DESIGN, CONSTRUCTION AND PERFORMANCE EVALUATION OF AXIAL
FLOW FANS

A THESIS SUBMITTED TO
THE GRADUATE SCHOOL OF NATURAL AND APPLIED SCIENCES
OF
MIDDLE EAST TECHNICAL UNIVERSITY

BY

HAYRETTİN ÖZGÜR KEKLİKOĞLU

IN PARTIAL FULFILLMENT OF THE REQUIREMENTS
FOR
THE DEGREE OF MASTER OF SCIENCE
IN
MECHANICAL ENGINEERING

SEPTEMBER 2019

Approval of the thesis:

DESIGN, CONSTRUCTION AND PERFORMANCE EVALUATION OF AXIAL FLOW FANS

submitted by **HAYRETTİN ÖZGÜR KEKLİKOĞLU** in partial fulfillment of the requirements for the degree of **Master of Science in Mechanical Engineering Department, Middle East Technical University** by,

Prof. Dr. Halil Kalıpçılar
Dean, Graduate School of **Natural and Applied Sciences**   _____

Prof. Dr. M. A. Sahir Arıkan
Head of Department, **Mechanical Engineering**   _____

Prof. Dr. Kahraman Albayrak
Supervisor, **Mechanical Engineering, METU**   _____

Examining Committee Members:

Assoc. Prof. Dr. Cüneyt Sert
Mechanical Engineering. METU   _____

Prof. Dr. Kahraman Albayrak
Mechanical Engineering, METU   _____

Assoc. Prof. Dr. Mehmet Metin Yavuz
Mechanical Engineering, METU   _____

Assist. Prof. Dr. Özgür Uğraş Baran
Mechanical Engineering, METU   _____

Assist. Prof. Dr. Ekin Özgirgin Yapıcı
Mechanical Engineering, Çankaya University   _____

Date: 03.09.2019

I hereby declare that all information in this document has been obtained and presented in accordance with academic rules and ethical conduct. I also declare that, as required by these rules and conduct, I have fully cited and referenced all material and results that are not original to this work.

Name, Surname: Hayrettin Özgür Keklikoğlu

Signature:

ABSTRACT

DESIGN, CONSTRUCTION AND PERFORMANCE EVALUATION OF AXIAL FLOW FANS

Keklikoğlu, Hayrettin Özgür
Master of Science, Mechanical Engineering
Supervisor: Prof. Dr. Kahraman Albayrak

September 2019, 127 pages

The primary purposes of this study are to examine the methods used in axial flow fan design, to perform these methods on the design of an axial fan, to develop a design application in order to reduce the design errors and spent time in the design process, and to determine the reliability of the application with numerical and experimental methods.

This study is concerned with the design of axial flow fans. It provides detailed information about the design process — additionally, a design code is implemented. All of the empirical data regarding axial fan design are digitized, and an airfoil database is generated in order to use in the code. In order to determine the pre-validity of the design code, computational fluid dynamics (CFD) methods are used. The aerodynamic characteristics of fans are examined in ANSYS CFX by using SST $k - \omega$ turbulence model. Moreover, the design code is enhanced by the construction process of the fan prototype. The manufacturing techniques used in the production of the fan parts are explained. Then, the test setup is prepared by using the Air Movement and Control Association (AMCA) standards, and several experiments are performed to reveal the accuracy of the design code.

The results of the study show that the generated design code gives logical suggestions on the axial flow fan design such that the value of the expected total pressure difference and volumetric flow rate are close enough to the obtained ones. Thus, an application that can help the designer in the design process has been developed and validated.

Keywords: Axial Flow Fan, Design Code, AMCA 210, Computational Fluid Dynamics

ÖZ

EKSENEL FANINLARIN TASARIMI, KONSTRÜKSİYONU VE PERFORMANS DEĞERLENDİRMESİ

Keklikoğlu, Hayrettin Özgür
Yüksek Lisans, Makina Mühendisliği
Tez Danışmanı: Prof. Dr. Kahraman Albayrak

Eylül 2019, 127 sayfa

Bu çalışmanın temel amaçları; aksiyal akışlı fan tasarımında kullanılan yöntemleri incelemek, aksiyal bir fan tasarımı üzerinde bu yöntemleri uygulamak, tasarım hatalarını ve tasarım sürecinde harcanan zamanı azaltmak için bir tasarım uygulaması geliştirmek, nümerik ve deneysel yöntemlerle bu uygulamanın güvenirliliğini belirlemektir.

Bu tez aksiyal akış fanının tasarımı ile ilgilidir. Tasarım süreci hakkında detaylı bilgi vermektedir. Buna ek olarak, bir dizayn kodu hayata geçirilmiştir. Eksenel fan tasarımı ile ilgili bütün ampirik veriler sayısallaştırılmıştır ve kod içerisinde kullanmak amacıyla bir kanat veritabanı oluşturulmuştur. Tasarım kodunun ön-geçerliliğini belirleyebilmek için, Hesaplamalı Akışkanlar Dinamiği (HAD) yöntemleri kullanılmıştır. Fanın aerodinamik özellikleri SST $k - \omega$ türbülans modeli kullanılarak ANSYS CFX'te incelenmiştir. Ayrıca, tasarım kodu, fan prototipin yapım süreci ile kapsamlandırılmıştır. Fan parçalarının üretiminde kullanılan imalat teknikleri açıklanmıştır. Air Movement and Control Association (AMCA) standartları kullanılarak test düzeneği hazırlanmış ve tasarım kodunun doğruluğunu ortaya çıkarmak amacıyla çeşitli deneyler yapılmıştır.

Çalışmanın sonuçları göstermektedir ki üretilen tasarım kodu eksenel akış fanı tasarımı üzerinde mantıklı önerilerde bulunmuştur; öyle ki, beklenen toplam basınç farkı ve debi değerleri elde edilen verilere oldukça yakın çıkmıştır. Böylece tasarım sürecinde tasarımcıya yardımcı olabilecek bir uygulama geliştirilmiş ve geçerliliği kabul edilmiştir.

Anahtar Kelimeler: Eksenel Akış Fanı, Tasarım Kodu, AMCA 210, Hesaplamalı Akışkanlar Dinamiği

To my parents and my lovely wife

ACKNOWLEDGEMENTS

TABLE OF CONTENTS

LIST OF TABLES

TABLES

LIST OF FIGURES

FIGURES

LIST OF ABBREVIATIONS

ABBREVIATIONS

AMCA	Air Movement and Control Association
CFD	Computational Fluid Dynamics
CAD	Computer-Aided Design
ASHRAE	The American Society of Heating, Refrigeration and Air Conditioning Engineers
SST	Shear Stress Transport
NACA	National Advisory Committee for Aeronautics

LIST OF SYMBOLS

SUBSCRIPTS

m	Mean
h	Hub; hydraulic
t	Tip
1	Inlet
2	Outlet
u	Tangential direction
f	Fluid
r	Radial direction
max	Maximum
avg	Average
$mech$	Mechanical
vol	Volumetric

SYMBOLS

ρ	Density
x, y, z	Cartesian coordinates
u_x, u_y, u_z	Cartesian velocity components
g	Gravitational acceleration
p	Pressure
Δp	Pressure difference
$\partial \tau_{ij}$	Viscous stress tensor
μ	Dynamic viscosity
υ	Kinematic viscosity
δ_{ij}	Kronecker delta
S_{ij}	Rate of strain tensor
σ_k	Closure coefficient
ε	dissipation
υ_T	Kinematic eddy viscosity
k	Turbulent fluctuation
l	Turbulence length scale
C_D	Closure coefficient of Prandtl
ω	Rate of dissipation of energy; rotational velocity (rad/s)
c	Chord length
s	Pitch length
F_L	Lift force

F_d	Drag force
Z_b	Number of blades
D	Diameter
r	Radius
C_L	Lift coefficient
C_{Li}	Isolated lift coefficient
C_d	Drag coefficient
b	Span length
β	Flow angle
H	Pressure head
W	Relative velocity
V	Absolute flow velocity
k_f	Cascade-influence factor
Q	Volumetric flow rate
N, n	Rotational velocity
ω_s	Nondimensional specific speed
Δ_s	Nondimensional specific diameter
ν	Hub ratio
ψ	Head coefficient
$\emptyset$	Flow coefficient
V_a	Axial velocity
U	Tangential velocity
γ	Stagger angle
α	Angle of attack
σ	Solidity
π	Dimensionless similarity parameter
P	Power
dB	Noise level
t	Time
c_t	Tip clearance
C_{dt}	Tip leakage loss coefficient
C_{da}	Annulus skin friction loss coefficient
C_{ds}	Secondary flow loss coefficient
η	Efficiency
A_{flow}	Flow area
Re	Reynolds number
R_r	Reaction ratio
δ_r	Drag over lift ratio
T	Torque; temperature
l_{tube}	Tube length
f_{pipe}	Pipe Friction Coefficient
p_{loss}	Pressure Loss

CHAPTER 1

INTRODUCTION

1.1. General

Axial flow fans are commonly used for heating, ventilating, air conditioning, tunnel and mining applications. In each form, the physical properties of the fan should be designed specifically for the application's needs. For example, in specific tunnel and mining applications, reaching the air at the operational area is vital. Therefore, the main design concern is to obtain the required pressure difference to transfer the required amount of fresh air. Moreover, in some heating applications, the flow rate becomes more critical since the heating rate is directly related to the flow rate. In that case, physical properties of the fan should be designed considering the air velocity and required heating rate of the application point. In addition to that, in some exhaust or fire applications, fan direction can be determined according to the location of the smoke. Therefore, the fan must be able to blow the air bi-directionally, and it should be designed using a proper airfoil profile which can generate flowrate in both directions. This wide-range usage calls for the utilization of different types of axial flow fans.

The subject of this thesis is the design, construction and performance evaluation of axial fan. In the design part, the commonly used empirical design methods in the literature are examined and employed. In the software implementation part; algorithm, design methodology, assumptions, database organizations and user interface are explained. Moreover, an example fan design is demonstrated using axial flow fan design software. In numerical analyses phase, Computer-Aided Design (CAD) model of the fan is generated by using the custom software and the model is analyzed by using the commercial Computational Fluid Dynamics (CFD) software with selecting

1

the proper mesh type, boundary conditions, solution methodology and turbulence model. In the construction and experimental test part, the axial flow fan is manufactured and tested experimentally. Finally, the accuracy of the axial flow fan design software is validated with the results of the CFD analysis and the experimental tests.

1.2. General Information on Axial Flow Fans

In axial flow fans, as the name suggests, the direction of the fluid flow is in the axial direction, it means that flow is parallel to the axis of rotation or parallel to the fan shaft. Ideally, the velocity of the fluid in flow has no radial component. On the other hand, there is a tangential velocity component caused by the rotation of the impeller. It supplies the required pressure rise to the fluid flow.

In many axial flow fan applications, the air is used as a working fluid at medium-pressure and low-speed. Since the operation range of air is mostly incompressible, the change in the air density is too small compared to the change in the air pressure; and therefore, can be neglected.

Fluid compressibility depends on various physical properties of axial flow fan. Increasing the diameter of the fan and the rotational speed of the motor lead to an increase in the velocity of the fluid at the tip. Changes in the fluid density can be neglected until 0.3 of Mach number, but when the fluid velocity is over 0.3 Mach, the fluid will be compressible [1]. So, there is a limit to the design parameters for obtaining an incompressible working fluid.

The main applications of axial flow fan are heating, ventilating, air conditioning in mines, tunnels, transportation, electronic devices, industrial applications, buildings and vehicles. In order to provide extensive range usage, there are different types of axial flow fan, and they are categorized according to their pressure rise and flow rate capabilities.

1.2.1. Classification of Axial Flow Fans

1.2.1.1. Propeller Fans

The first kind of axial flow fan widely used in industrial applications is propeller fans or sometimes called panel fans. These fans have a low-pressure rise and high flow rate capabilities. They are generally used for exhausting air from a room or a factory. The hub-tip ratio for these fans is generally less than 0.3, and they have low production cost.

Propeller fans are generally mounted on the walls or windows of the buildings. They can be used with other propeller fans on the same wall and operated in parallel to obtain a higher flow rate. Propeller fans have two types of drive arrangements, namely belt-drive or direct-drive arrangement [2].

In the direct-drive arrangement, the electric motor is directly mounted to the rotor of the fan. The production cost is lower compared to belt-drive arrangement as a belt and pulleys are not used. Moreover, the direct-drive arrangement is more efficient than belt-drive since no losses are stemming from friction and transmission [2]. A propeller fan in a direct-drive arrangement is shown in Figure 1.1.

Figure 1.1. Propeller Fan in Direct-Drive Arrangement [3]

In belt-drive arrangement, the rotational motion of the electric motor is transferred using a belt and pulleys. Since the reduction ratio of the pulley can be adjusted, the rotational speed range of belt-drive arrangement is more comprehensive that of the direct-drive arrangement. This speed control feature allows the use of belt-drive arrangements in larger size propeller fan applications [2]. A propeller fan in belt-drive arrangement is shown in Figure 1.2.

Figure 1.2. Propeller Fan in Belt-Drive Arrangement [4]

1.2.1.2. Tube-Axial Fans

Tube-axial fans are similar to propeller fans; however, they have physical properties specific to them. These fans have cylindrical housings up to one diameter long, and their hub-tip ratio range is generally between 0.3 and 0.5. The electric motor can rotate faster than the motor used in propeller fans, and therefore, tube-axial fans can produce higher pressure rise. Driving methods are similar to propeller fans, and the electric motor can be mounted to the rotor by using a belt or directly [2]. A tube-axial fan in a direct-drive arrangement is shown in Figure 1.3.

Figure 1.3. Tube-Axial Fan in Direct-Drive Arrangement [5]

There are two ways to mount tube-axial fans: They can be mounted both to the inlet and outlet of the application area. It means that they can be used as an air source or an exhaust. Since tube-axial fans have no guide vanes, air leaves the propeller spinning. In this case, the outlet length plays a vital role in determining the pressure loss generated by spinning. In other words, longer outlet length results in a higher-pressure loss for the tube-axial fans. Thus, the best way to mount tube-axial fans is to mount them from the propeller side as an air source fan and to mount from the outlet side as an exhaust fan [2].

1.2.1.3. Vane-Axial Fans

In vane-axial fans, there are guide vanes located inside of the cylindrical housing of the fan. The length of the cylindrical housing is generally one diameter long. According to the type of the application, guide vanes can be used before or/and after the propeller. The purpose of using guide vanes before the propeller is to adjust the inlet angle of the incoming flow while using guide vanes after the propeller prevents air spin at the outlet of the fan.

As mentioned in the tube-axial fan, air spin determines the way of mounting of the fan. It is not the case in vane-axial fans, where air spin is prevented at a vast scale, and pressure loss due to spinning is eliminated. As a result, high static pressure rise is obtained.

Vane-axial fans have bigger hub-tip ratio than previous fan types. Their hub-tip ratio range is generally between 0.5 and 0.8. Vane-axial fans can also be driven by an electric motor using a belt or directly. A vane-axial fan in a direct-drive arrangement is shown in Figure 1.4.

Figure 1.4. Vane-Axial Fan in Direct-Drive Arrangement [6]

1.2.1.4. Two-Stage Axial Flow Fans

In two-stage axial flow fans, there are two propellers which can be rotated in the same direction or reverse direction. They are used in the applications in which higher static pressure rise is needed in order to transfer the air at the target area. The directions of rotation are determined according to the presence of guide vanes. The guide vanes used between the propellers adjust the inlet angle of coming flow from the first stage to the second stage, and propellers can turn in the same direction. If there are no guide vanes between propellers, they must turn in the reverse direction to obtain proper inlet angle from the first stage to the second stage.

The configuration without guide vanes is shown in Figure 1.5. Two identical electric motors must be used to obtain the same rotational motion, increasing the production cost.
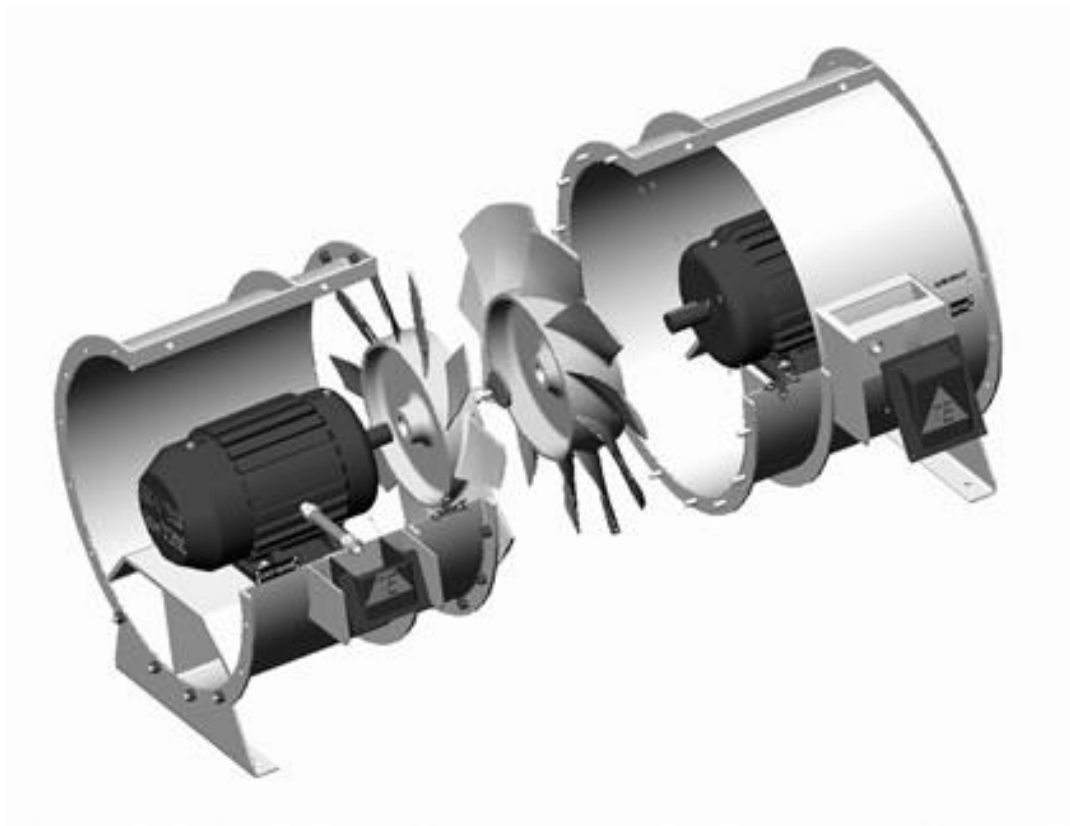
Figure 1.5. Two-Stage Axial Flow Fan without Guide Vanes [7]

Typical features of axial flow fans with direct-drive arrangement are given in the Table
1.1.

Table 1.1. *Typical Features of Axial Flow Fans* [2]

	Propeller fan	*Tube-axial fan*	*Vane-axial fan*	*Two-stage axial-flow fan*
Casing	Mounting ring or Mounting panel	Short cylindrical housing	Cylindrical housing	Long cylindrical housing
Motor Support	Inlet side of panel preferred	Inside housing, outlet side preferred	Inside housing, outlet side preferred	Inside housing, between the two stages
Guide vanes	None	None	Past fan wheel preferred	Between the two stages or none
Hub-tip ratio	0-40%	30-50%	45-80%	50-80%

1.2.2. Performance of Axial Flow Fans

Performance of axial flow fans is determined by performing specific tests. These tests
are prepared according to some standards and executed in laboratory conditions. The
Air Movement and Control Association, Inc. (AMCA) and The American Society of
Heating, Refrigeration and Air Conditioning Engineers, Inc. (ASHRAE) were
supported to prepare these fan standards. They establish uniform methods to determine
flow rate, pressure rise, power consumption and efficiency [8]. The performance
curves of a fan can be constituted with these parameters. In Figure 1.6, a sample
performance curve of a fan is shown.
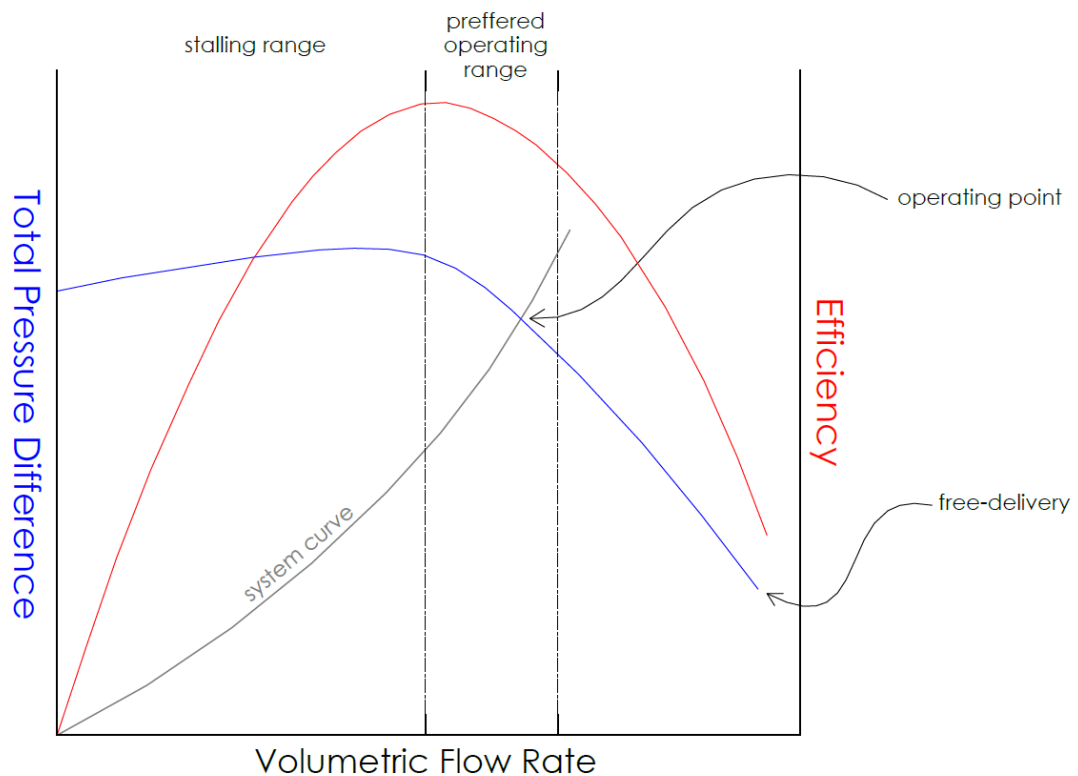
Figure 1.6. Performance Curves of an Axial Flow Fan

In Figure 1.6, the point at which the volumetric flow rate reaches its maximum value is called the free-delivery point. Pressure difference approaches zero while approaching to this point. The point at which fan operates is called the point of operation. Its location is determined with respect to the characteristic of the system in which the fan is used [8]. An increase in the flow resistance leads to a decrease in the flow rate and an increase in the pressure difference of the fan. It means that the point of operation moves left on the pressure curve.

Movement of the operating point to the left on the performance curve will increase the pressure difference up to the stalling range. After the stalling range, pressure difference starts to decrease, and then, fan no longer can work efficiently.

Point of operation should be kept away from stalling range since it means low efficiency and high noise for axial flow fans. In order to design an efficient and low noise axial flow fan, the operating range should be located between the free-delivery and stalling range. Preferred operating range is also shown in Figure 1.6.

1.3. Literature Survey

The focus of most of the studies on the axial flow fans is regarding the design methods. These are generally about the fan blade and the axial flow fan design methods. In the blade design methods, isolated airfoil approach versus cascade airfoil approach is mostly compared. In axial flow fan design methods, the differences between the design steps are compared and analyzed.

Design methods are compared with respect to numerical and experimental studies. In the numerical studies, analyses are performed using Computational Fluid Dynamics (CFD) tools and other mathematical models. The turbulence models used in the CFD tools are compared according to their performances. In experimental studies, performance curves of fan are obtained experimentally, and the results are compared with numerical ones. Additionally, airfoil types are also compared. In this case, the impellers of the axial fans constructed by using different airfoil types are compared.

Castegnaro [9] studied the differences in the design methods for low-speed axial flow fans. The choice of the airfoil and the solidity distribution, the computation of the stagger angle of the blade elements and the determination of the number of blades are the methodological differences among the classical design methods. Three tube-axial flow fans and two types of airfoil, C4 and NACA 65, are used in this work. The purpose of the first fan is to find out the best airfoil and obtain the most accurate formula for the stagger angle. The second fan is used in determining the convenient solidity distribution. In the last fan, Reynolds number effect on the flow deflection is examined. The results show that C4 airfoil is the most convenient airfoil type for the axial fan applications and $\gamma = \beta_m - \alpha$ is the recommended formula for the stagger angle due to the achievement in the required flow deflection and the fan pressure. In

12

order to get the optimum solidity distribution, two blade types are used, and results show that the blade designed according to a linear diffusion factor criterion has higher efficiency than the C_L criterion-based blade. Lastly, it is found in the third fan that the flow deflection reduces about 12% when the fan works at 1000 rpm instead of 2000 rpm for the same propeller.

In another study of Castegnaro, the cascade and the isolated airfoil approaches on the blade design are analyzed [10]. It is stated that the cascade approach is valid for high solidity ($\sigma \geq 1$), isolated airfoil approach is valid for low solidity ($\sigma \leq 0.7$) and for medium solidity values ($1 > \sigma > 0.7$) modified isolated approach is generally used. The aim of this work is to compare the performances of the modified isolated airfoil approach, modified cascade approach and their mixed form on the medium solidity blades. In the scope of the study, two rotor-only axial flow fans are tested experimentally and numerically. The airfoil type using in the blade profile of both fans is chosen from NACA 65 series. In the CFD model, the $k - \omega$ model of Wilcox is applied in the solution. The analyses are performed on the commercial code CD-Adapco StarCCM+©. The experimental results show that the modified isolated approach is an effective design method for blade design, while it is proven that the mixed approach is the most accurate approach for medium solidity values. Moreover, the cascade approach is found not enough to supply the required flow deflection for low-solidities.

Ahmed et al. [11] examine the effects of solidity ratios, and stagger angles on the flow field around NACA 0012 airfoils numerically using the turbulence model as $k - \varepsilon$ model. The flow separation on the training edge of the airfoil for different angles of attack is predicted for solidity ratios and stagger angles. The angles of attack are varied from 0 to 24 degrees, and the stagger angle is varied from 10 to 30 degrees while the solidity is ranged from 0.55 to 0.83; and the resulting pressure, lift and drag coefficients are recorded. The results show that the decrease in the solidity ratios causes to start the flow separation earlier. Boundary layer thickness increases with the increase in the angle of attack but increasing rate comes down with the decrease in the

solidity ratios. Pressure coefficient at the suction side increases with the decrease in the solidity. The lift coefficient decreases when the flow separation starts and it is observed that the lift and drag coefficients increase with a reduction in the stagger angle at high incidences.

Masi et al. [12] study on the design criterion for high efficiency for tube-axial fans. In the tube-axial fans, the desired pressure rise requirements may not be achieved in the application due to not having guide vanes or straightener. It is stated that this problem may be overcome by the knowledge of the design constraints such as maximum size and rotational speed. Thus, one of the aims of this work is to give a suggestion about the sizing for high-efficient tube-axial fans. The second aim is to help the fan designer to give efficiency diagrams, and therefore, the designers can check whether their fan is acceptable or not. Two design scenarios are used in the experiments. The design objective of the first scenario is to obtain maximum efficiency, and it is called unconstrained design scenario. The design objective of the other scenario is to obtain maximum efficiency with fixed rotational speed and external diameter, which is called as a design under constraints on fan size and rotational speed. The analysis shows that the fan efficiency depends on the trade-off between axial diffusion losses and the swirl velocity at the rotor outlet, and the fan sensitivity improves with the increase in the volumetric flow rate. It is suggested that hub-tip ratio should be as low as possible since the fans having a low hub-tip ratio are less sensitive with respect to the application types. If it is not possible, the tail cone diffuser is suggested for utilization.

Venter et al. [13] study the tip clearance effect on the performance of an axial flow fan. In the study, a new approach where not only changes in the static fan pressure and fan static efficiency are evaluated but also volumetric flow rate changes are employed, is used. The test code used in the study is BS 848: 1980: Type A, which implies that free inlet and free outlet conditions prevail. The fan used in the application is 8-bladed 1542 mm of diameter axial flow fan. Six different tip clearances are used, and their sizes are varied between 3.0 mm to 10.5 mm. The analysis shows that an increase in the tip clearance ends up with a decrease in the static pressure, the static efficiency,

the power consumption and the volumetric flow rate of the fan. Moreover, it is also found that the type of the application and size of the rotor have an impact on fan performance.

Pogorelov et al. [14] also study the effects of tip clearance on the flow field in an axial flow fan. Numerical analysis is performed by using large-eddy simulation. Compressible Navier-Stokes equations are used in the solution. The computations are performed for two different tip clearances, $s/D_0 = 0.01$ and $s/D_0 = 0.005$, with the same fixed flow rate coefficient. The purpose of the numerical analysis is to find out the impact of the clearance width on the overall flow field, and it is observed that decreasing the tip clearance completely affects the flow field: First of all, the blade-wake interaction is removed for $s/D_0 = 0.005$. Secondly, the amplitude of the tip clearance vortex, and lastly, the noise-level decreases with decreasing tip clearance.

Yilbas et al. [15] study the numerical simulation of flow field developed around a cascade of NACA 0012 airfoils. Two-dimensional incompressible Navier-Stokes equations are used in the numerical solution of the flow field. Turbulence effects are also included in the solution by using $k - \varepsilon$ model. Lift, drag and pressure coefficients are calculated for different angles of attack varying between 0 and 24 degrees and different solidities swept between 0.55 and 0.83. According to the results, it is concluded that the pressure coefficient of the suction side of trailing edge increases with decreasing solidity. However, it is predicted that the lift coefficient drops suddenly when the flow separation starts, and no drastic reduction in the lift coefficient is observed. It is also seen that the increase in the solidity causes the incidence angle to increase at which maximum lift occurs. Moreover, the effect of rotation of leading edge on the drag coefficient is also examined and it is concluded that the rotation causes the drag coefficient to decrease, increase the lift coefficient.

CHAPTER 2

DESIGN OF THE AXIAL FLOW FAN

2.1. Introduction

Design of the axial flow fan is a procedure in which the expected performance parameters from the fan are used as inputs at the beginning of the design process. These input parameters are the total pressure difference and the volumetric flow rate. There is an additional input parameter. It is the rotational velocity of the electric motor. At the end of this chapter, a sample fan design procedure is shown, but there are a lot of approaches, methods, rules and empirical graphs regarding the fan design which should be known by the designer.

In this chapter, the methodologies and approaches used in the blade design, the rules and empirical graphs used in the axial flow fan design, and the parameters used in the design steps are explained and investigated.

2.2. Axial Flow Fan Blade Design Methods

Interaction between the fan blades is a critical state affects the fan design. The lift and drag coefficients obtained from a blade on the impeller can be affected by the neighbor blade according to the distance between them. It is called the pitch distance and can be seen in Figure 2.1.
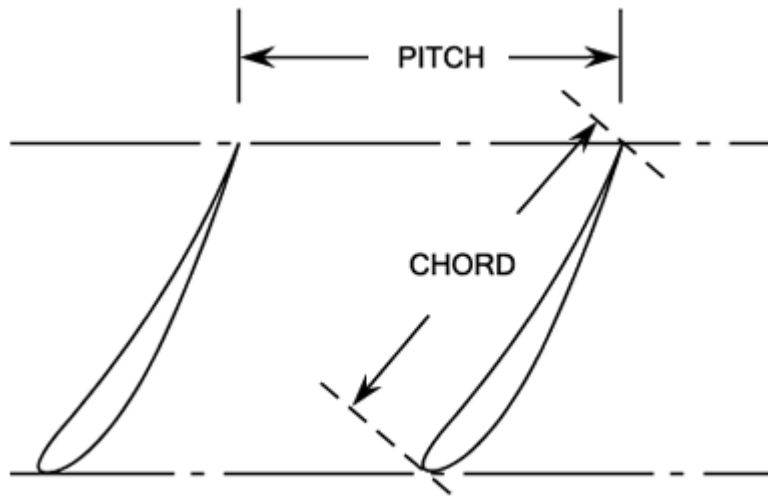
Figure 2.1. The Pitch Distance Between Fan Blades

There is a relation between the chord c and the pitch s of the blades and it is called blade solidity. It is used for specifying whether the blades affect each other or not. It can be expressed as

$$solidity = \sigma = c/s \qquad (2.1)$$

There are two approaches in the design of an axial flow fan blade. These are the isolated airfoil approach and the cascade approach. The decision of which approach is used in the axial flow fan blade design can be determined by calculating the blade solidity.

In the study of Castegnaro, the validity of using solidity ranges in the determination of the design approach is examined [10]. It is found that the isolated airfoil approach is valid for low solidities which is smaller than 0.7, and the cascade approach is valid for high solidities bigger than 1.0. In addition, the mixed approach, which is the combination of the cascade and the isolated airfoil approaches, is validated for the solidity ranges between 0.7 and 1.0.

2.2.1. Isolated Airfoil Approach

A control volume, which is given in Figure 2.2, is created around a single airfoil in the isolated airfoil approach. When the flow field is applied to this control volume, the airfoil will be under the influence of some forces, which are the viscous force and the pressure distribution force.
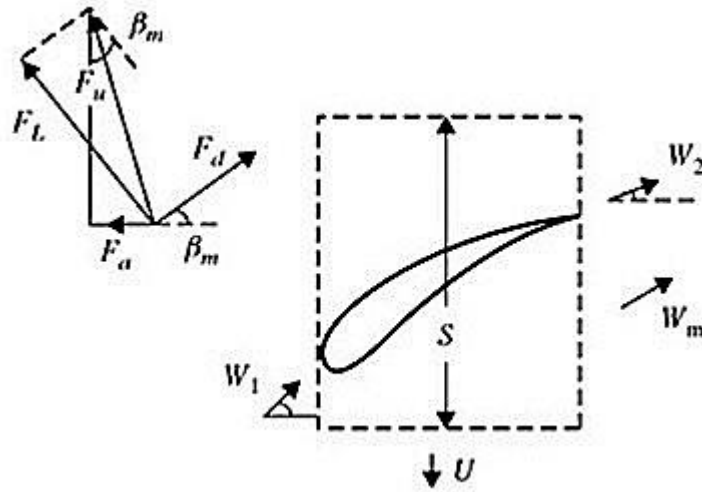
Figure 2.2. Forces Acting on Isolated Airfoil [16]

As shown in Figure 2.2, the force F_d, which is parallel to the direction of the relative mean velocity W_m, is called drag force and the force F_L, which is normal to the drag force, is called the lift force.

The pitch distance of an impeller is calculated as

$$s = \frac{2\pi r_m}{Z_b} \tag{2.2}$$

where r_m is the mean radius of the fan and Z_b is the number of blades. Mean radius can be calculated using the tip radius, r_t and the hub radius, r_h of the fan.

$$r_m = \sqrt{\frac{1}{2}(r_t^2 + r_h^2)} \qquad (2.3)$$

Determination of the number of blades will be explained detailed in the following sections.

The lift and the drag forces can be written in terms of the lift and the drag coefficients, C_L and C_d respectively.

$$F_L = C_L bc \left(\frac{1}{2}\rho W_m^2\right) \qquad (2.4)$$

$$F_d = C_d bc \left(\frac{1}{2}\rho W_m^2\right) \qquad (2.5)$$

where b is the span length of the fan blade and W_m is the relative mean flow velocity.
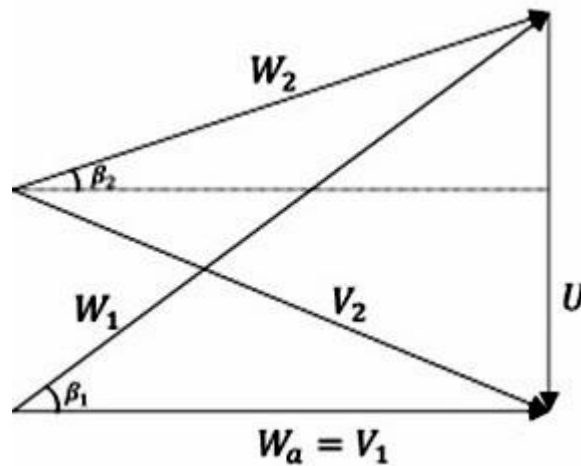
Figure 2.3. The Velocity Triangles Applied on an Airfoil

Figure 2.3 shows the detailed velocity triangles applied on an airfoil. The velocity triangles can be used for the calculation of the lift and drag coefficient as follows [16]

$$tan\beta_m = \frac{1}{2}(tan\beta_1 + tan\beta_2)$$

(2.6)

$$C_L = 2\left(\frac{s}{c}\right)(tan\beta_1 - tan\beta_2)\cos\beta_m$$

(2.7)

$$C_d = \left(\frac{s}{c}\right)\left(\frac{\Delta p}{\rho W_1^2/2}\right)$$

(2.8)

where W_1 is the relative inlet flow velocity, β_1 is the inlet flow angle, β_2 is the outlet flow angle, β_m is the mean flow angle and Δp is the total pressure difference. The lift and the drag coefficients directly affect the performance of axial flow fans.

Pressure fields of the blades start to affect each other when the solidity ratios increase. In this case, the actual lift value obtained by the blades is different from the theoretical lift value. Therefore, the isolated airfoil approach is not enough for creating an efficient fan having higher solidity [17].

2.2.2. Cascade Approach

As mentioned at previous sections, the interactions of pressure fields passing on the blades are affected from the pitch distance, the chord distance and the stagger angle. Moreover, these interactions lead to change the actual lift coefficient obtained from a blade, and therefore, the efficiency of the axial flow fan. In order to get rid of this problem, Scholz find a relation between the actual lift coefficient and the effected lift coefficient [18]. According to their research, there is a ratio between the cascade lift coefficient and the isolated lift coefficient, and it is called as cascade-influence factor k_f.

$$k_f = \frac{C_L}{C_{Li}} \tag{2.9}$$

where C_L is the cascade lift coefficient and C_{Li} is the isolated lift coefficient.

The graphs of the cascade-influence factor for the circular-arc camber line profile airfoils is given in Figure 2.4, respectively. In both graphs, cascade-influence factor lines are the function of the solidity and the stagger angle.

22
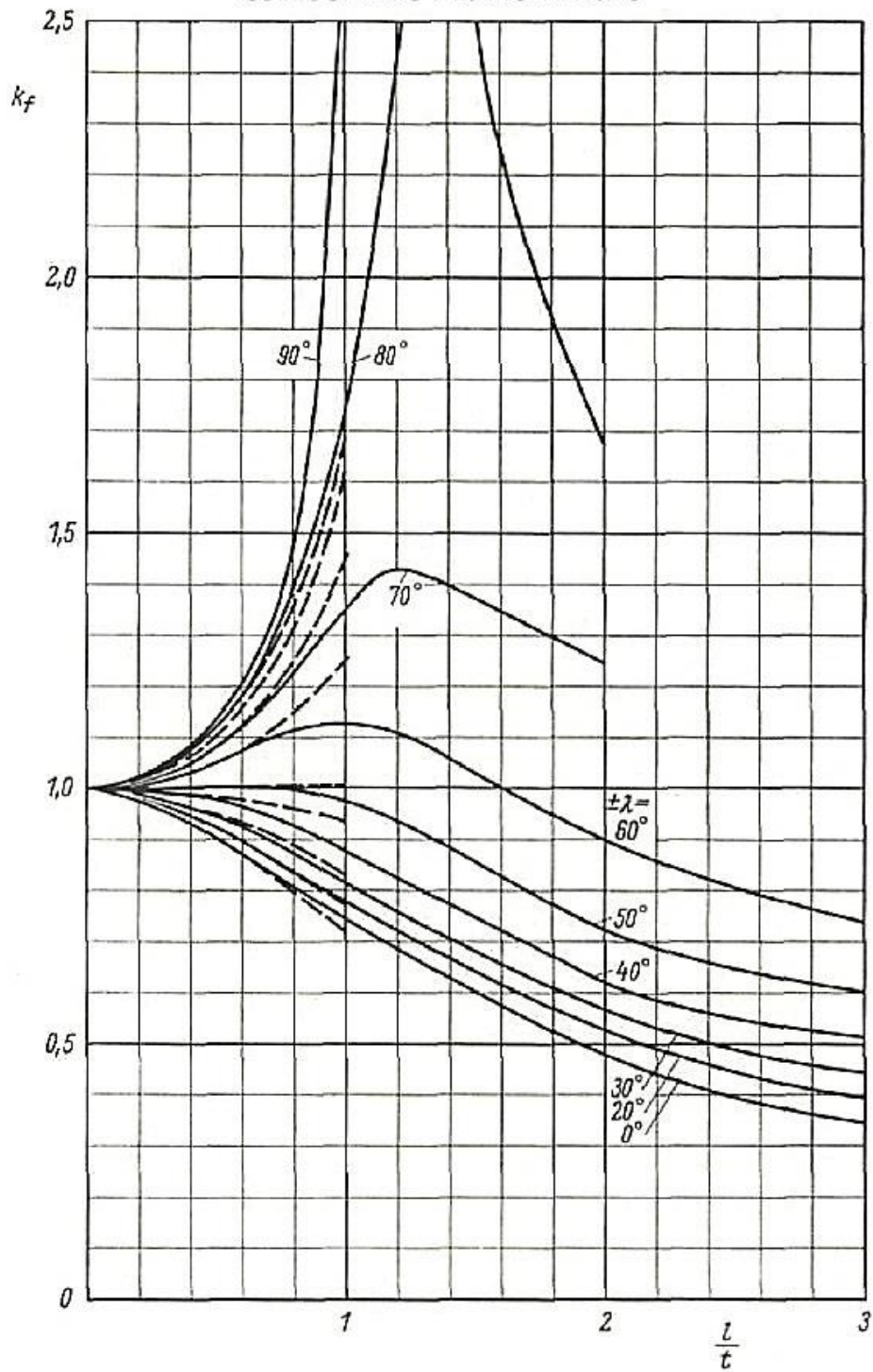
Figure 2.4. Cascade-Influence Factor for the Circular-Arc Camber Line Profile Airfoils [18]

23

According to Figure 2.4, when the blade solidity, l/t approaches zero, cascade-influence factor approaches unity. It means that, the value of lift coefficient obtained from isolated airfoil approach is nearly equal with the one obtained from the cascade approach for low solidities. Nevertheless, isolated airfoil approach gives more accurate results than the cascade approach for solidity value smaller than 0.7 [10].

In the software implementation part, both the isolated airfoil and the cascade approaches are used in the algorithm. For the solution with the cascade approach, the cascade-influence factor in Figure 2.4 is used since the database consists of circular-arc camber type of airfoil entirely.

2.3. Preliminary Design Procedure

At the beginning of the design process, some input parameters are required to start the design of the axial flow fan. These are the volumetric flow rate (Q), the total pressure difference (Δp) and the rotational speed of the impeller (ω). The volumetric flow rate and the total pressure difference can be determined in accordance with the application needs. In fact, these input parameters are the goal of the fan designer. At the end of the design, the fan should be able to give that flow rate at that total pressure difference.

Apart from these, the rotational speed of the impeller is the other important input parameter of the fan design. It is directly related to the rotational speed of the motor. It should be considered that there is a limit for the rotational speed of the motor in the incompressible design. It is known that axial flow fans are considered to operate in the incompressible range. There is another well-known fact that air starts to become compressible after a certain speed and pressure. If the speed of the air flow exceeds 0.3 Mach number, compressible range starts [1]. The highest speed obtained in the axial flow fan is the tangential speed at the tip of the impeller. The main parameters which determine the value of tangential speed are the rotational speed of the electric motor and the diameter of the fan, and therefore, these parameters should be selected and calculated carefully to design a fan works in the incompressible range.

In order to calculate the diameter of the fan, the empirical Cordier diagram is used.

2.3.1. Cordier Diagram

The first thing which is thought at the beginning of the fan design is efficiency, and it is directly related to the physical properties of the fans. Even the design quality is dependent on the experience of the fan designer, the physical properties of the fan should be controlled and calculated using an empirical diagram called the Cordier diagram whether the type of the fan is in the design limit or not. The Cordier diagram is shown in Figure 2.5.
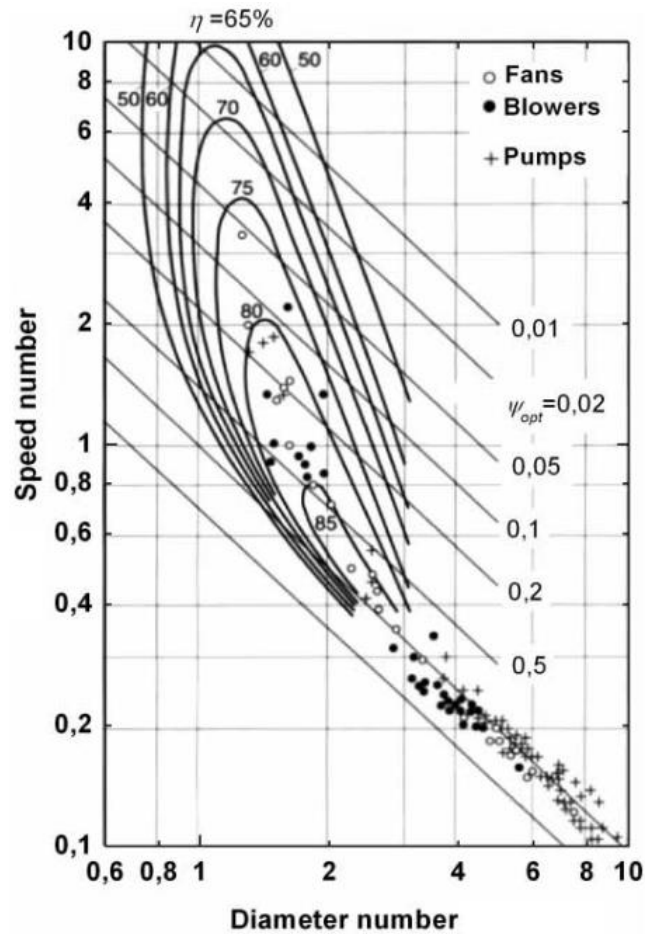
Figure 2.5. Cordier Diagram [19]

In order to design an efficient turbomachine, Otto Cordier had established a relation between the design parameters at the operating point and the size of the turbomachines by using two dimensionless numbers [19]. These are the speed number (specific speed) and the diameter number (specific diameter). They can be defined as respectively

$$\omega_s = \frac{\omega \sqrt{Q}}{(\Delta p / \rho)^{3/4}} \tag{2.10}$$

$$\Delta_s = \frac{D(\Delta p / \rho)^{1/4}}{\sqrt{Q}} \tag{2.11}$$

The Cordier diagram for fans can be seen in Figure 2.6.

26
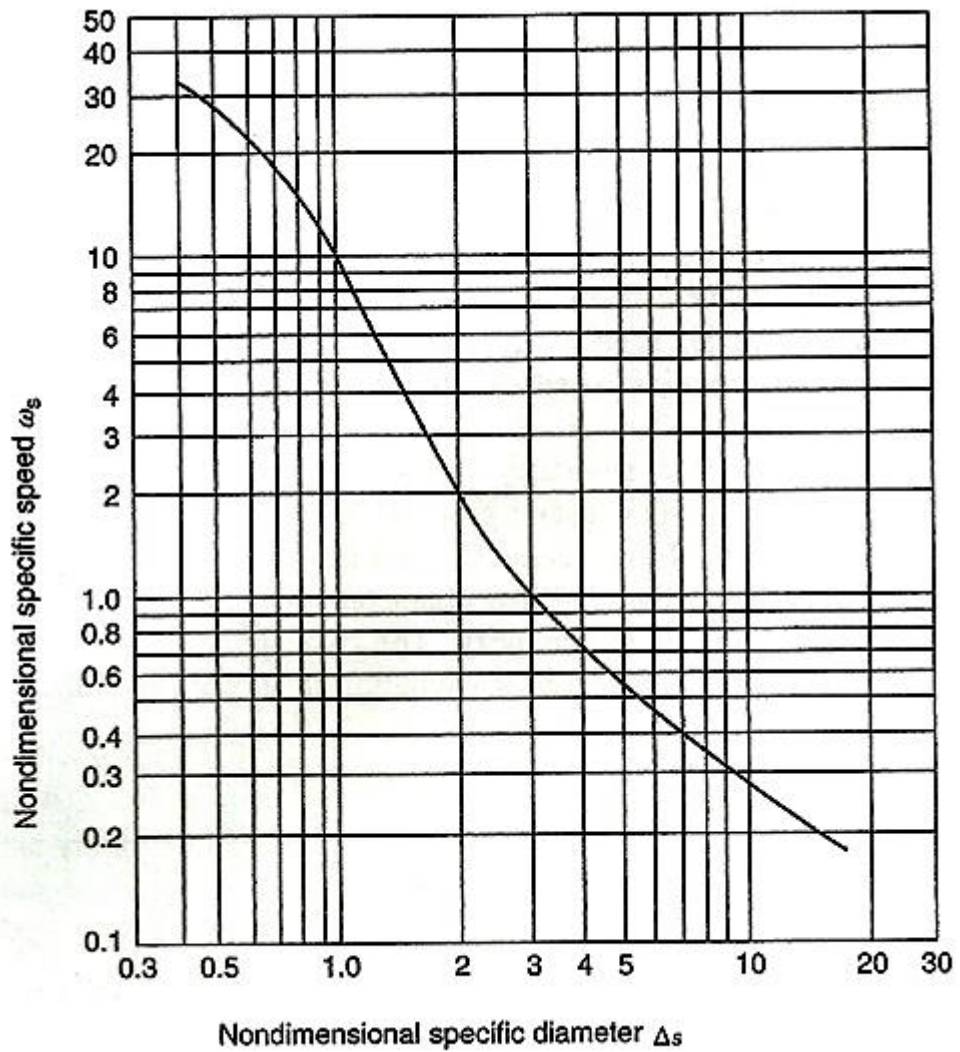
Figure 2.6. Cordier Diagram for Fans [16]

It is known that turbomachines can be classified according to their impeller type as axial, mixed (diagonal) and radial, and all of them work in different ranges of volumetric flow rate and total pressure difference. In the study of Epple at al. [20], the types of the impellers are classified on the Cordier Diagram and it is given in Figure 2.7.
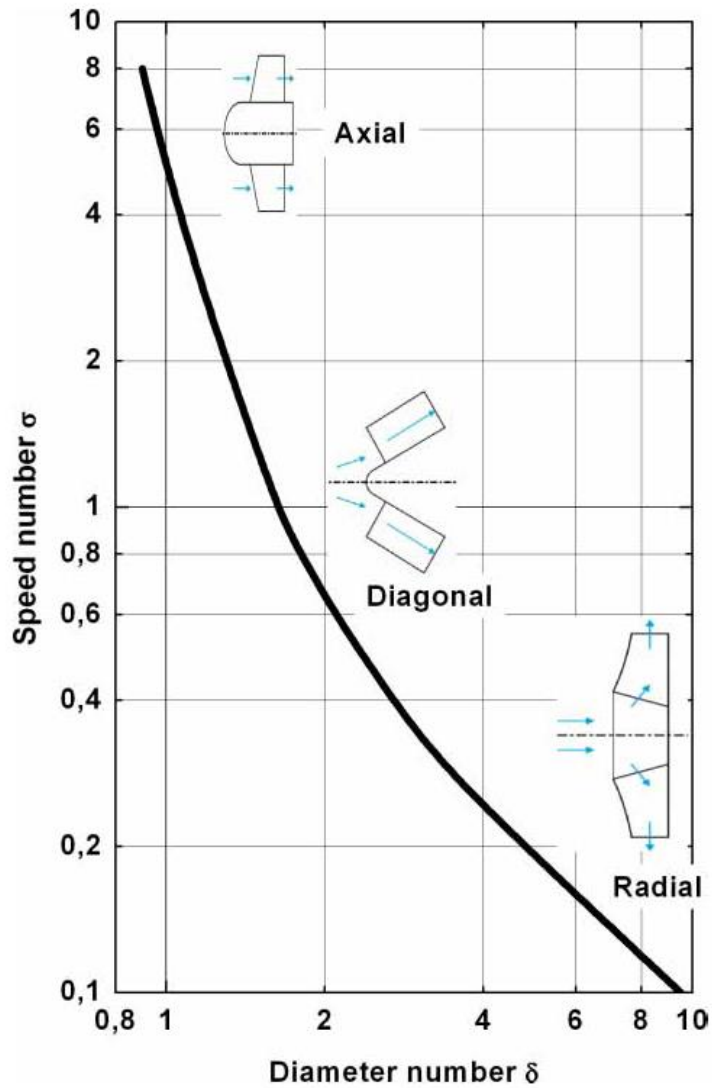
Figure 2.7. Classification of Impeller Types on the Cordier Diagram [20]

2.3.2. Hub Diameter and Number of Blades

After the determination of the fan diameter and the control of the impeller type, the next topic is the calculation of the hub diameter. As explained in the previous chapter, the types of axial flow fans can be classified with their hub-tip ratio.

The hub-tip ratio range of propeller type axial flow fans is less than 0.3, the tube-axial fan is between 0.3 and 0.5, and the vane-axial fan is between 0.5 and 0.8 [2].
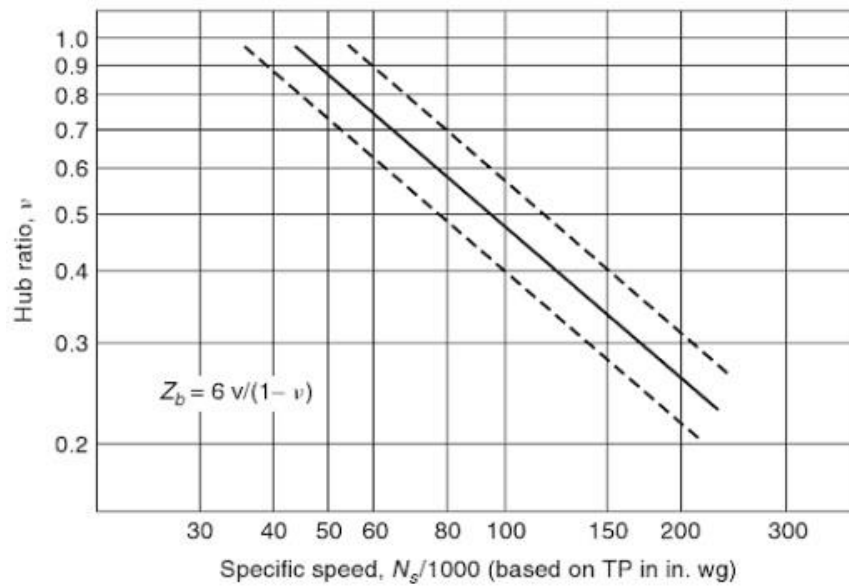
Figure 2.8. The Optimum Hub-Tip Ratio Range for Axial Flow Fans [16]

Figure 2.8 shows the optimum hub-tip ratio range for axial flow fans. v presents hub-tip ratio and it can be calculated as

$$v = \frac{D_h}{D_t} \tag{2.12}$$

where D_t is the tip diameter and D_h is the hub diameter.

There is a relation between the hub ratio, v and the number of blades, and it is given as

$$Z_b = \frac{6v}{1-v} \tag{2.13}$$

Increasing the hub-tip ratio leads to an increase in the number of blades. According to Eleftherios, the number of blades affects the efficiency and noise level. Increasing the number of blades cause the efficiency to decrease and increase the noise level [17].

2.3.3. The Guide Vanes

As mentioned in the previous chapter, air leaves the fan in spinning, and the primary duty of guide vanes is eliminating the air spin. Guide vanes can be used before or after the impeller for different purposes.

The guide vanes located inlet side of the fan adjust the angle of the incoming flow to the impeller and the flow leaves the impeller in the axial direction. The shape of the inlet guide vanes is also too valuable. Since the mistakes in the guide vanes design result spinning in the outlet flow. In case of existing a turbulent flow at the inlet side of the fan, the inlet guide vanes work better than the outlet guide vanes but the noise-level increases when reducing the turbulence-level. In addition, inlet guide vanes accelerate the velocity of fluid flow.

The outlet guide vanes have an extra duty besides adjusting the angle of the leaving air. They produce a certain ratio of the static pressure rise of the axial fan while the velocity of the fluid flow decreases because of them. According to Bleier, the shape of the outlet guide vanes is not as critical as the shape of the rotating impeller. It can be assumed that the velocity of the fluid flow, which passes the stationary outlet guide vanes does not change as much as that passes rotating impeller [2]. The outlet configuration of the guide vanes can be seen in Figure 2.9.

Figure 2.9. The Outlet Guide Vane Configuration [21]

The number of the guide vanes can be selected concerning the number of the blades used in the impeller. Since there can be a vibration problem in the blades because of resonance when the number of blades and guide vanes are equal. It can be expressed as [22]

$$frequency_{blades} = Z_{blade}\frac{n}{60} \qquad (2.14)$$

$$frequency_{guide\ vanes} = Z_{guide\ vane}\frac{n}{60} \qquad (2.15)$$

where n is the rotational speed of the impeller, Z_{blade} is the number of blades and $Z_{guide\ vane}$ is the number of guide vanes.

In order to prevent the resonance

$$frequaency_{blades} \neq frequaency_{guide\ vanes} \qquad (2.16)$$

and it means that

$$Z_{blade} \neq Z_{guide\ vane} \qquad (2.17)$$

According to Piolenc et al [23], if the number of guide vanes are selected as even number, resonance problem is prevented.

There are empirical studies about the size and the number of the guide vanes, but there is not an exact formula about the calculation of the number of the guide vanes.

2.3.4. Head and Flow Coefficients

The head and flow coefficients are the dimensionless parameters of the fan field. These parameters can be used to compare a fan to the other fans without comparing their total pressure rises and volumetric flow rates. They provide convenience in the comparison due to being universal parameters and calculating in the same way for all fans.

Head coefficient which is sometimes called as pressure coefficient or work coefficient, can be calculated for incompressible flow as

$$\psi = \frac{\Delta p}{\frac{1}{2}\rho V_a^{\ 2}} \qquad (2.18)$$

Flow coefficient is related about the axial velocity, V_a and the tangential velocity, U. It can be obtained as

$$\emptyset = \frac{V_a}{U} \qquad (2.19)$$
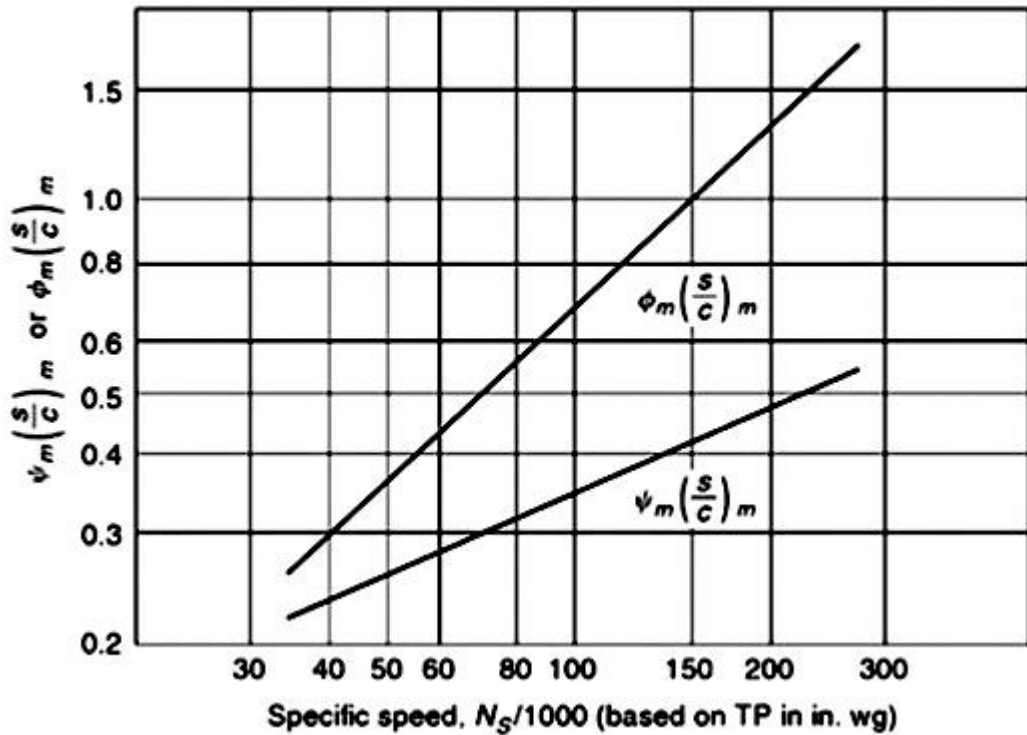
Figure 2.10. Specific Speed vs Flow and Head Coefficients [16]

Figure 2.10 shows the relations between the specific speed versus flow and head coefficients. The chord length of the blade can be calculated by using the flow or head coefficient.

2.3.5. Velocity Diagrams, Flow Angles and Blade Angles

The fluid flow and the blades are examined in a two-dimensional plane in the isolated airfoil and cascade approaches. It was thought that there is no velocity component in the radial direction. It means that there is no third component of the fluid velocity, and therefore, the fluid flow and the blade profiles can be drawn and examined in the two-dimensional plane.

33

There are two assumptions on the fluid flow. The first assumption is that the blockage effect occurred by the projection area of the blades can be ignored. In this way, the axial velocity component of the fluid flow is thought to be constant throughout the fan. The second assumption is that the characteristic of fluid flow can be considered as free-vortex. It provides simplicity in the calculations and gains more efficiency in the fan design. Figure 2.11 can be obtained by using these two assumptions.
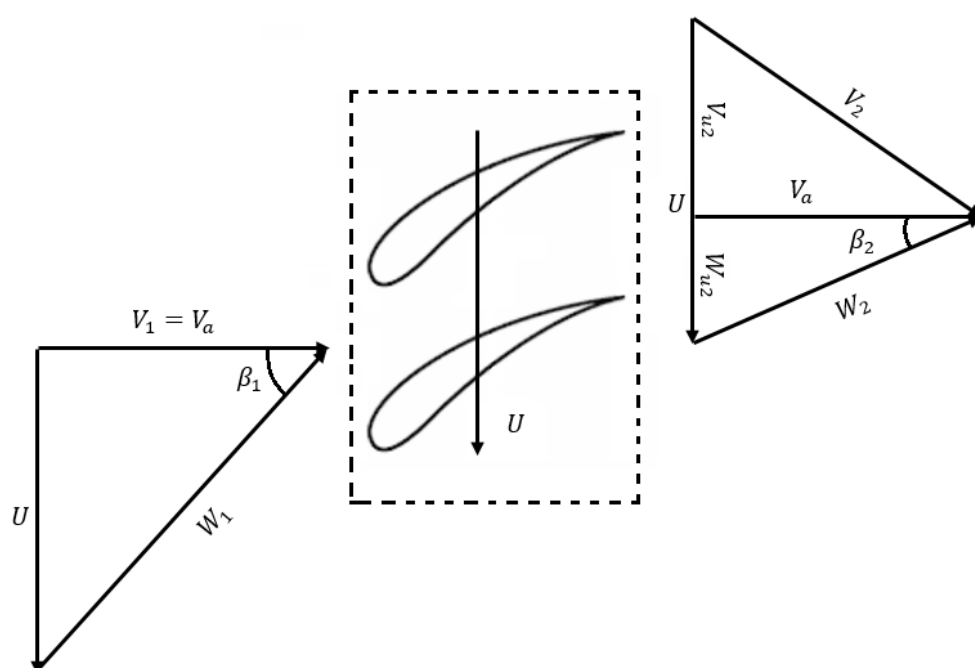
Figure 2.11. Velocity Triangles in Axial Flow Fan

At the velocity diagram in Figure 2.11, the flow angles and the blade angles are shown. It can be seen that the axial velocity, V_a is constant throughout the axial fan.

The fluid angles and bladed angles can be calculated as;

$$\beta_1 = \tan^{-1}\left(\frac{U}{V_a}\right)$$

(2.20)

34

$$\beta_2 = \tan^{-1}\left(\frac{W_{u2}}{V_a}\right) \tag{2.21}$$

$$\beta_m = \tan^{-1}\left(\frac{tan\beta_1 + tan\beta_2}{2}\right) \tag{2.22}$$

where β_1 is inlet flow angle, β_2 is outlet flow angle, β_m is mean flow angle.

Velocity components can be calculated as;

$$V_1 = V_a = \frac{Q}{\frac{\pi(D_t^2 - D_h^2)}{4}} \tag{2.23}$$

$$W_1 = \sqrt{V_a^2 + U^2} \tag{2.24}$$

$$U = \frac{\pi DN}{60} \tag{2.25}$$

$$W_{u2} = U - V_{u2} \tag{2.26}$$

$$V_{u2} = \frac{gH_t}{\eta_h U} \tag{2.27}$$

$$V_2 = \sqrt{V_a^2 + V_{u2}^2} \tag{2.28}$$

$$W_2 = \sqrt{V_a^2 + W_{u2}^2} \tag{2.29}$$

where W_1 is relative inlet flow velocity, W_2 is relative outlet flow velocity, V_1 is absolute inlet flow velocity, V_2 is absolute outlet flow velocity, V_{u2} is tangential

component of absolute outlet flow velocity, W_{u2} is tangential component of relative outlet flow velocity.

Stagger angle of an airfoil in axial flow fan configuration is shown in Figure 2.12.
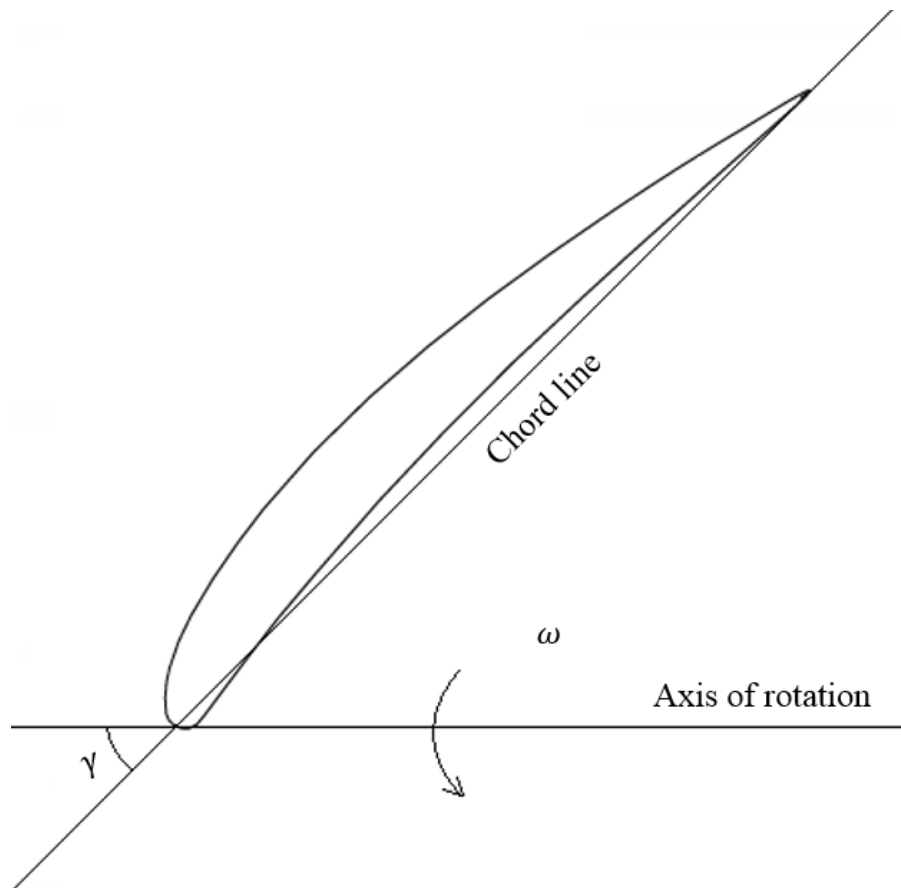
Figure 2.12. Stagger Angle

Stagger angle can be calculated as

$$\gamma = \beta_m - \alpha \tag{2.30}$$

where α is angle of attack of the airfoil.

36

2.3.6. Details in Airfoil Selection

The lift coefficient, C_L is nearly determined during the first iteration of the design process and the designer should select a proper airfoil which satisfies the lift requirement of the fan. The selection is important due to affecting the power consumption of the electric motor, and therefore, the fan efficiency.

It can be said that many airfoils can supply the desired lift coefficient at different angles of attack, α but not all of them can give a good performance. Even their lift coefficients are equal, their drag coefficients are possibly different. In addition, their performances are determined from the ratio of lift and drag coefficients C_L/C_d, and therefore, the designer should control the value of the drag coefficient, C_d of the selected airfoil as much as the lift coefficient.

According to Turner, high lift coefficient can increase the risk of approaching stalling range while low lift coefficient can come up with a result with low efficiency due to low C_L/C_d ratio [24]. In the study, it is suggested that the lift coefficient should be chosen from 0.6 to 0.7 at the tip and should not be exceed 1.0 at the hub. Moreover, solidity should be smaller than 1.1 to get rid of the stalling problem. These suggestions can be showed in brief

$$0.6 < C_L < 0.7 \ at \ the \ tip \tag{2.31}$$

$$C_L \leq 1.0 \ at \ the \ hub \tag{2.32}$$

$$\sigma \leq 1.1 \ \& \ C_L \leq 1.0 \ at \ the \ hub \ for \ no \ stalling \tag{2.33}$$

According to Downie et al. [25], the lift coefficient should not exceed 1.3 at the hub and 0.7 at the tip of the fan. These limits are suggested for the design based on the isolated airfoil approach.

Besides the limits of the values of the lift and drag coefficients at the hub and the tip of the fan, all airfoils have a stall limit. When the angle of attack of the airfoil reaches a point at which the lift coefficient is maximum or when the pressure difference of a fan reaches a value at which stalling range of the fan starts, the fan starts to work unstable.

In the design of the axial flow fan, the designer calculates a lift value for satisfying the application needs. Then, the proper airfoils are selected from the airfoil database according to the Reynolds number of the fluid flow on the fan blade. These selected airfoils are compared with respect to their C_L/C_d ratio and one of them is selected. It should be remembered that higher C_L/C_d ratio means higher efficiency and lower power consumption, and therefore, the type of airfoil used in the design is too important.

In the research of Stefano et al. [9], the most favorable and the most efficient airfoils, which are C4 and NACA-65 airfoils, are examined. C4 type of airfoil shows higher performance than NACA-65 type in his research. Moreover, the most proper type of airfoil for axial fan application is also found as a C4 type of airfoil.

In the code part of the software implementation phase, the calculation of the lift coefficient and the selection of the airfoil are implemented carefully in order not to design a fan works in the stalling range. Moreover, the airfoil which has the highest C_L/C_d ratio is re-selected from the airfoil database for each iteration of the design. The details of them are given in the software implementation part.

2.3.7. Similarity Laws

Similarity laws or sometimes called fan laws are used to estimate the performance curves of a turbomachine work in different conditions. It means that, if the performance of a fan is known for a specific condition, it is possible to calculate its performance or its scaled model for operating at different conditions.

According to Dixon [26], there are two important reasons for using similarity laws. One of them is that the performance curve of a fan can be estimated by using its small-scaled model without spending too much money and time. The other reason is that the most proper type of turbomachine can be specified according to the needs of the application. In addition, the rotational speed can be named as control variable since the rotational speed can be controlled by the supplied voltage of the electric motor. The density will be changed when the working fluid is changed; therefore, density can be named as fluid property, and fan diameter can be called as the geometric variable.

There are four non-dimensional parameters used in the similarity laws. These parameters are called as π terms and they are consisted by the diameter D, the volumetric flow rate Q, the rotational speed of the impeller N, the density of working fluid ρ_f, the dynamic viscosity of the working fluid μ, the power P and the head gH. These π terms can be formulized as

$$\pi_Q = \frac{Q}{ND^3} \tag{2.34}$$

$$\pi_H = \frac{gH}{N^2D^2} \tag{2.35}$$

$$\pi_P = \frac{P}{\rho_f N^2 D^5} \tag{2.36}$$

$$\pi_\mu = \frac{\mu}{\rho_f ND^2} \tag{2.37}$$

If the density of the working fluid and fan diameter is constant

- The volumetric flow rate changes directly with the rotational speed

$$\frac{Q_2}{Q_1} = \frac{N_2}{N_1} \tag{2.38}$$

39

- The pressure difference change with the square of the rotational speed

$$\frac{\Delta p_2}{\Delta p_1} = \left(\frac{N_2}{N_1}\right)^2 \qquad (2.39)$$

- The power consumption changes with the cube of the rotational speed

$$\frac{P_2}{P_1} = \left(\frac{N_2}{N_1}\right)^3 \qquad (2.40)$$

- The noise level changes with the logarithm of the rotational speed [2]

$$dB_2 - dB_1 = 50 \log\left(\frac{N_2}{N_1}\right) \qquad (2.41)$$

- The variation of the efficiencies can be seen in Figure 2.13. It can be said that efficiency curves of the fan for different rotational speeds are similar, but it is shifted left in the volumetric flow rate axis.
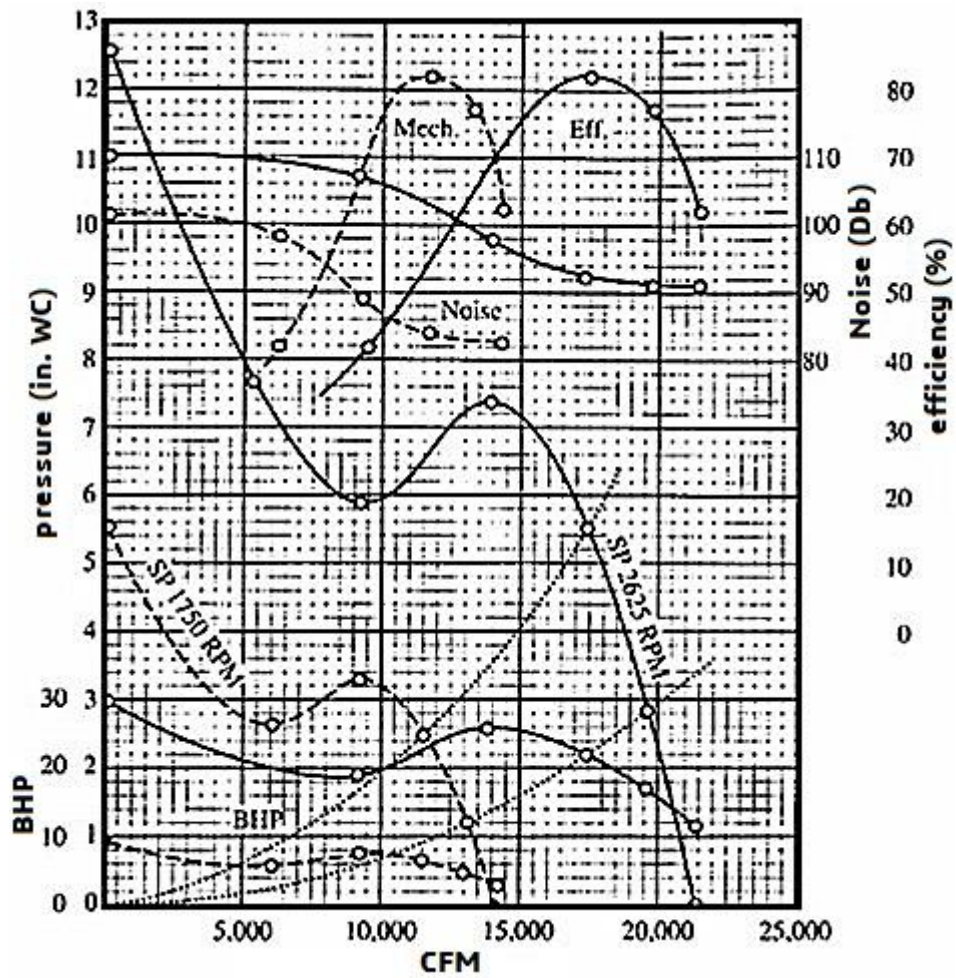
Figure 2.13. Performance Curves at 1750 and 2625 rpm [2]

The density of the working fluid can be changed with the temperature during the application, or the axial fan can be worked with a different working fluid. If the fan diameter and the volumetric flow are constant,

- Pressure difference changes directly with the density

$$\frac{\Delta p_2}{\Delta p_1} = \frac{\rho_2}{\rho_1} \qquad (2.42)$$

41

- The power consumption changes directly with the density

$$\frac{P_2}{P_1} = \frac{\rho_2}{\rho_1}$$

(2.43)

- The noise level and the efficiency remain constant.

The geometric variable is mostly used for its economic advantage. Tests are performed for the small-scaled axial flow fan. After the performance curves are obtained, an actual-scale fan prototype is produced.

If the number of blades, the blade and flow angles, airfoil types, the rotational speeds of both actual and small-scaled fan are the same

- The volumetric flow rate changes with the cube of the diameter

$$\frac{Q_2}{Q_1} = \left(\frac{D_2}{D_1}\right)^3$$

(2.44)

- The pressure difference changes with the square of the diameter

$$\frac{\Delta p_2}{\Delta p_1} = \left(\frac{D_2}{D_1}\right)^2$$

(2.45)

- The power consumption changes with the fifth power of the diameter

$$\frac{P_2}{P_1} = \left(\frac{D_2}{D_1}\right)^5$$

(2.46)

- The noise level changes with the logarithm of the rotational speed [2]

$$dB_2 - dB_1 = 50 \log\left(\frac{D_2}{D_1}\right)$$

(2.47)

- The efficiency remains constant.

2.4. Three-Dimensional Flow Effects

Axial flow fans are under the effects of intense three-dimensional flow. Some of these effects lead to results with a loss in the pressure difference generated by the fan. The details of them are given in the next sections.

One of the effects of three-dimensional flow is about the tangential velocity distribution of the fluid flow on a blade from hub to tip.

2.4.1. Radial Equilibrium Requirement

The tangential velocity distribution of the fluid flow can be controlled by the designer with a selection of the proper airfoil profile from the hub to the tip. In order to do that, the three-dimensional momentum equation for inviscid flow is written in the cylindrical coordinate system as

$$-\frac{1}{\rho}\frac{\partial p}{\partial r} = V_r\frac{\partial V_r}{\partial r} + \frac{V_u}{r}\frac{\partial V_r}{\partial \theta} + V_a\frac{\partial V_r}{\partial z} - \frac{V_u^2}{r} \tag{2.48}$$

It is assumed that there is no radial velocity component of fluid flow in the axial flow fan. Therefore, this equation can be reduced as

$$\frac{1}{\rho}\frac{\partial p}{\partial r} = \frac{V_u^2}{r} \tag{2.49}$$

It can be said from this simplified version of the momentum equation that there is a relation between the pressure term and the centrifugal force term causing from the tangential velocity of the fluid particle. This relation is called as a radial equilibrium requirement of a fluid particle.

The momentum equation with an assumption of no radial velocity component for a fluid particle along a streamline is given as [16]

$$\frac{1}{\rho}\frac{\partial p}{\partial r} + V_u\frac{dV_u}{dr} + V_a\frac{dV_a}{dr} = 0 \tag{2.50}$$

Equation 2.49 is integrated into Equation 2.50

$$\left(\frac{V_u}{r}\right)\frac{d(V_u r)}{dr} + V_a\frac{dV_a}{dr} = 0 \qquad (2.51)$$

Bruneau indicates that there are two types of tangential velocity distributions can satisfy Equation 2.51 [27]. These are free-vortex and non-free vortex flow.

2.4.1.1. Free-Vortex Flow

The general power law of fluid flow is given as

$$V_u r^n = constant \qquad (2.52)$$

For free-vortex flow assumption, it is accepted that $n = 1$ and $V_u r = constant$. This assumption provides an easiness in the calculations and it is the commonly used assumption in the impeller design of the axial flow fan. In addition, axial velocity component of the fluid flow is constant throughout the fan from hub to tip since dV_a term in Equation 2.51 should be equal to zero.

2.4.1.2. Non-Free Vortex Flow

The other tangential velocity distribution is called as non-free vortex flow. Even the purpose of using non-free vortex flows is to get rid of the design problems caused by the free-vortex assumption; it is not preferred due to complexities and severe control abilities. There are three non-free vortex flow types.

2.4.1.2.1. The Constant Flow Angle Design

This assumption is similar to the free-vortex assumption, and it can be formulized with using $n = -1$ as

$$V_u/r = constant \qquad (2.53)$$

There is a swirl problem of this design due to the similarity with the free-vortex flow design. Untwisted blades and guide vanes are used in the constant flow angle design. It means that the production process is not too tricky compared with the free-vortex flow design.

2.4.1.2.2. The Super-Vortex Design

There is also a swirl problem in the super vortex design. The flow deflection angle arising from the blade twist is higher than the free-vortex flow design. Moreover, Bruneau indicates that the exit velocity variation cannot be controlled for the fans have a hub-tip ratio greater than 0.6 [27]. It can be formulized with $n = 2$ as

$$V_u r^2 = constant \qquad (2.54)$$

2.4.1.2.3. The Constant Swirl and Forced-Vortex Design

The swirl problem is fixed slightly in the constant swirl and forced-vortex design. However, the exit velocity variation cannot be controlled for the fans which have a hub-tip ratio higher than 0.2. It can be formulized with $n = 0$ as

$$V_u = constant \qquad (2.55)$$

2.4.2. Losses in the Axial Flow Fans

As mentioned previously, some of the three-dimensional flow effects are results with a loss in the generated pressure difference of the fan. The details and explanations of them are given in followings.

2.4.2.1. Duct Losses

According to Wallis [28], the duct losses are composed of the combination of some losses, and they affect the total pressure difference in the fluid flow. These losses can be listed as

- Skin Friction
- Flow Separation
- Secondary Flow
- Discharge Loss

2.4.2.1.1. Skin Friction

The surface roughness of the components of the axial flow fan leads to occur a skin friction loss. The flow resistance and the fluid shear increase on the components which contact with the working fluid directly, and therefore, it results with a loss. These components of the axial flow fan are rotor, stator, inside wall of housing, guide vanes and blades.

2.4.2.1.2. Flow Separation

Fluid flow applied on a blade can separate when the angle of attack reaches its critical value. In some cases, even the angle of attack is constant; fluid flow can be separated due to the changing of the blade angles. In addition, flow over the flat plate can be separated at the location of sudden enlargements or discontinuities. All of these separations end up with a pressure loss.

2.4.2.1.3. Secondary Flow

In the flow passes over the fan blades, there sometimes occurs a secondary flow which is in normal direction to the fluid flow. It occurs when the flow capacity of the fluid is smaller than its design value. It means a design mistake, and it leads to occur secondary flow.

2.4.2.1.4. Discharge Loss

Some of the kinetic energy of the fluid flow dissipates, and air leaves from the fan with a loss. It is named as discharge loss, and dissipated energy turns to heat in the application.

2.4.2.2. Tip Clearance Leakage Loss

The pressure difference between the upper and bottom sides of the blades calls forth a leakage of the fluid flow when it faces with a gap or short-cut. Unfortunately, there is a permanent gap between the tip of the impeller and the inner wall of the fan housing. It means that some portion of the fluid flow leak from that gap continuously. Thus, there is a permanent loss caused by the tip clearance in the design.

These duct losses can be formulized as a component of the drag coefficient as [16]

$$C_{dt} = 0.29 \left(\frac{c_t}{b}\right) C_L^{\frac{3}{2}} \tag{2.56}$$

$$C_{da} = 0.02 \left(\frac{s}{b}\right) \tag{2.57}$$

$$C_{da} = 0.018 C_L^2 \tag{2.58}$$

where c_t is the tip clearance, b is the span length of the blade, s is the pitch distance, C_{dt} is the tip leakage loss coefficient, C_{da} is the annulus skin friction loss coefficient and C_{ds} is the secondary flow loss coefficient.

2.4.3. Tip Clearance Effects

As explained in the previous section, tip clearance is the permanent gap between the blade tip and the inner wall of the cylindrical housing. It can be seen in Figure 2.14.

Figure 2.14. Sample Tip Clearance of an Axial Flow Fan [29]

The tip clearance is one of the main parameters which affects the fan efficiency directly. The primary purpose of the designer about the tip clearance is to obtain the smallest clearance as possible. Even the changes in the tip clearance are small, the outputs on the fan performance cannot be tolerated. The study about the effects of small changes in the tip clearance on the mechanical efficiency and the noise level is presented in Table *2.1*.

Table 2.1. *Tip Clearance Effect on Mechanical Efficiency and Noise Level* [2]

Tip Clearance	Mechanical Efficiency	Noise level
1/16 in	82%	73.5 dB
5/16 in	72%	-
13/16 in	60%	76 dB
1 in	58%	-

As seen in Table *2.1*, small increments in the tip clearance lead to decrease the mechanical efficiency considerably and increase the noise level.

The length of the tip clearance also affects the volumetric flow rate, the pressure difference and the power consumption. They are reduced when the used tip clearance is increased. The effect on the pressure difference is given in Figure 2.15.

AXIAL FLOW FAN PERFORMANCE
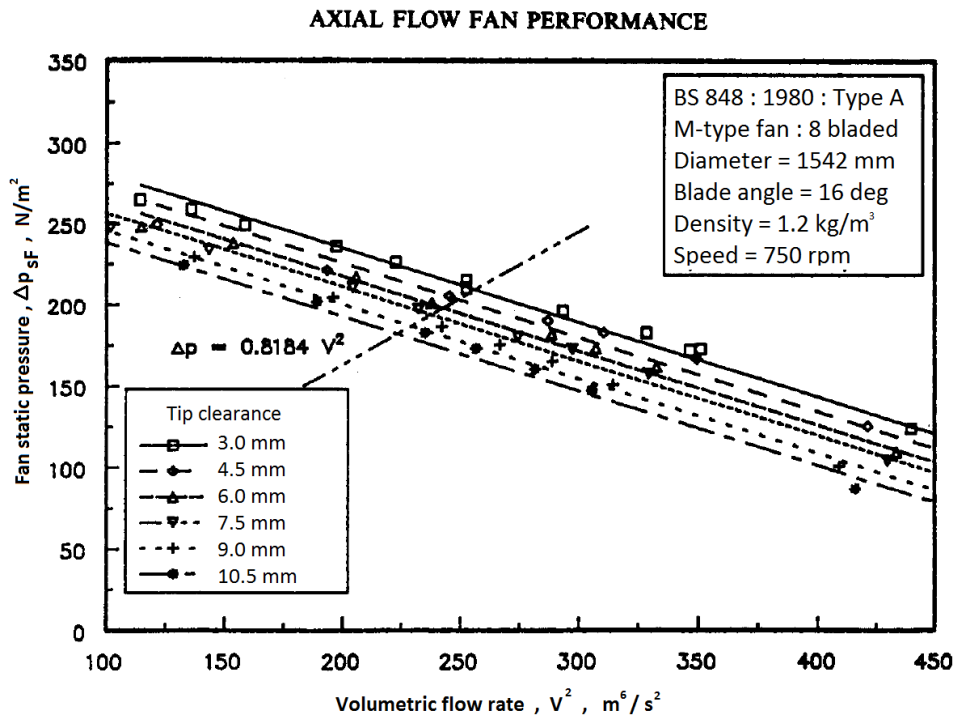
Figure 2.15. Tip Clearance Effect on Pressure Difference [13]

Eck also studies the tip clearance effect on the maximum efficiency of an axial flow fan. It is stated that the maximum efficiency obtained with nearly zero tip clearance is 90%. The results of the study show that a 1% increment in the tip clearance leads to a 2% reduction in efficiency. The results are shown in Table *2.2*.

Table 2.2. *Tip Clearance Effect on the Efficiency of an Axial Flow Fan* [30]

Clearance %	*1*	*2*	*3*	*4*	*5*
η_{max} %	88	86	84	82	80

2.5. Sample Design

All of the components in the axial flow fan affect each other directly or indirectly. It means that the values or the ratios of them take into account as an input to calculate the parameters in the next step and it results with a complexity in the design, and therefore, a sample design of an axial flow fan is presented in this part to emphasize the design procedure and the relations between the design steps.

The first step in the axial flow fan design is determining the input parameters, which are the volumetric flow rate, the total pressure rise and the rotational speed of the impeller. These parameters are called as desired parameters of the fan.

As an example, the input parameters are selected as $Q = 0.26 \, m^3/s$, $\Delta p = 155 \, Pa$, $N = 5000 \, rpm \rightarrow \omega = 523.6 \, s^{-1}$.

- Calculation of the fan diameter

Specific speed can be calculated as

$$\omega_s = \frac{\omega\sqrt{Q}}{(gH)^{0.75}} = \frac{\omega\sqrt{Q}}{(\Delta p/\rho_{air})^{0.75}} = 6.897 \tag{2.59}$$

Specific diameter can be read from the Cordier diagram in Figure 2.6 using nondimensional specific speed ω_s as

$$\Delta_s \approx 1.2 \tag{2.60}$$

Fan diameter can be calculated by using specific diameter such that

$$\Delta_s = \frac{D_{fan}(gH)^{0.25}}{\sqrt{Q}} \rightarrow D_{fan} = \frac{\Delta_s\sqrt{Q}}{(gH)^{0.25}} \rightarrow D_{fan} = 167 \ mm \tag{2.61}$$

- Calculation of the hub diameter

Specific speed (in.wg) can be calculated as

$$N_s = \frac{N\sqrt{Q}}{\left(\frac{\Delta p}{\rho_{water}g}\right)^{0.75}} = 1.67 \times 10^5 \tag{2.62}$$

From Figure 2.8, hub-tip ratio is selected as $\nu = 0.3$

Hub diameter can be obtained as;

$$\nu = \frac{D_{hub}}{D_{fan}} \rightarrow D_{hub} = \nu D_{fan} \rightarrow D_{hub} = 51 \ mm \tag{2.63}$$

- Calculation of the number of blades Z_b and span length b

$$Z_b = \frac{6\nu}{(1-\nu)} \rightarrow Z_b = 3 \tag{2.64}$$

$$b = \frac{D_{fan} - D_{hub}}{2} \rightarrow b = 58 \ mm \tag{2.65}$$

- Calculation of the axial velocity;

The flow area of the axial flow fan can be obtained using D_{fan} and D_{hub}

$$A_{flow} = \frac{\pi \left(D_{fan}^2 - D_{hub}^2 \right)}{4} \rightarrow A_{flow} = 0.02\ m^2 \tag{2.66}$$

The axial velocity can be calculated as

$$V_a = \frac{Q}{A_{flow}} \rightarrow V_a = 13\ m/s \tag{2.67}$$

Up to this point, some general parameters which determine the outer shape of the fan are calculated. From this point, the detailed calculations, flow angles, blade angles, and efficiency are presented.

In order to increase resolution of the design and obtain a better impeller, blades are sliced into equal parts along the span length. A sample sliced fan blade can be seen in Figure 2.16.
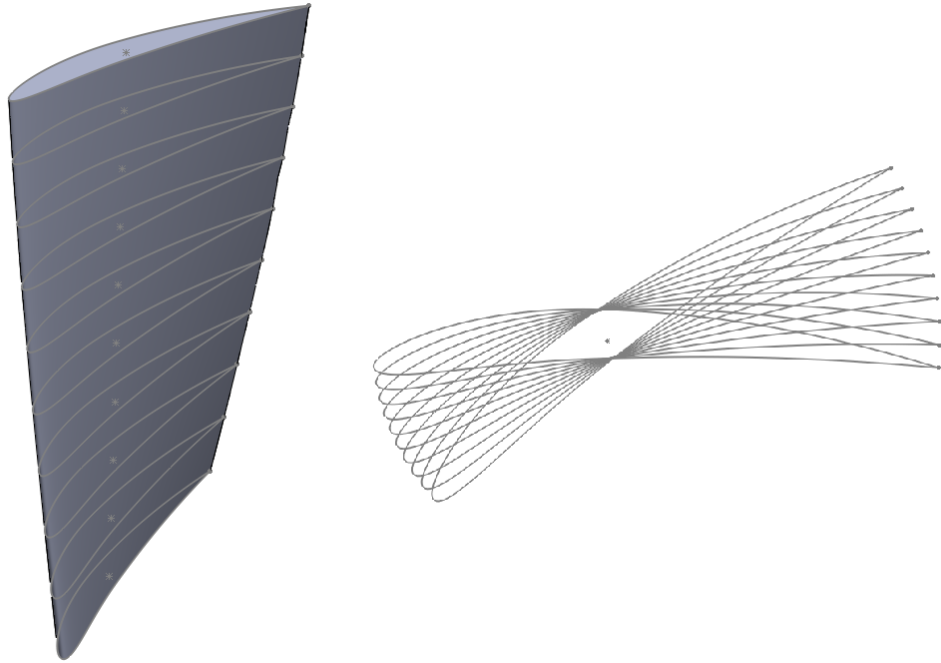
Figure 2.16. Sliced Fan Blade

The span length is divided into five slice points. The next calculations are performed for the diametral points of D_1, D_2, D_3, D_4, D_5. All of the parameters are given in a table at the end of this part but a calculation step for the mean diameter of $D_3 = 110 \ mm$ is presented.

- The tangential velocity is calculated as

$$U_3 = \frac{\omega D_3}{2} \rightarrow U_3 = 28.7 \ m/s \tag{2.68}$$

- The flow coefficient

$$\emptyset_3 = \frac{V_a}{U_3} \rightarrow \emptyset_3 = 0.45 \tag{2.69}$$

- Calculation of the chord length and the blade solidity

From Figure 2.10, $\emptyset\left(\frac{s}{c}\right)$ can be read as

$$\emptyset_3\left(\frac{s_3}{c_3}\right) \approx 1.1 \tag{2.70}$$

The pitch distance and the chord length are calculated respectively

$$s_3 = \frac{\pi D_3}{Z_b} \rightarrow s_3 = 115 \ mm \tag{2.71}$$

$$\emptyset_3\left(\frac{s_3}{c_3}\right) = 1.1 \rightarrow c_3 = 47 \ mm \tag{2.72}$$

The blade solidity can be found as

$$\sigma_3 = \frac{c_3}{s_3} \rightarrow \sigma_3 = 0.41 \tag{2.73}$$

At this point, the iteration process of the design starts. There should be an assumption about the hydraulic efficiency as an initial value for starting the iteration.

The hydraulic efficiency is assumed as $\eta_{h_3} = 0.95$

- Calculation of inlet, outlet and mean flow angles

$$\beta_{1_3} = \tan^{-1}\left(\frac{U_3}{V_a}\right) \rightarrow \beta_{1_3} = 65.4 \ deg \tag{2.74}$$

$$\beta_{2_3} = \tan^{-1}\left(\frac{U_3 - V_{u2_3}}{V_a}\right) \rightarrow \beta_{2_3} = 57.6 \ deg \tag{2.75}$$

$$\beta_{m_3} = \tan^{-1}\left(\frac{\tan\beta_{1_3} + \tan\beta_{2_3}}{2}\right) \rightarrow \beta_{m_3} = 62\ deg \tag{2.76}$$

- Calculation of flow velocities

The inlet, outlet and mean flow velocities can be found, respectively

$$W_{1_3} = V_a/\cos(\beta_{1_3}) \rightarrow W_{1_3} = 31.4\ m/s \tag{2.77}$$

$$W_{2_3} = \sqrt{V_a^2 + (U_3 - V_{u2_3})^2} \rightarrow W_{2_3} = 24.4\ m/s \tag{2.78}$$

$$W_{m_3} = V_a/\cos(\beta_{m_3}) \rightarrow W_{m_3} = 27.7\ m/s \tag{2.79}$$

The locations of these calculated flow angles and flow velocities can be seen in Figure 2.11.

- Calculation of the Reynolds number on a blade

$$Re_3 = \frac{W_{m_3}c_3}{\nu_{air}} \rightarrow Re_3 = 86155 \tag{2.80}$$

Flow is found as turbulent because its value is higher than critical Reynolds number of 2300 [31].

- Calculation of the lift coefficient [16]

$$C_{L_3} = 2\left(\frac{s_3}{c_3}\right)(\tan\beta_{1_3} - \tan\beta_{2_3})\cos(\beta_{m_3}) \rightarrow C_{L_3} = 1.39 \tag{2.81}$$

At this point, there is a critical selection regarding the blade design approach. According to the blade solidity, the isolated airfoil approach is logical.

Then, the type of the airfoil can be determined with respect to the calculated lift coefficient or called required lift coefficient of the fan. Even it can be supplied by

many types of airfoils, the airfoil whose C_L/C_d is highest should be selected with considering its stall point.

NACA6409 type of airfoil is selected due to supplying the required lift coefficient and having a high C_L/C_d ratio

The specifications of NACA6409

- $Re_3 \approx 100000$
- $C_{L_3}/C_{d_3} \approx 57$
- Angle of attack $\alpha_3 = 7.4$
- $C_{d_3} = 0.024$
- Calculation of stagger angle

$$\gamma_3 = \beta_{m_3} - \alpha_3 \rightarrow \gamma_3 = 54.6 \; deg \tag{2.82}$$

- Calculation of final efficiency in the first iteration

Reaction ratio

$$R_{r_3} = \emptyset_3 \times \tan(\beta_{m_3}) \rightarrow R_{r_3} = 0.84 \tag{2.83}$$

Ratio of drag and lift coefficients

$$\delta_{r_3} = \frac{C_{d_3}}{C_{L_3}} \rightarrow \delta_{r_3} = 0.0175 \tag{2.84}$$

Then, hydraulic efficiency [16]

$$\eta_{h_3} = \emptyset_3 \left[\frac{R_{r_3} - \emptyset_3 \delta_{r_3}}{\emptyset_3 + R_{r_3} \delta_{r_3}} + \frac{1 - R_{r_3} - \emptyset_3 \delta_{r_3}}{\emptyset_3 + \delta_{r_3}(1 - R_{r_3})} \right] \rightarrow \eta_{h_3} = 0.96 \tag{2.85}$$

The final hydraulic efficiency is found as $\eta_{h_3} = 96$. It can be said that the value of the final hydraulic efficiency is close with its initial value, and therefore, iteration can be stopped.

The values of all design steps are given in the Table *2.3*.

Table 2.3. *Calculated Parameters of Sample Axial Flow Fan Design*

	D_1	D_2	D_3	D_4	D_5
Diameter (mm)	51	80	110	138	167
Inlet Flow Angle (deg)	45.6	58	65.4	70	73.4
Outlet Flow Angle (deg)	17.8	37.9	57.6	66.4	71.3
Mean Flow Angle (deg)	33.84	50	62	68.4	72.4
Axial Velocity (m/s)	13	13	13	13	13
Relative Inlet Velocity (m/s)	18.7	24.7	31.4	38.4	45.6
Relative Outlet Velocity (m/s)	13.7	16.6	24.4	32.7	40.7
Relative Mean Velocity (m/s)	15.7	20.3	27.7	35.5	43.2
Tangential Velocity (m/s)	13.3	20.9	28.7	36.1	43.7
Airfoil Type	NACA4412	S1210	NACA6904	NACA6904	S1223RTL
Chord Length (mm)	47	47	47	47	47
Angle of Attack (deg)	9.8	8.6	7.4	3.8	-1.48
Stagger Angle (deg)	24	41.3	54.6	64.6	73.8

CHAPTER 3

SOFTWARE IMPLEMENTATION

3.1. Introduction

The design steps of the axial flow fan are explained in the sample design part of the previous chapter. It can be seen that there are many calculations and long iteration process. Moreover, in the blade design part, the blade is divided into several parts along the span length, and all of these computations are re-calculated for all diametral locations.

Generally, in the industry, the designs are performed with respect to the mean diameter of the fan. It means that one blade profile is used for all of the blade sections at the end of the design. It can bring about an efficiency drop in the performance, and the design specifications will not be achieved accurately.

This work aims to generate an airfoil database in which all of the necessary information about airfoils is contained and to connect this database with the computation process of the fan design using an algorithm. In this way, the user can divide the blade into small parts easily, and the software will give the proper airfoils suggestion for all diametral slice points.

3.2. Database Generation

There are many types of airfoils, but some of them cannot be used in the axial flow fan design due to some reasons. For example, an airfoil has a thin section should not be used near the hub of the impeller because it can break at that section due to the rotational force arising from high revolutions. Therefore, the logical preference is to use a thick airfoil at the hub section. In this work, to ensure that the implemented

software can give reasonable suggestions at the results screen, the airfoils in the literature are selected carefully to use in the database.

There are about 35 airfoils in the database. The list of them is given in Appendix A. The lift, drag, angle of attacks and Reynolds Number information of all the airfoils are embedded in it by using MATLAB. Some of them can be seen in Figure 3.1.

Airfoil_Type	Reynolds_Number	Ncrit	Alpha	CL	CD
'EPPLER 1211'	50000	9	1x90 double	1x90 double	1x90 double
'EPPLER 1211'	50000	5	1x84 double	1x84 double	1x84 double
'EPPLER 1211'	100000	9	1x81 double	1x81 double	1x81 double
'EPPLER 1211'	100000	5	1x100 double	1x100 double	1x100 double
'EPPLER 1211'	200000	9	1x133 double	1x133 double	1x133 double
'EPPLER 1211'	200000	5	1x130 double	1x130 double	1x130 double
'EPPLER 1211'	500000	9	1x141 double	1x141 double	1x141 double
'EPPLER 1211'	500000	5	1x134 double	1x134 double	1x134 double
'EPPLER 1211'	1000000	9	1x139 double	1x139 double	1x139 double
'EPPLER 1211'	1000000	5	1x135 double	1x135 double	1x135 double
'MH 112'	50000	9	1x70 double	1x70 double	1x70 double
'MH 112'	50000	5	1x86 double	1x86 double	1x86 double
'MH 112'	100000	9	1x104 double	1x104 double	1x104 double
'MH 112'	100000	5	1x104 double	1x104 double	1x104 double
'MH 112'	200000	9	1x116 double	1x116 double	1x116 double
'MH 112'	200000	5	1x118 double	1x118 double	1x118 double
'MH 112'	500000	9	1x121 double	1x121 double	1x121 double
'MH 112'	500000	5	1x121 double	1x121 double	1x121 double
'MH 112'	1000000	9	1x120 double	1x120 double	1x120 double
'MH 112'	1000000	5	1x125 double	1x125 double	1x125 double
'CYR 24'	50000	9	1x75 double	1x75 double	1x75 double
'CYR 24'	50000	5	1x88 double	1x88 double	1x88 double
'CYR 24'	100000	9	1x101 double	1x101 double	1x101 double
'CYR 24'	100000	5	1x112 double	1x112 double	1x112 double
'CYR 24'	200000	9	1x115 double	1x115 double	1x115 double
'CYR 24'	200000	5	1x116 double	1x116 double	1x116 double
'CYR 24'	500000	9	1x120 double	1x120 double	1x120 double
'CYR 24'	500000	5	1x115 double	1x115 double	1x115 double
'CYR 24'	1000000	9	1x129 double	1x129 double	1x129 double
'CYR 24'	1000000	5	1x134 double	1x134 double	1x134 double

Figure 3.1. Airfoil Database

60

3.3. Software Implementation

The calculations and the iterations in the design process are coded by using MATLAB. At the beginning of the coding process, the code cooperates with a few airfoils; therefore, the iteration process could not complete with reasonable accuracy. It is found that the lift coefficient of available airfoils could not meet the lift requirement of some designs involve a high volumetric flow rate. This problem is solved by adding numerous airfoils in the database.

After the adjustments in the database, user interface part of the code is improved. Typically, the design starts with the determination of the input parameters, which are the expected performance parameters from the fan. Therefore, the user starts with the input parameters by filling them in the blanks. The picture of the user interface is given in Figure 3.2.
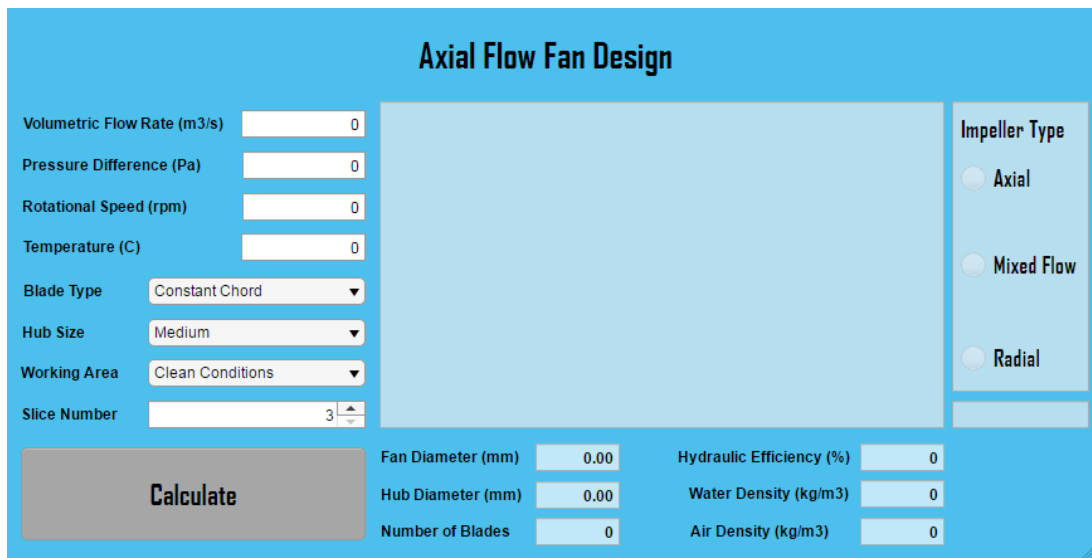
Figure 3.2. User Interface of Axial Flow Fan Design Software

It can be seen in Figure 3.2, the volumetric flow rate, the total pressure difference, the rotational speed of the motor and the working temperature are the input parameters of

the software. Then, the user can customize the blade and the hub size of the fan. After that, the working conditions of the fan are selected. It is explained that the code can divide the blade from hub to tip. According to the number of selected diametral slice points, the code gives the proper airfoils up to the selected value. Finally, the user presses the "Calculate" button, and the design software calculates these output parameters:

- Fan Diameter
- Hub Diameter
- Number of Blades
- Diameter of Slice Point and Corresponding Airfoil Type
- Stagger Angle
- Chord Length
- Hydraulic Efficiency
- Impeller Type

Sample design in Chapter 2 is re-performed by using the design software, and it can be seen in Figure 3.3.
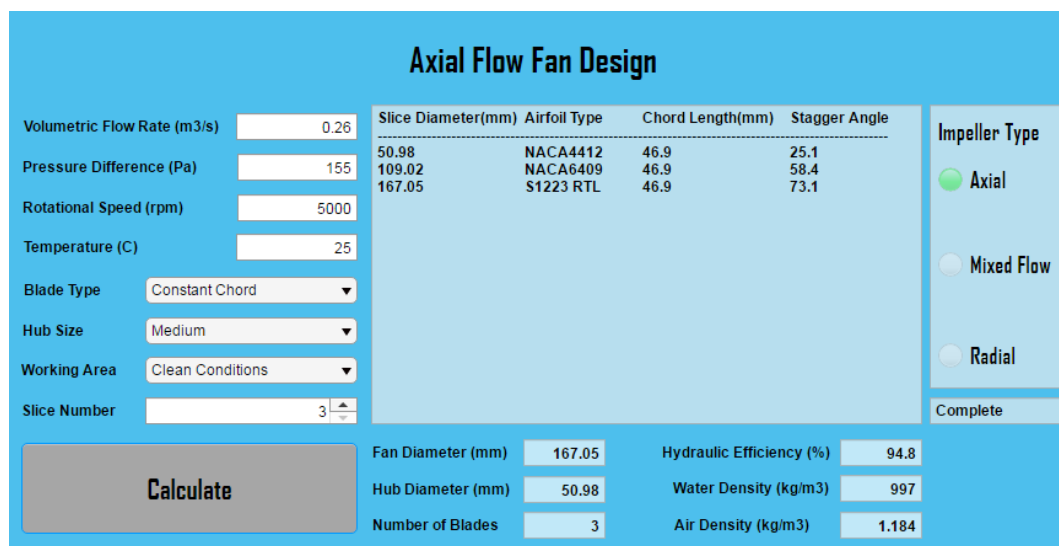
Figure 3.3. Sample Axial Flow Fan Design

It can be seen in Figure 3.3; the software suggests different airfoil types for all diametral slice points. It means that the blade can be constructed by using different airfoil profiles from hub to tip. In industry, because of the limited allocated time to the design, the blade profile, which is selected according to the mean diameter, is used for the whole of the blade sections. However, the lift coefficient requirements of the diametral locations are not the same. Therefore, using one blade profile for the whole sections is not an efficient way of design.

The good thing in the usage of this implemented software is that it suggests a proper airfoil for each diametral location. In addition, the diametral slice points can be increased. It can affect the resolution of the design directly. The user can cut into numerous slices to the designed fan blade, and the software recalculates all of the design steps for each diametral location. Then, the best airfoil for related diametral point is determined from among all profiles in the database.

3.3.1. Airfoil Selection

In the design of the axial fans, there is an iteration process. In the first iteration, a required lift coefficient is calculated according to the desired volumetric flow rate. Then, a literature search is performed to find a proper airfoil which can meet the lift requirement. After the determination of the airfoil profile, the other data of the airfoil, which is the drag coefficient and the angle of attack are used as inputs into the iteration process. At the end of the first iteration, the initial and the final hydraulic efficiencies are compared. If the difference is higher than the selected threshold value, the second iteration is performed.

The calculated lift coefficient changes during the iterations. It means that the required lift coefficient may not remain the same during the iteration process, and the determined airfoil profile may not be used in the next iterations. Therefore, the process of airfoil selection is repeated. If the threshold value of the iterations is selected small, too many iterations are required. In addition, these iterations are performed only for

one diametral slice point. As a result, designing a detailed axial flow fan with hand calculations turns to be a painful process for a designer.

In this work, to get rid of this painful process and to obtain a reliable axial flow fan, all of these calculations, iterations and airfoil selections are turned a software with user-interface. All of them are computed in seconds. In addition, the errors likely to stem from hand calculation are eliminated.

Besides the time wasting and the calculation errors, selection of the airfoil is also an essential subject in the fan design because it directly affects the efficiency of the fan. Therefore, a methodology of airfoil selection should be generated. In this work, when the code comes to the point at which the lift coefficient is calculated, the entire airfoil database is scanned to determine the airfoils which satisfy the required lift coefficient. Then, the lift to drag ratios of these airfoils are compared. The generated methodology is selecting the airfoil has the highest lift to drag ratio. Thus, the most proper and most efficient airfoil can be identified.
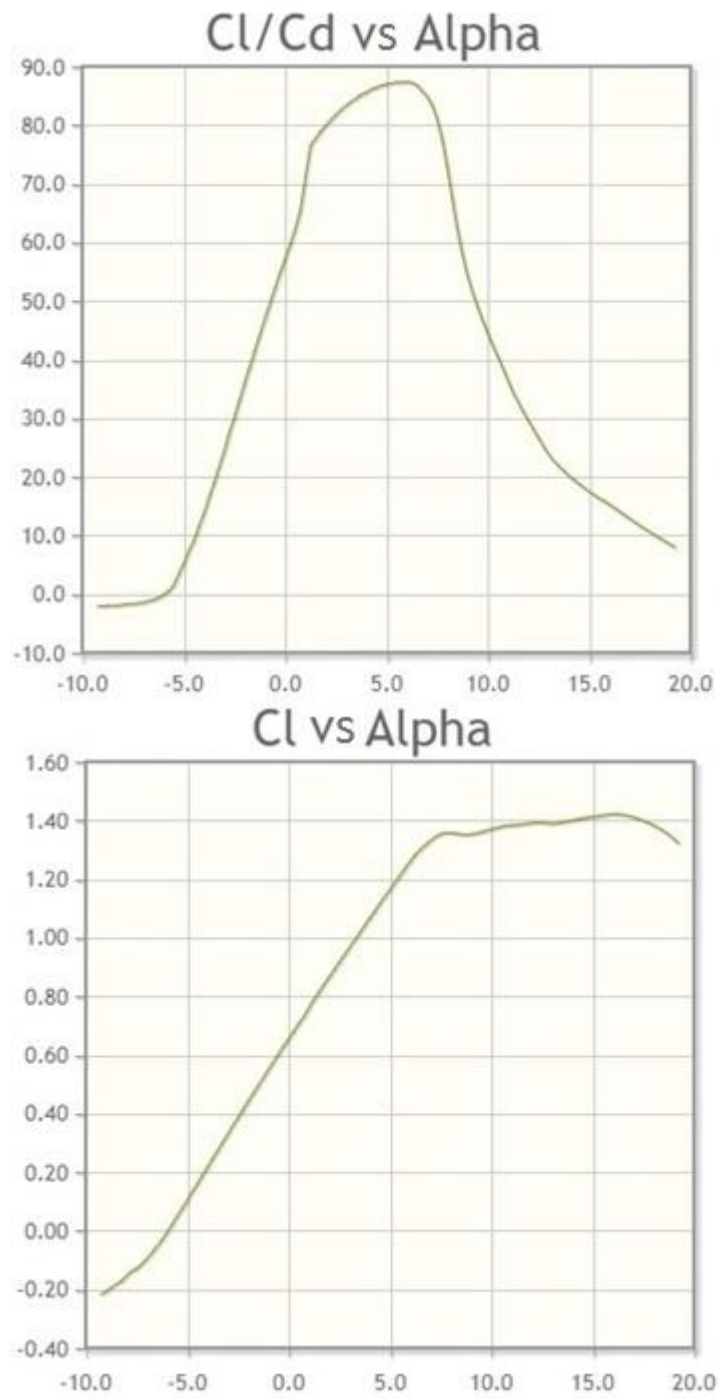
Figure 3.4. Lift and Drag Coefficients of NACA6409 [32]

Comparing the airfoils about their lift to drag ratios and selecting the airfoil has the highest ratio can be risky in some circumstances. It can be seen in Figure 3.4; an airfoil may give the highest lift over drag ratio at around its stall point. Working with this type of airfoils may create an unstable operation. Therefore, the selected airfoil is checked whether it works at its stall point or not.

3.3.2. Flow Chart of the Code

The code is composed of four different parts. In the first part, the outer dimensions of the fan are calculated. These are the fan diameter, the hub diameter and the number of blades. The second part is about the number of diametral slice points. According to the input value of the user, the blade is divided into small parts, and the corresponding diameter of these parts are calculated to use in the next calculations. In the third part, the iteration process is performed. There are three error checks in the code. Iterations are continued until all of the errors are smaller than the determined threshold value. The calculations in the third part are recomputed with respect to the number of diametral slice points. In this way, the software can suggest proper airfoils as the user wants. In the final part, the results are prepared and printed on the output screen of the software.

The flow chart of the code can be seen in Figure 3.5.
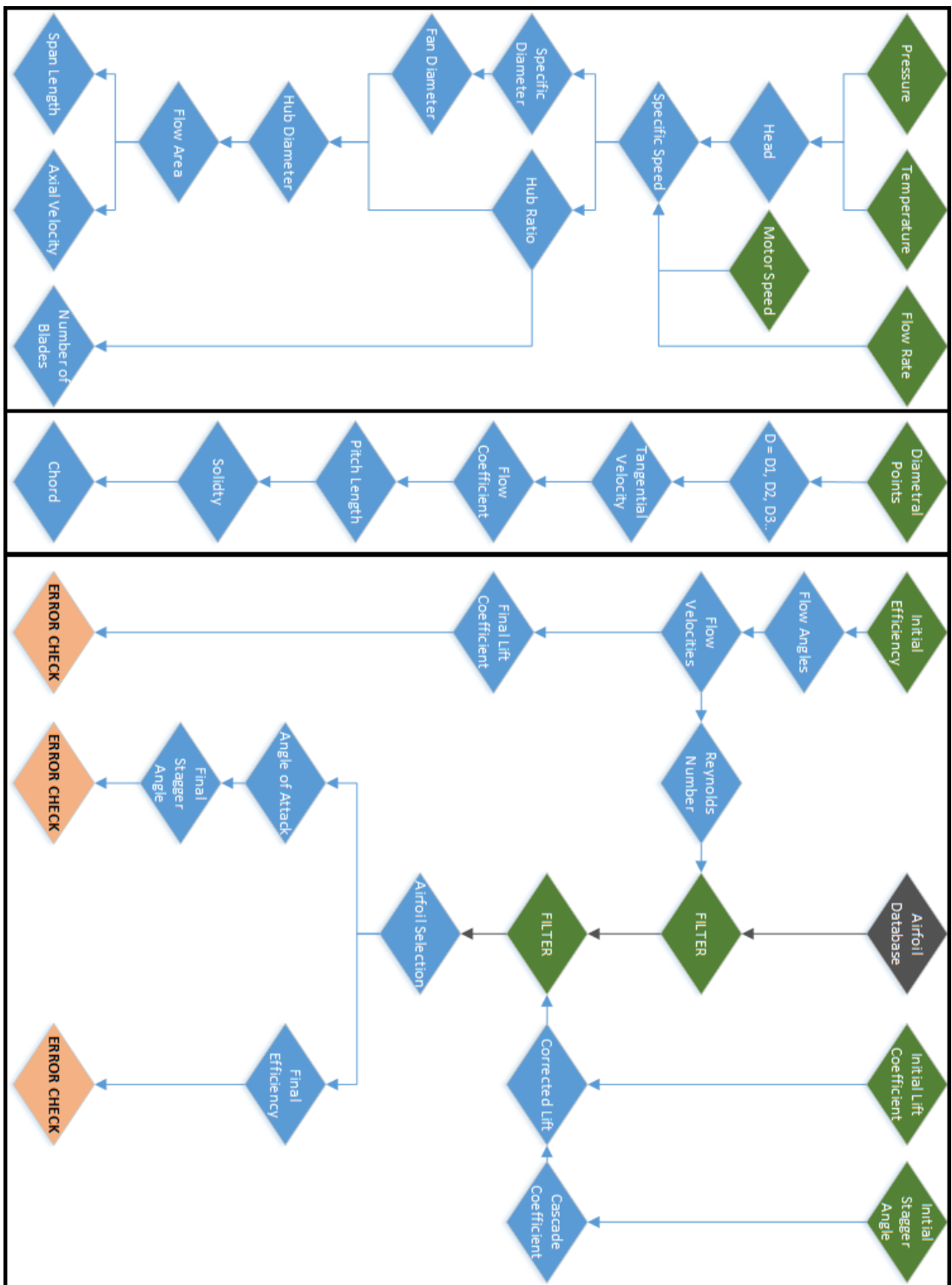
Figure 3.5. Flow Chart of the Code

3.4. An Axial Flow Fan Design by using Design Software

An axial flow fan is designed by using the design software, and therefore, the accuracy of the implemented software can be validated. The input parameters of the fan are determined, and they are filled in the blanks on the user-interface.

These input parameters are

- Volumetric Flow Rate = 50 m^3/s
- Pressure Difference = 1250 Pa
- Rotational Speed of the AC Motor = 1500 rpm
- Working Temperature = 25 Celsius

The generated design parameters of the implemented software are given in Figure 3.6.
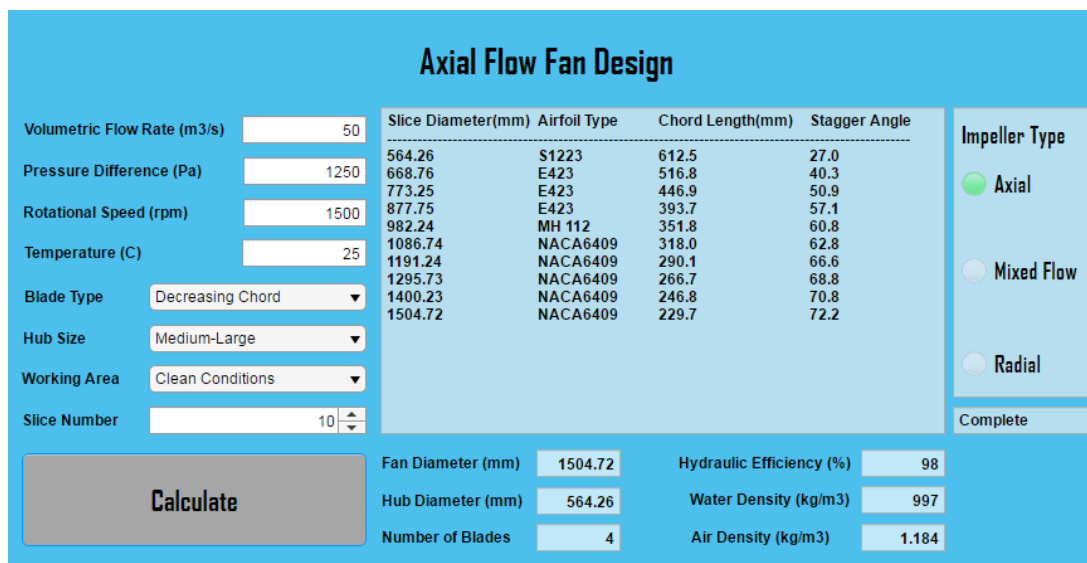
Figure 3.6. Generated Design Parameters

It can be seen in Figure 3.6; the blade is divided into ten sections along span length. Four different types of airfoils are suggested to use at those sections. The fan diameter is calculated as 1504 mm, and the hub diameter is calculated as 564 mm. The impeller

of the fan is composed of four blades. In addition, in order to draw the 3D model of the fan, chord lengths and stagger angles are given.

In the next chapters, the accuracy of the design software is determined by the help of the numerical and the experimental methods.

CHAPTER 4

CFD ANALYSES OF THE AXIAL FLOW FAN

4.1. Introduction

A Computational Fluid Dynamics (CFD) methods can be used to observe the aerodynamic characteristics of the fluid flows in the designed system. Most of the time, engineers choose to validate their design with the help of CFD methods instead of preparing experimental setups. Also, it can be used to prevent design errors before the manufacturing process starts. Therefore, the period of time allocated for the design process decreases. Moreover, the details of the fluid flow such as streamlines, velocity distributions, pressure distributions, temperature distributions can be observed by using post-processing tools of the CFD software.

In this study, the CFD analyses of the fan are performed by using commercial CFD software, CFX. In the analyses, the simplified 3D geometry of the fan is used, and then, the mesh model is created. After the setting-up of the boundary conditions and turbulence model, analyses are run for different outlet pressures.

The performance curves of the fan can be plotted by using the results of the analyses. Then, the performance parameters expected from the fan are compared with the plotted performance graph, and the accuracy of the implemented software will be interpreted.

4.2. General Information on Computational Fluid Dynamics

Computational Fluid Dynamics (CFD) provides well-rounded modeling capabilities for vast range fluid flow problems. Parameters of fluid flows on complex geometries are calculated with the help of a comprehensive range of mathematical models provided by CFD tools and programs.

71

In the mathematical model, there are differential equations that define the fluid flow. They are chosen by the CFD software according to the properties of the flow. For example, the compressibility range and viscosity of the working fluid determine the characteristics of the differential equations, which can simplify the mathematical model.

4.2.1. Differential Equations Using in the CFD Calculations

4.2.1.1. The Conservation Equations

The conservation equations are the main equations in the mathematical model. These are the mass conservation equation (the continuity equation) and the momentum conservation equation (Navier-Stokes equation).

The mass conservation equation can be written as

$$\frac{\partial \rho}{\partial t} + \frac{\partial (\rho u_i)}{\partial x_i} = \frac{\partial \rho}{\partial t} + \frac{\partial (\rho u_x)}{\partial x} + \frac{\partial (\rho u_y)}{\partial y} + \frac{\partial (\rho u_z)}{\partial z} = 0 \qquad (4.1)$$

where ρ is density, x_i $(i = 1, 2, 3)$ or x, y, z are the Cartesian coordinates and u_x, u_y, u_z are the Cartesian velocity components of the fluid flow.

If the only body force is gravitational force, the momentum conservation equation can be written as

$$\frac{\partial (\rho u_i)}{\partial t} + \frac{\partial (\rho u_j u_i)}{\partial x_j} = -\frac{\partial p}{\partial x_i} + \frac{\partial \tau_{ij}}{\partial x_j} + \rho g_i \qquad (4.2)$$

where g_i is the gravitational acceleration, p is the pressure and $\partial \tau_{ij}$ is viscous stress tensor.

Viscous stress tensor can be written as

$$\tau_{ij} = 2\mu S_{ij} - \frac{2}{3}\mu \delta_{ij} \frac{\partial u_i}{\partial x_j} \qquad (4.3)$$

where μ is dynamic viscosity of the flow, δ_{ij} is the Kronecker symbol ($\delta_{ij} = 1$ when $i = j$, otherwise $\delta_{ij} = 0$) and S_{ij} is the rate of strain tensor such that

$$S_{ij} = \frac{1}{2}\left(\frac{\partial u_i}{\partial x_j} + \frac{\partial u_j}{\partial x_i}\right) \tag{4.4}$$

For incompressible and isothermal flow, the density and the viscosity of the fluid are assumed to be constant. Therefore, the mass and momentum conservation equations are given in Equation 1.1 and Equation 1.2 reduce to;

$$\frac{\partial u_x}{\partial x} + \frac{\partial u_y}{\partial y} + \frac{\partial u_z}{\partial z} = 0 \tag{4.5}$$

$$\frac{\partial u_i}{\partial t} + \frac{\partial (u_j u_i)}{\partial x_j} = -\frac{1}{\rho}\frac{\partial p}{\partial x_i} + \frac{1}{\rho}\frac{\partial \tau_{ij}}{\partial x_j} + g_i \tag{4.6}$$

If the flow is inviscid (i.e., Euler flow), the effects of viscosity are neglected. Inviscid flow is often utilized in high-Reynolds-number applications for compressible flows [33]. In these applications, the effect of inertial forces becomes critical when the effect of viscous forces is considered. The mass conservation equation does not change; however, the momentum conservation equation reduces to Euler equation:

$$\frac{\partial (\rho u_i)}{\partial t} + \frac{\partial (\rho u_j u_i)}{\partial x_j} = -\frac{\partial p}{\partial x_i} + \rho g_i \tag{4.7}$$

If the flow is nonisothermal, the properties of the fluid can be changed with heat transfer or temperature alteration. In this type of flow, Boussinesq Approximation is employed for simplifying to solve the conservation equation. As a result, the necessity for solving all parts of the momentum conservation equation for compressible flow diminishes. The accuracy of the approximation is dependent on the change in the density. It is assumed that the density change does not affect the fluid flow, and it is

73

omitted from all parts of the momentum conservation equation except the body force term.

The mass conservation equation is also affected by Boussinesq Approximation because only the density in the body force term changes with temperature. As a result, the mass conservation equation changes to its form used in the incompressible flows.

4.2.1.2. The Turbulence Energy Equation Models

The main equation using in all turbulence models is the turbulence kinetic energy equation. It can be written as

$$\frac{\partial k}{\partial t} + u_j \frac{\partial k}{\partial x_j} = \tau_{ij} \frac{\partial u_i}{\partial x_j} - \varepsilon + \frac{\partial}{\partial x_j}\left[\left(v + \frac{v_T}{\sigma_k}\right)\frac{\partial k}{\partial x_j}\right] \quad (4.8)$$

where σ_k is the closure coefficient, ε is dissipation, v_T is kinematic eddy viscosity and it is given as $v_T = \rho k^{1/2} l$.

The terms on the left-hand side of Equation 1.8 are called as local change and convective transport, respectively. The terms on the right-hand side are production of Reynolds stresses, dissipation and diffusion of Reynolds stresses, respectively.

The rate of conversion from turbulence kinetic energy to internal thermal energy is called dissipation, ε. The value of dissipation is proportional to the turbulence kinetic energy of turbulent fluctuations, k and the turbulence length scale, l:

$$\varepsilon \sim \frac{k^{3/2}}{l} \quad (4.9)$$

The dissipation term is expressed in various forms in different types of turbulence energy equation models.

4.2.1.2.1. One-Equation Models

"One-equation models are incomplete as they relate the turbulence length scale to some typical flow dimension." [34].

Prandtl assumes that there is a closure coefficient in the formula of the dissipation [35] and it can be expressed as

$$\varepsilon = C_D \frac{k^{3/2}}{l} \tag{4.10}$$

Thus, with the new dissipation term of Prandtl, the kinetic energy equation given in Equation 1.8 can be written as

$$\frac{\partial k}{\partial t} + U_j \frac{\partial k}{\partial x_j} = \tau_{ij} \frac{\partial U_i}{\partial x_j} - C_D \frac{k^{\frac{3}{2}}}{l} + \frac{\partial}{\partial x_j}\left[\left(v + \frac{v_T}{\sigma_k}\right)\frac{\partial k}{\partial x_j}\right] \tag{4.11}$$

Spalart and Allmaras developed a detailed one-equation model. Their field of interest in the turbulence energy equation is the kinematic eddy viscosity term. Their model contains three damping functions and eight closure coefficients [36].

Baldwin and Barth also develop a model in terms of the kinematic eddy viscosity [37]. There are seven closure coefficients and three functions in this model. Two of these functions are the empirical damping functions, and one of them describes the turbulence length scale.

In the study of Sai and Lutfy, it is found that the Spalart-Allmaras model has better performance than the Baldwin-Barth Model [38]. On the other hand, both of these models are not good enough compared to the $k - \omega$ model which is categorized in the two-equation models.

It can be said that due to some deficiencies, one-equation models cannot be implemented on all turbulent flows (especially separated flows) as a universal turbulence model. In the one-equation models, the effects of eddy viscosity on the

75

turbulence length scale are included. Nevertheless, in order to obtain an accurate universal model, the transport effects should also be examined. One of the approaches which include the transport effects is two-equation models.

4.2.1.2.2. Two-Equation Models

"Two-equation models provide an equation for the turbulence length scale or its equivalent and are thus complete." [34]. Two-equation models are preferred due to implementing on the fluid flow efficiently. There is no need to know any information about the fluid flow to predict the characteristics of the turbulent flow.

Kolmogorov introduced the first two-equation turbulence model [34]. The parameters used in his model is the kinetic energy of turbulence fluctuations, k and the rate of dissipation of energy in unit volume and time, ω.

Many studies have been conducted to develop the $k - \omega$ turbulence model of Kolmogorov which has been modified over the years. One of them is called as standard $k - \omega$ model and developed by Wilcox [34]. Normally, it is not suggested to use the $k - \omega$ model in the fluid flows having a low-Reynolds number, but the adjustments for the low-Reynolds number effects have been done by Wilcox for his model [39].

The SST $k - \omega$ model was published by Menter [40] and the term SST is the shear stress transport. Menter mixes the two types of two-equation models in the regions of the boundary layer. His model uses the $k - \omega$ model of Wilcox to obtain its accuracy in the inner region (near-wall region) of the boundary layer and uses the standard $k - \varepsilon$ model in the outer region of the boundary layer to have freestream independence for free shear flows. These abilities provide the SST $k - \omega$ model to have more accurate and reliable results than the standard $k - \omega$ model.

The $k - \varepsilon$ turbulence model is the other two-equational model. It is based on the kinetic energy of turbulence fluctuations, k and the dissipation rate of it, ε. The improved form of this model was published by Jones and Launder [41]. It is the most

popular two-equation model in the literature because of its robustness, time saving and accuracy for a wide range of turbulent flows [39]. It is called as the Standard $k - \varepsilon$ model.

The RNG $k - \varepsilon$ model was developed to minimize the inadequacies in the standard $k - \varepsilon$ model. The RNG term in the model stands for renormalization group modeling. It is a statistical technique used in the derivation of the $k - \varepsilon$ model and the accuracy of the standard $k - \varepsilon$ model gets better for rapidly strained flows. Standard $k - \varepsilon$ model is suitable for the flows having a high-Reynolds number but the convenience for the flows having a low-Reynolds number is enhanced by using the RNG modeling. On the other hand, proper treatment is needed at the near-wall. The swirl effect is also added in the RNG $k - \varepsilon$ model, and therefore, the accuracy is increased for swirling flows.

Another form of the two-equation model developed by using the standard $k - \varepsilon$ model is $k - \varepsilon$ Eddy Viscosity Model which is also known as Realizable $k - \varepsilon$ model and developed in the studies of Shih et al. [42]. They test their model for different types of flows and the results show that the performance of their model is better than the standard $k - \varepsilon$ model in almost all of the flow types. Moreover, according to the studies made for separated flows and flows having complex secondary flow feature, it is found that the Realizable $k - \varepsilon$ model has the best performance among the all forms of the $k - \varepsilon$ models [39].

4.3. Geometry

On the output screen of the implemented software, the dimensional information of the blade, which is the type of the airfoils, stagger angles and chord lengths, are given for all determined diametral locations. The 2D data files of all the airfoils are prepared with respect to the given chord lengths.

The 3D drawing of the blade is given in Figure 4.1.
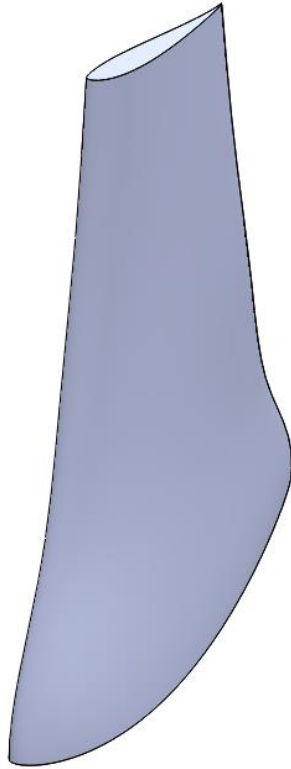
Figure 4.1. 3D Model of the Designed Fan Blade

It can be seen from Figure 4.1, the trailing edge of the blade is sharp. Moreover, the blade has a twisted shape due to increasing stagger angle from the hub to the tip. These two properties of the blade lead to some difficulties in the meshing part of the analyses and the construction process, also.

In addition, the details of the assembly can influence the mesh file unfavorably. The number of elements used in the small details of the impeller will increase the mesh size remarkably. The meshing of small ineffective details such as nuts and screws is unnecessary for obtaining fluid flow in the analyses. Therefore, the geometry should be simplified to decrease the size of the mesh file and to obtain good results.

The simplified fan geometry can be seen in Figure 4.2.
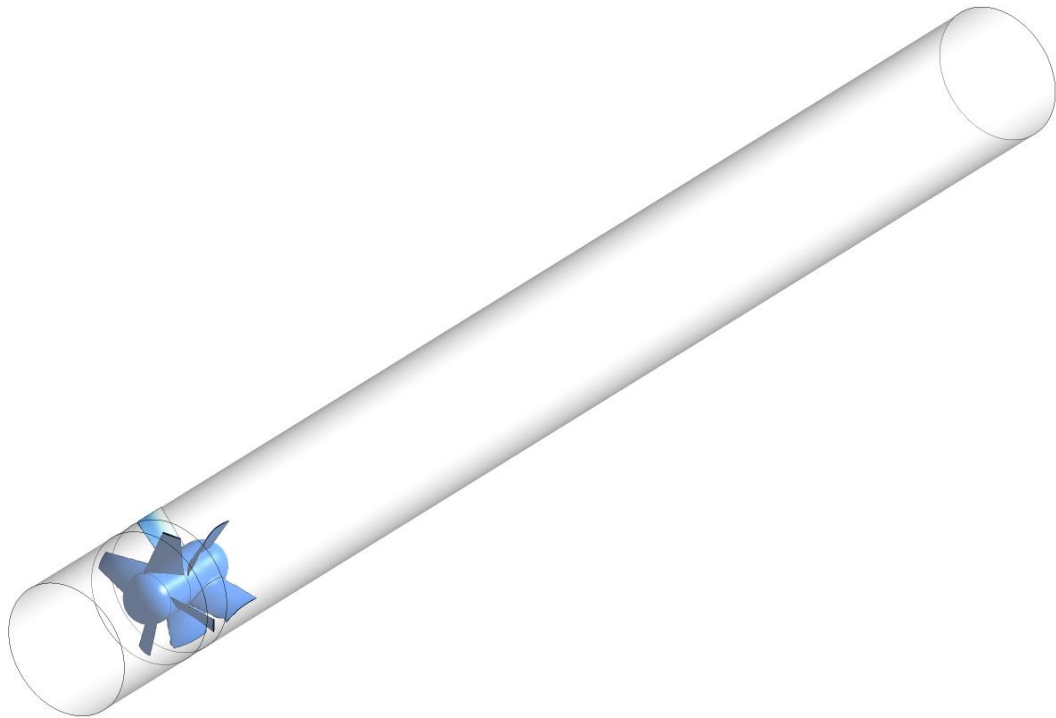
Figure 4.2. Simplified Fan Geometry

4.4. Meshing

The meshing part of the analysis has an essential role in having accurate fluid flow at the end of the numerical analyses. Therefore, the type, the size, the number of elements and nodes, and the other geometric properties of the mesh should be selected with considering the geometric features of the axial flow fan.

In order to capture boundary layer gradients at the interfaces between the wall boundary and the fluid domain, the thin cells are generated on the fan blades in the main mesh. These thin cells are called inflation. Since the blade geometry has a sharp edge at the trailing edge, it ends up a low-quality mesh in the inflation layers. In order to pass over this quality problem, mesh size properties which are edge size, face size, and body size are inserted on the parts of the axial fan in detail. After these corrections,

a high-quality mesh is obtained, but the number of mesh is poorly affected. Detailing of the mesh properties can increase the number of elements and nodes in the mesh file.
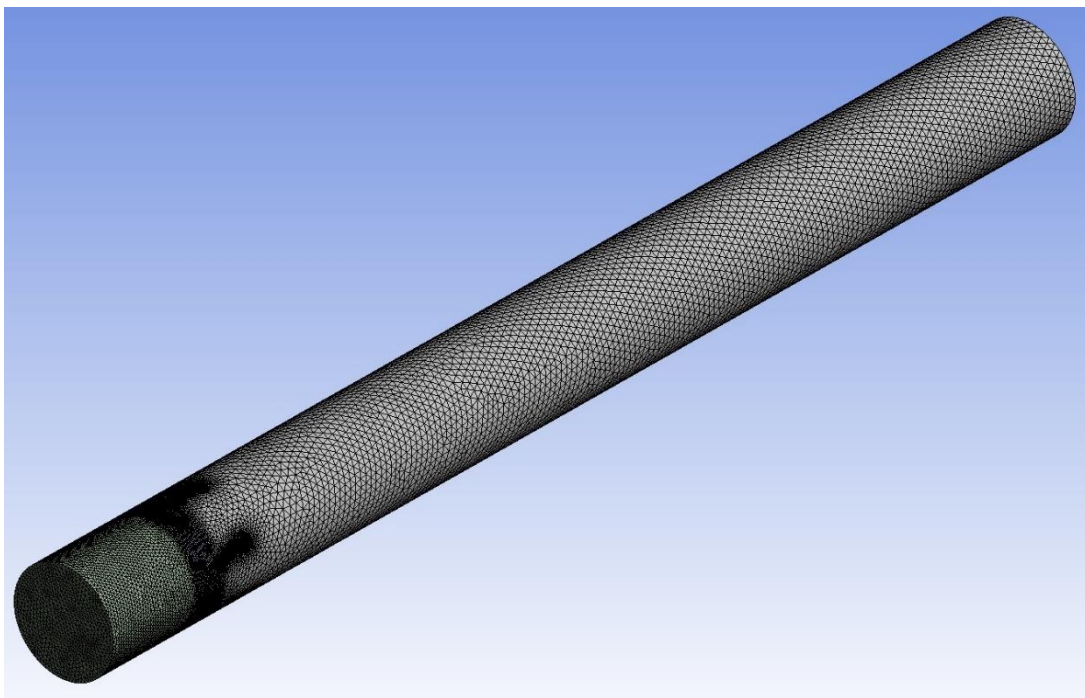
Figure 4.3. Meshed View of the Axial Fan Geometry
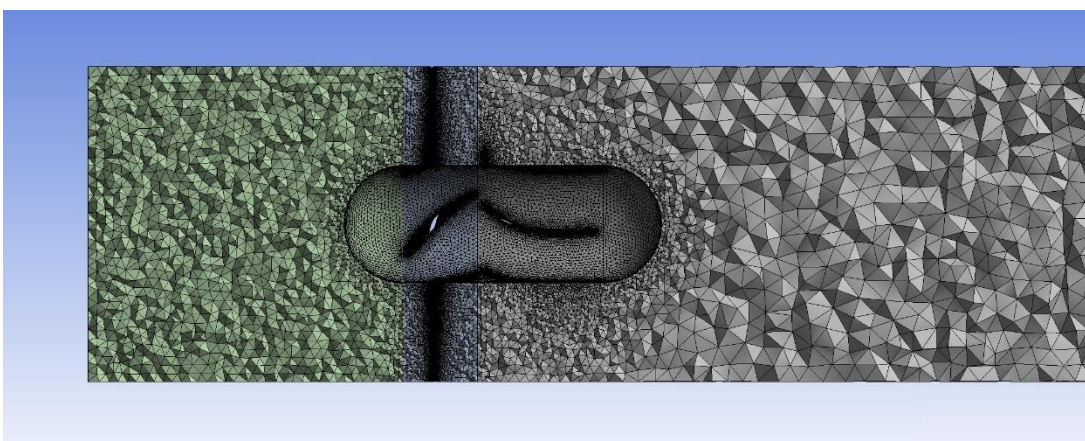
Figure 4.4. Sectional View of the Meshed Geometry

Mesh file of the fan geometry is shown in Figure 4.3 and Figure 4.4. Tetrahedrons method is used as mesh method; therefore, the domain consists of tetrahedral elements and triangular prisms (in inflation layers). Since the geometry of the fan blade is complex, mesh details are increased to obtain a good quality mesh. As a result of these elaborations, the number of nodes in the domain is approximately 5.3 million, and the number of elements in the domain is approximately 15 million.

Logically, increasing the number of elements and nodes provide to obtain reliable results. After a point at which the details of the mesh file are enough for solving the analysis accurately, increasing the number of elements and nodes do not affect the solution. This point is called as Mesh Independency. A mesh independence study for the current fan geometry is shown in Figure 4.5.
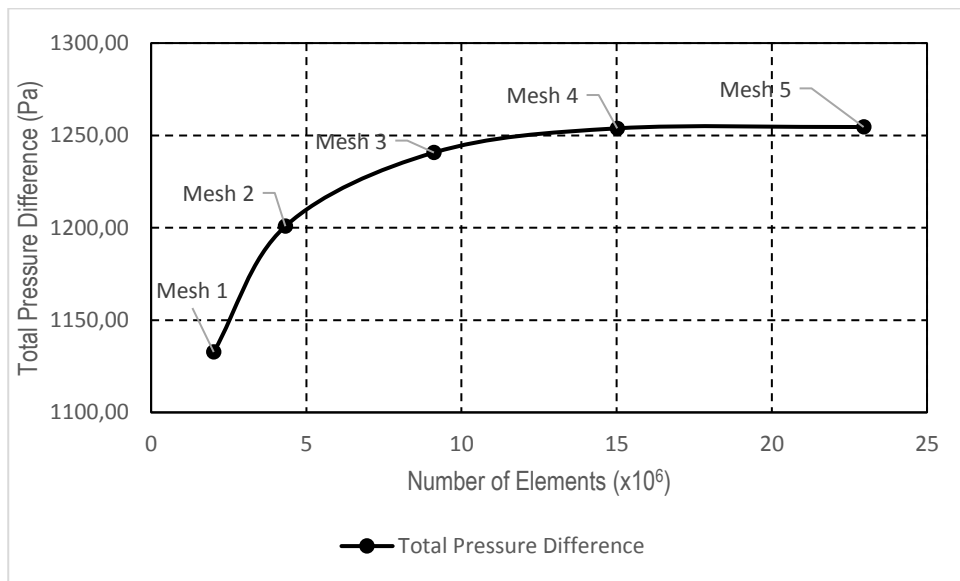
Figure 4.5. A Mesh Independence Study

In the mesh independency study shown in Figure 4.5, it is found that the total pressure differences measured from the fan outlet are changed with increasing the number of elements in the mesh file up to Mesh 4; however, they stay almost unchanged between

Mesh 4 and Mesh 5. The analyses can be solved with Mesh 5, but it would be reasonable to use Mesh 4 to reduce the analysis load.

In addition, as a quality indicator of the mesh file, the maximum skewness is found as 0.84 in the all domain.

4.5. Boundary Conditions

Boundary conditions are defined to explain the working conditions to the analysis software. There are several ways of defining inlet and outlet boundary conditions. The most used of them are velocity inlet – pressure outlet, pressure inlet – pressure outlet and pressure inlet – mass flow outlet.

In order to plot the performance curve of the fan, outlet pressure is increased from the first iteration to the last iteration, and produced flow rates are recorded. Selecting the boundary conditions as pressure inlet and pressure outlet means that the volumetric flow rate is computed according to the existing pressure difference of the fan up to convergence point. Therefore, in this work, the boundary conditions of the axial flow fan are selected as a pressure inlet and pressure outlet.

In the static frame total pressure option of the inlet boundary condition of CFX, the inlet pressure is the gauge total pressure. It is taken to be zero in the series of analyses. It means that fan inlet is opened at atmosphere. Turbulence Intensity at the inlet zone is assumed as 5%.

The outlet boundary condition of the fan is chosen as a pressure outlet. In CFX, it can be selected by using a static pressure option, and it is taken to be gauge static pressure. In the current series of analyses, outlet static pressure is increased from the first iteration to the last iteration, just like being in the experimental test procedure. In the experimental test of the axial fans, there is a throttling device at the outlet section, and it is used to decrease the outlet flow area of the test tube. The details of them are given in the next chapter, but the primary purpose of decreasing flow area is to increase the static pressure at the outlet.

The rotor domain consists of air, and it is rotational. As a design parameter of the axial fan, the rotational velocity of the motor is determined as 1500 rpm (157.08 rad/s). In order to give the rotation to the domain, the domain is selected as rotating.

The last boundary conditions are about the housing, the hub, the blade and the guide vane. These boundaries are defined as wall. Typically, the inside wall of the housing is stationary, but the domain is rotating. In CFX, this situation can be supplied by using a counter-rotating wall option. The hub and the blade walls are the rotating walls. As the rotational velocity of the air domain is equal to the rotational velocity of the impeller, the blade and hub walls rotate at a speed of zero relatives to the adjacent cell zone.

Details of the boundary conditions are given in the Table *4.1*.

Table 4.1. *Boundary Conditions*

Surface Name / Domain Name	Boundary Type
Inlet	Pressure Inlet
Inlet Domain	Stationary
Outlet	Pressure Outlet
Guide Vanes	Stationary Wall
Outlet Domain	Stationary
Blades	Rotating Wall
Hub	Rotating Wall
Cylindrical Housing Wall	Counter Rotating Wall
Rotor Domain	Rotating

4.6. Turbulence Model and Solver Options

In CFX, if there is no heat transfer, compressibility and turbulence in the domain, the calculations are performed by using the mass and the momentum conservation equations. For turbulent flow, additional transport equations are involved.

In this application, the fluid domain contains a high turbulent flow, and therefore, capturing the boundary layer on the impeller wall directly affect the analyses results. Therefore, the selected turbulence model should have a solution capability, just like the capability of the $k - \omega$ model in the near-wall region. In addition, the fluid domain consists of rotating, swirl dominant and rapidly strained flow. It means that the outer regions of the boundary layer or the free-shear layers are also important for accuracy. The selected turbulence model should also have solution capability of the standard $k - \varepsilon$ model in the swirl dominant flows. All of these requirements can be supplied by the SST $k - \omega$ model. The accuracy and calculation performance of this model is validated in the studies of Bardina et al [43]. Therefore, the SST $k - \omega$ model is used as the turbulence model in all analyses.

In the solver control panel of CFX, there are some options about the calculation of the advection terms in the discrete finite-volume equations. High-Resolution Scheme is selected. In the ANSYS CFX Theory Guide, it is said that the High-Resolution option in Turbulence Numerics uses the High-Resolution Advection Scheme. Therefore, in the calculation of the Turbulence Numerics, High-Resolution option is selected [44].

4.7. Iterations

As explained in the boundary conditions, inlet gauge total pressure is taken to be zero, but outlet gauge static pressure is increased from the first analysis to the last analysis. In addition, the designed rotational speed of the fan is taken as 1500 rpm. The iterations are performed for different outlet gauge static pressures. At the end of each iteration, the total pressure difference between the inlet and outlet of the fan and the corresponding volumetric flow rate are recorded.

4.8. Results

The input performance parameters of the implemented software are $1250\ Pa$ for the desired total pressure rise and $50\ m^3/s$ for desired flow rate. Besides, it is assumed that the fan is working in a clean condition, and the rotational speed of the AC motor is selected as $1500\ rpm$ ($157.08\ rad/s$).

In order to see the convergence state of the iterations, monitor points are located at the outlet of the fan. Total pressure and mass flow rate at the outlet are plotted in each iteration. They are used for the judgment of the convergence at that target. In Figure 4.6, the convergence history of the outlet of the fan is given.
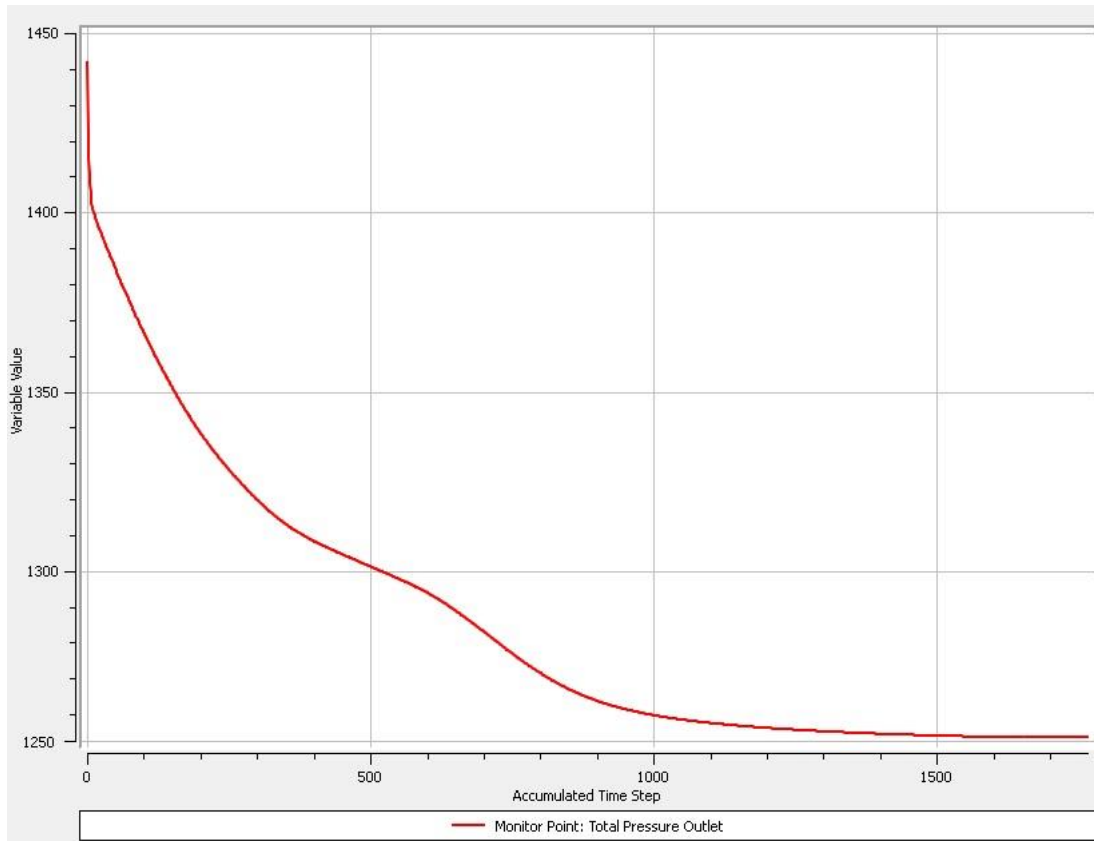
Figure 4.6. The Convergence History at the Fan Outlet

According to the results of the analyses, the performance of the fan suggested by the implemented software is found. It can be said that there is a consistency between the design parameters of the implemented software and the CFD results. The values of them are close to each other. The desired volumetric flow rate of $50\ m^3/s$ is found at the total pressure rise of about $1200\ Pa$ on the performance graph.

The error of the implemented software with respect to the CFD results can be calculated as

$$Relative\ Error = \frac{\Delta p_{software} - \Delta p_{CFD}}{\Delta p_{CFD}} \times 100\% \approx 5\% \qquad (4.1)$$

It is acceptable that there is an agreement between the results of the analyses and the implemented software.

The iteration results are given in Table *4.2*.

Table 4.2. *Iteration Results*

Volumetric Flow Rate (m^3/s)	Total Pressure Difference (Pa)	Torque (Nm)	Hydraulic Efficiency (%)
63.11	677.02	367.22	74.07
61.49	752.49	381.89	77.13
60.39	802.83	391.30	78.87
59.26	852.80	400.43	80.34
58.12	903.57	409.17	81.70
55.69	1002.87	425.93	83.48
53.14	1101.60	440.81	84.54
50.41	1199.46	453.28	84.92
48.96	1253.82	458.39	84.85
47.44	1295.58	462.60	84.58
45.82	1342.42	465.69	84.08
44.07	1387.93	467.44	83.30
42.14	1431.54	467.44	82.16
39.95	1448.30	465.31	79.17
37.35	1452.71	460.62	74.99
35.75	1458.95	457.29	72.62
28.57	1469.94	433.42	61.68

There is an efficiency column in Table *4.2*. It represents the hydraulic efficiency of the axial flow fan, and it can be calculated as

$$\eta_h = \frac{Q \Delta p_t}{T \omega} \qquad (4.2)$$

where Q is volumetric flow rate, Δp_t is the total pressure difference generated by the fan. The multiplication of these gives fluid power. T is the net torque acting on the rotor and ω is the rotational speed of the fan, and they are used to obtain the shaft power.
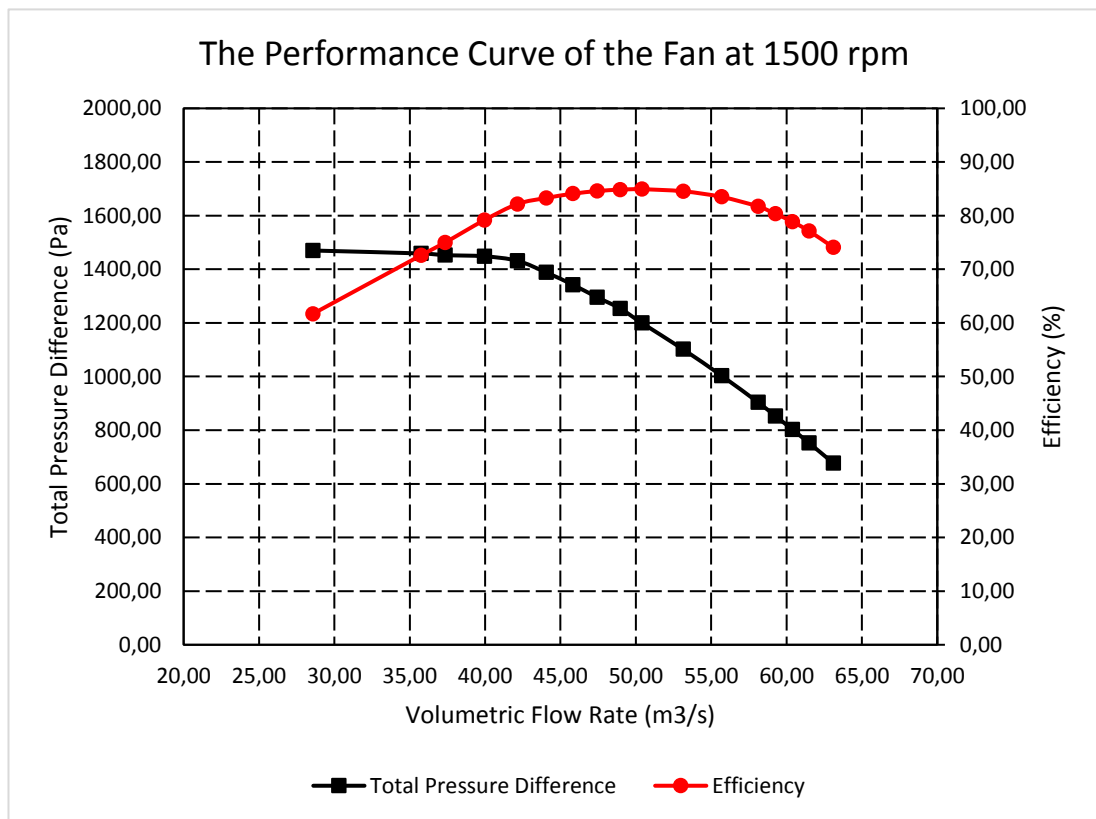
Figure 4.7. Calculated Performance Curves of the Fan

The performance curves of the current fan are given in Figure 4.7. It can be seen that the stall starts at the volumetric flow rate of 40 m^3/s. Operating the fans at its stall point can be inefficient and noisy. Therefore, for achieving safe operation range, the working point should be higher than 40 m^3/s for the current fan. It is also seen that the maximum efficiency is obtained at the suggested operating range of the fan.

At the end of each analysis, the velocity streamlines and the pressure distributions are investigated carefully to check the behavior of the fluid flow. Within this scope, the followings are given for 50.41 m^3/s volumetric flow rate and 1199.46 Pa total pressure difference.

Figure 4.8 and Figure 4.9 shows the velocity streamlines in the fan.
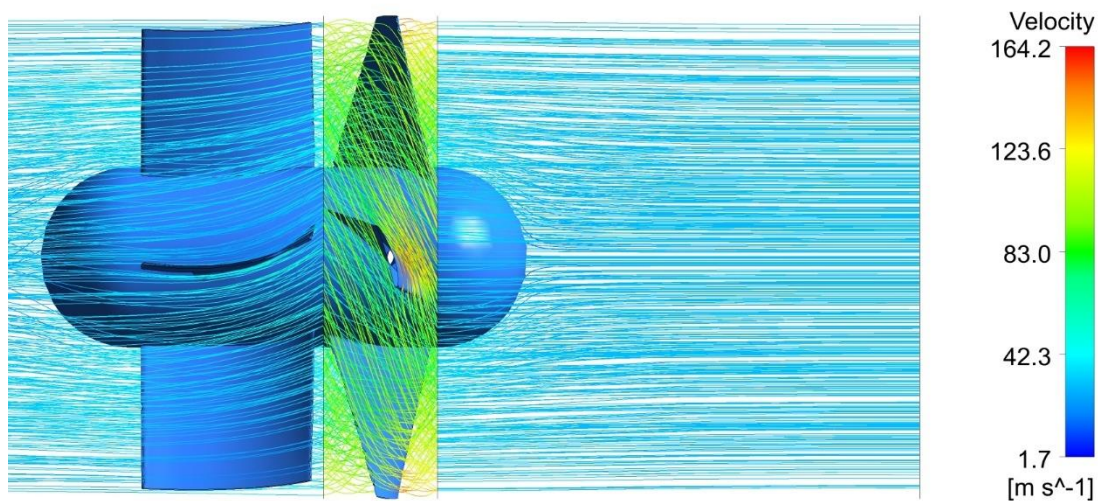
Figure 4.8. Velocity Streamlines – Side View
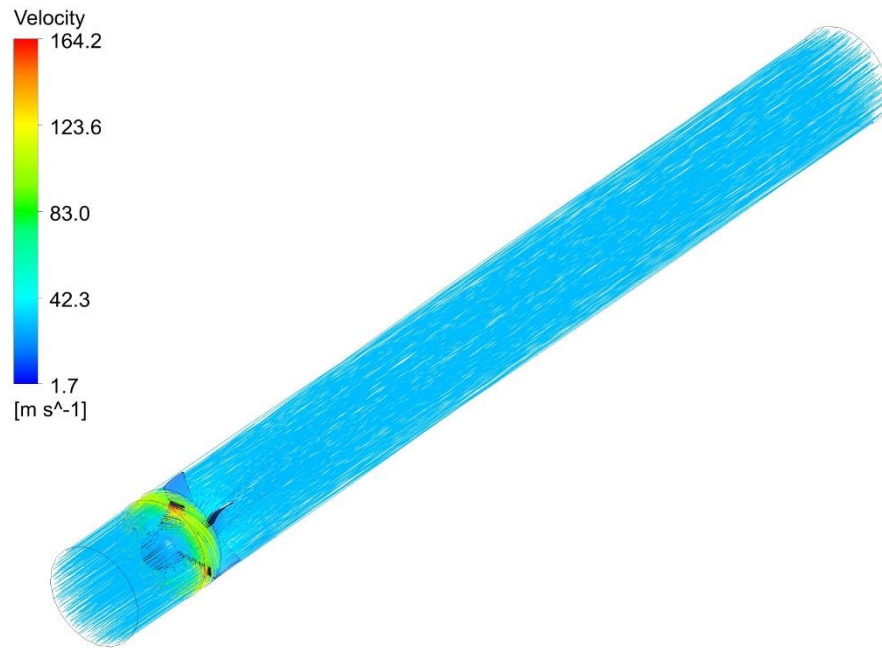
Figure 4.9. Velocity Streamlines – Isometric View

According to the obtained velocity streamlines shown in Figure 4.8 and Figure 4.9, it can be said that there is no inlet whirl at the fan inlet. When fluid flow enters the rotor domain, it starts to rotate at a rotational speed of 1500 rpm. Normally, change in the fluid density can be neglected for the fluid velocities smaller than 0.3 Mach. According to the velocity legend of the streamlines, fluid velocity exceeds 0.3 Mach (nearly $104 \; m/s$ for this application) at some points in the rotor domain. It means that the incompressible working range is exceeded. Because of having a small footprint in the fluid flow, the effects of the streamlines are neglected and all analyses are performed in incompressible working range. When fluid flow enters the outlet domain, it faces with stationary guide vanes. They are used for eliminating air spin at the fan outlet. According to the flow pad of the streamlines, it can be said that air spin is eliminated at the fan outlet.
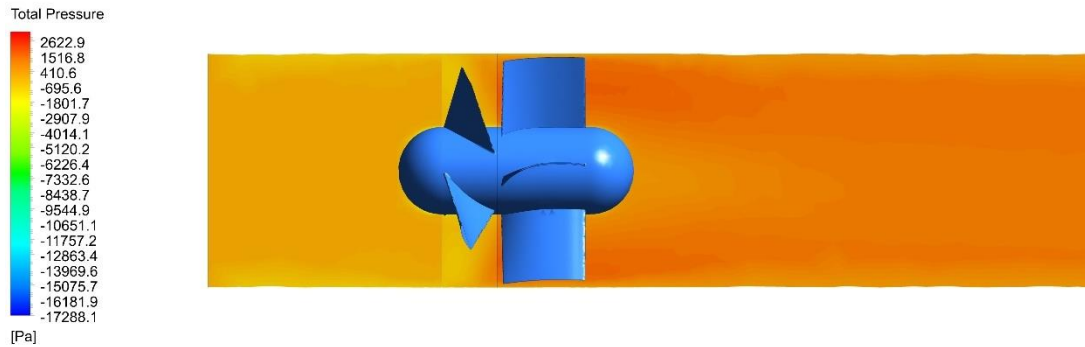
Figure 4.10. Total Pressure Distribution Throughout the Fan

Total pressure distribution throughout the fan is given in Figure 4.10. Red color represents high pressure values and orange color represents low pressure values. It can be said that the total pressure is increased in the rotor domain. It is logical since axial flow fans generate a flow rate by increasing the total pressure of the working fluid. There are jumps in the colors at the interfaces of the domains. It means that transitions of the total pressures between the interfaces are not smooth. These differences are due to interface settings. Interfaces are selected as mixing-plane (stage-interface) and the total pressures are kept constant between the stages. It means that there is no loss in the total pressure of the working fluid during the crossing of the interface and total pressure is averaged to calculate the velocity of the fluid flow in the second side of the interface. Using the total pressure averaged results in a color jump in the interface transitions since the total pressure on the second side of the interface is calculated by using average total pressure on the previous side.

90

CHAPTER 5

CONSTRUCTION, EXPERIMENTAL FACILITIES AND PERFORMANCE EVALUATION OF THE AXIAL FLOW FAN

5.1. Introduction

At the beginning of the design process, the input parameters, or the desired performance parameters of the fan when it works at the operating point, are determined. After that, the size and the types of the airfoils, the fan diameter, the hub diameter, the number of blades, and the other important design parameters of the axial fan are calculated by using design software tool which is examined and explained in the previous chapters.

After the design process, the 3D model of the fan is analyzed in CFD software. The design parameters obtained from implemented software are validated, and the accuracy of the design tool is found enough for starting the construction process.

This chapter of the thesis consists of the construction process of the axial flow fan and its performance evaluation by the help of experimental methods.

In the construction process, the producible 3D model of the parts of the fan are drawn with the help of the 3D modeling CAD tool, SolidWorks. Then, these parts are produced by using different manufacturing processes. The details of them are given in the construction part of this chapter. The manufactured parts of the fan are the blades, the hub, the cylindrical housing, the inlet and the outlet duct, and the guide vanes.

In the experimental facilities and performance evaluation part, the experimental test and the test procedures of the current fan are performed. The aerodynamic characteristics of the fan are obtained, and all the design parameters are verified by

the help of an experimental test. The test is prepared according to AMCA 210: Laboratory Methods of Testing Fans for Aerodynamic Performance Rating [8].

5.2. Construction

All of the production and assembly activities of the parts of the axial flow fan is carried out within the workplace of the TEKNIMA CleanAir Technology.

5.2.1. Blade Construction

The blades are constructed by using an aluminum casting process. Aluminum is selected as a working material for some reasons. First of all, the fan rotates at high rotational velocity; therefore, the raw material used in the blade construction must resist the existing bending and centrifugal force when impeller rotates. At this circumstance, aluminum becomes the right choice due to its strength. Secondly, there is a cost advantage of the casting of aluminum. It has low production cost in the manufacturing on demand (MOD) type of production process.

The first step in the blade construction is preparing a wooden prototype of a designed blade by using CNC machining. Then, this machined wooden blade is used in the aluminum casting process as a mold.

The constructed blades are shown in Figure 5.1.

Figure 5.1. Constructed Fan Blades

5.2.2. Guide Vane Construction

Sheet metal is used as a raw material in the construction of the guide vanes. It can be formed the desired shape quickly by using a press tool. The formed condition of one of them can be seen in Figure 5.2.

Figure 5.2. Constructed Guide Vane

5.2.3. Cylindrical Housing Construction

The raw material of cylindrical housing is sheet metal. Sheet metal roller is used to give a cylindrical shape to it. Then, the edges of the rounded sheet are welded to obtain a robust cylindrical housing. It is challenging to have a perfectly round shape due to deteriorations originated by high temperature in the welding process. Unfortunately, the circular cross-section turns to be elliptic form at some locations due to high temperatures. Also, the tip clearance is affected by this condition unfavorably. Although the tip clearance is achieved at some locations on the housing, there are some inevitable clearances whose dimensions are different from desired tip clearance. The constructed housing of the current fan can be seen in Figure 5.3.

Figure 5.3. Constructed Cylindrical Housing

5.2.4. Hub Construction

The hub of the fan is constructed by using CNC machining. The raw material of the hub is steel. It is machined from a steel sheet. In the construction of the hub, there are some small geometric tolerances have vital importance to obtain balance when impeller rotates. Designed and constructed hub of the fan is shown in Figure 5.4.
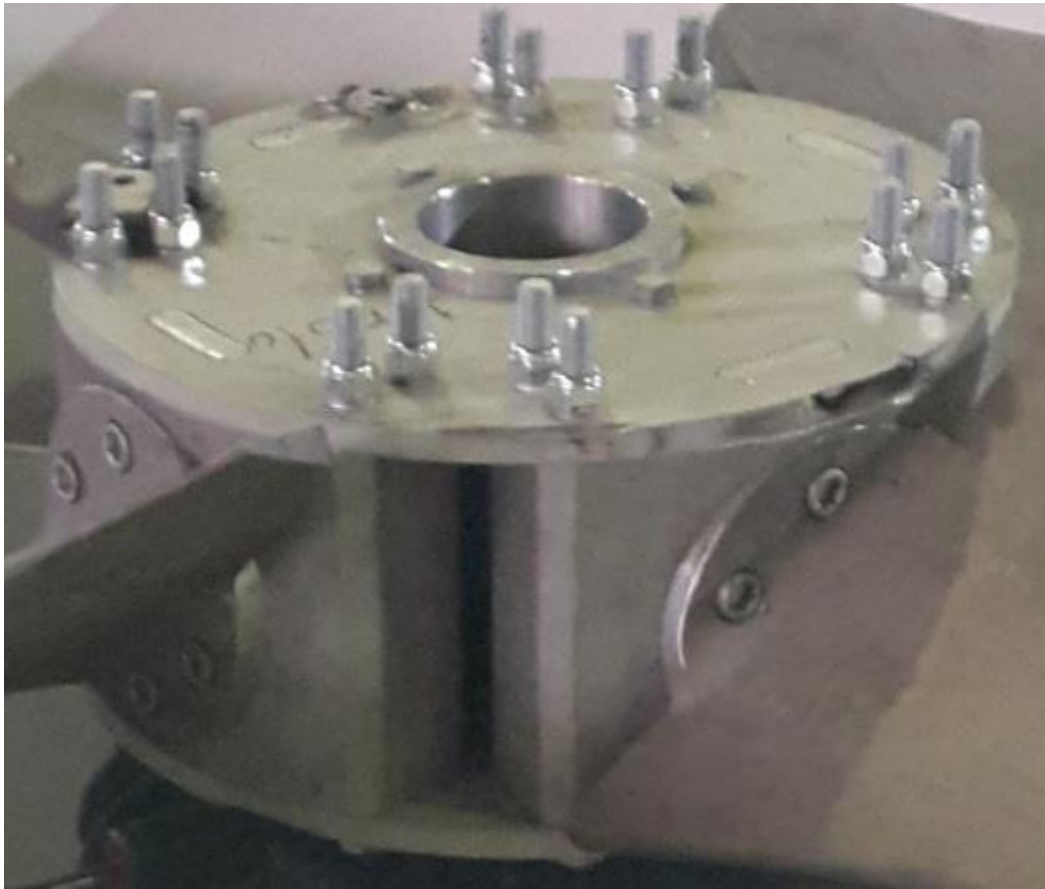
Figure 5.4. Constructed Hub

It can be seen from Figure 5.4; there are gaps in the cylindrical side of the hub. They are used to mount blades to the hub. These gaps have a property which is sought after

by most of the designers; they allow for rotating blades in order to adjust the stagger angle.

5.2.5. Impeller Assembly

After the construction process of blades and their hub, they are assembled. The stagger angles of each blade should be the same, and therefore, the necessary adjustments are implemented one by one. Then, the outer diameter of the impeller is determined. In order to do that, determined tip clearance is subtracted from the diameter of the inner diameter of the housing. To obtain sufficient tip clearance between the impeller and the inner wall of the housing, the tip of the blades is machined with turning. At the final step, as being in all rotating systems, the balance of the impeller should be adjusted. The impeller is mounted on the balance machine, and necessary small mass blocks are welded on the inner side of the hub. The impeller of the current fan is shown in Figure 5.5.
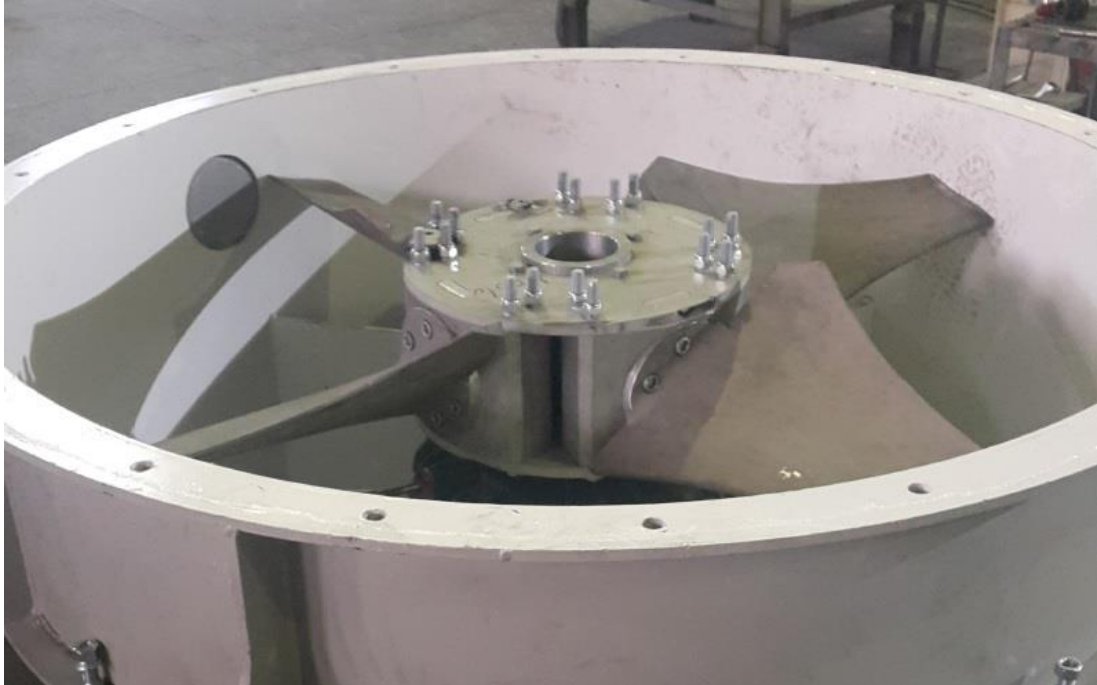
Figure 5.5. Assembled Impeller

5.2.6. Fan Assembly

After all parts of the axial flow fan are constructed, the fan is ready to assemble. First of all, the AC motor is mounted on its base plate in the cylindrical housing. Then, the impeller is assembled on the shaft of the motor. In order to decrease the noise level of the fan, two silencer ducts are mounted to the inner and outer side of the fan. The final state of the axial flow fan can be seen in Figure 5.6.

Figure 5.6. Assembled Axial Flow Fan

5.3. Test of the Axial Flow Fan

In this part, the details of the test setup and the test procedure are presented and expounded. All of these works are performed within the laboratory of TEKNİMA CleanAir Technology.

The designed and manufactured axial flow fan is tested at three different rotational speeds. During the test process, the total and static pressures at the cross-section of the measurement point is recorded for different locations of the throttling device. The power consumption of the AC motor is also recorded to calculate the efficiency of the

fan. Moreover, the temperature and static pressure of the air at the test area are recorded.

5.3.1. Test Setup

There is a standard for the calculation of the aerodynamic performance ratings of the fans by using experimental methods. The test setup is built up with respect to the rules of it. In this work, ANSI/AMCA 210 Outlet Duct Setup - Pitot Traverse in Outlet Duct model is used, and the schematic view of the test setup is shown in Figure 5.7.
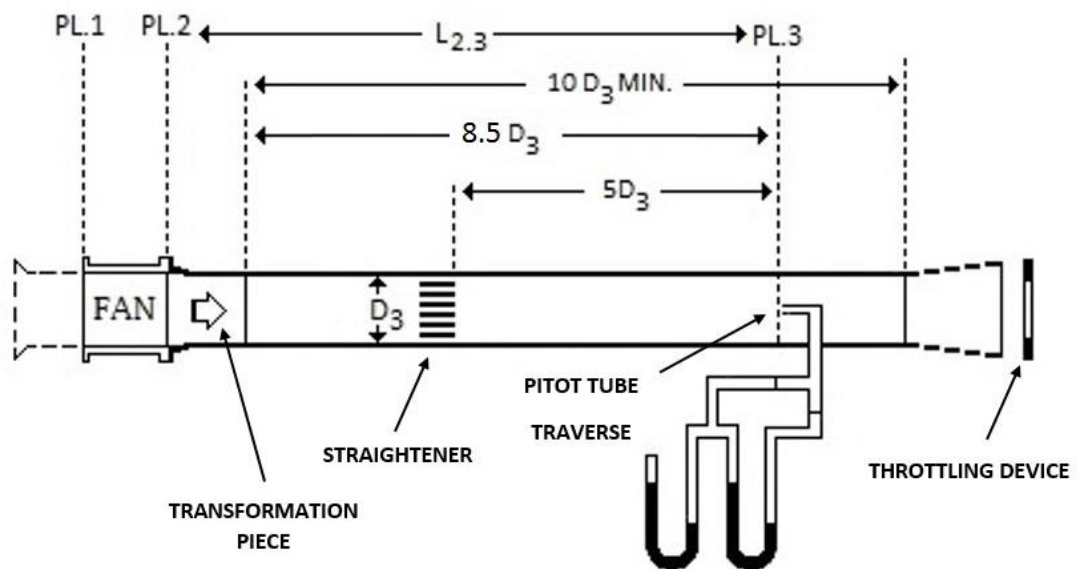
Figure 5.7. Outlet Duct Setup-Pitot Traverse in Outlet Duct [8]

According to the schematic in Figure 5.7, the minimum length of the test setup should be ten times the diameter of the test tube. In this study, the diameter of the test tube is 1.5 meters. Therefore, the length of the test setup is 15 meters long. The prepared test setup can be seen in Figure 5.8.

Figure 5.8. Test Setup

In order to determine the velocity profile of the fluid flow in the test tube, Pitot tubes are used, and they are placed in the test section in a rule shown in Figure 5.9.
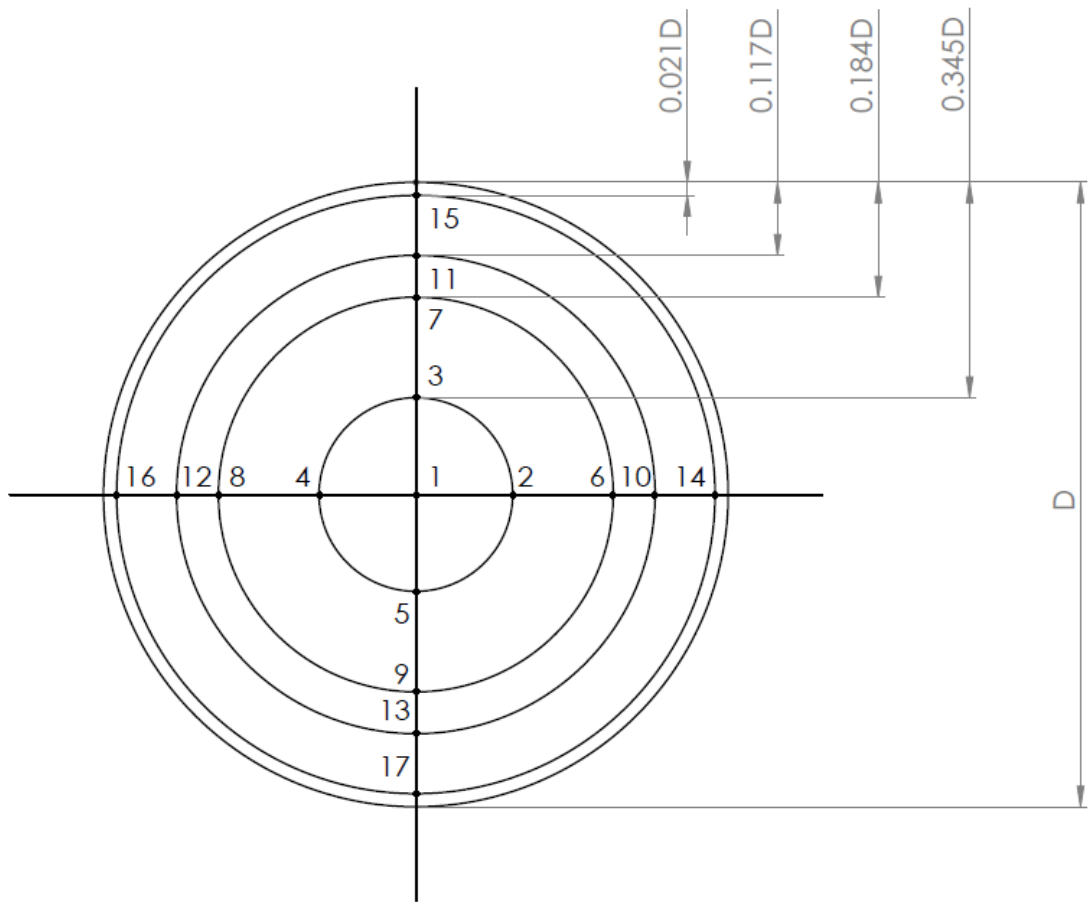
Figure 5.9. Positioning of the Pitot Tubes

There are 17 points on the cross-sectional area of the test tube. These are used for locating Pitot tubes in the flow area. The constituted Pitot tube section of the test setup is shown in Figure 5.10.

Figure 5.10. Pitot Tube Section of the Test Tube

5.3.2. Test Procedure

In this work, measurements are carried out to obtain the performance curve of the current fan. Normally, the fan is designed for the rotational speed of 1500 rpm. In order to view the effect of rotational speed on the results, the fan is also tested at 800 rpm and 1000 rpm. In order to clarify the test process, the test procedure is given as follow.

1. Control the connection between the AC motor and the control panel.
2. Adjust the rpm values of the AC motor.
3. Adjust the location of the throttling device.
4. Start the AC motor of the fan.
5. Record the total pressures and static pressure from the Pitot tubes.
6. Record the power consumption of the AC motor.
7. Close the AC motor of the fan.
8. Repeat the steps from 3 to 7 until the stall point of the fan achieved.

During the test process, the total pressures of the working fluid when it flows in the testing tube are measured for different locations of the throttling device. The Pitot tubes are used for reading the total pressures of the working fluid. The locations of them are given in Figure 5.9.

The first measurement is performed for the location of a fully opened state of the throttling device. The total pressures of all points are recorded with a handheld digital pressure meter, and the measuring process can be seen in Figure 5.11.

Figure 5.11. Measurement Process of the Total Pressures

In order to calculate the efficiency of the fan, the power consumption of the AC motor is also recorded from the control panel of the AC motor. After that, the location of the throttling device is shifted to the left. It means that the outlet flow area of the test tube is decreased and the static pressure in the testing tube is increased. The next measurement is performed for this circumstance. The picture of the throttling device is given in Figure 5.12.

Figure 5.12. Throttling Device at the Outlet Section of the Test Tube

The rest measurements are performed in this way, and the test is ended when the stall point of the working fan is achieved. At that point, the working fluid becomes

unstable, and the backflow comes into existence at the inlet location due to lack of flow area of the test tube.

5.3.3. Results

At the end of the test procedure, the obtained pressure data and power consumption values are gathered, and they are given in Table *5.1*.

Table 5.1. *Measured Data of the Experiment at 1500 rpm*

Throttling Device Position	1200 mm	900 mm	600 mm	300 mm
Pitot Tube Location	Total Gauge Pressures (Pa)			
1	294	505.52	730.66	1008.72
2	332.64	511.2	772.31	1020.6
3	379.68	553.8	833	1030.32
4	420	599.24	866.32	1031.4
5	561.12	690.12	866.32	1048.68
6	567.84	711.42	896.07	1048.68
7	588	724.2	897.26	1053
8	619.92	731.3	905.59	1057.32
9	619.92	734.14	907.97	1061.64
10	635.04	734.14	912.73	1062.72
11	650.16	734.14	918.68	1064.88
12	658.56	742.66	922.25	1064.88
13	702.24	755.44	923.44	1064.88
14	717.36	759.7	924.63	1067.04
15	722.4	773.9	931.77	1071.36
16	757.68	788.1	938.91	1072.44
17	762.72	809.4	944.86	1086.48
Static Pressure (Pa)	125	240	530	910
Power Consumption of the AC Motor	70 kW	72 kW	74 KW	56 kW
Ambient Pressure of Ankara on April 2, 2019	90600 Pa			
The temperature of the Test Ambient	16°C			

In order to emphasize the steps of plotting the performance graph of the current axial flow fan, a sample calculation is presented, and the obtained data of a fully opened state of the throttle device (1200 mm) is used.

- The diameter, length and cross-sectional area of the test tube

$$D = 1.5 \ m \tag{5.1}$$

$$l_{tube} = 15 \ m \tag{5.2}$$

$$A_{tube} = \frac{\pi \times D^2}{4} = 1.77 \ m^2 \tag{5.3}$$

- The temperature (dry bulb) of the test ambient

$$T_{ambient} = 16 \ °C \approx 289 \ K \tag{5.4}$$

- Air density at 16°C & 1 atm

$$\rho_0 = 1.184 \ kg/m^3 \tag{5.5}$$

$$1 atm = p_0 = 101325 \ Pa \tag{5.6}$$

- Ambient pressure of Ankara on April 2, 2019 [45]

$$p_{atm} = 90600 \ Pa \tag{5.7}$$

- Air density at Ankara

$$\rho_{air} = \rho_0 \times \frac{P_{atm}}{P_0} = 1.06 \ kg/m^3 \tag{5.8}$$

- Gauge static pressure

$$p_{static} = 90 \ Pa \tag{5.9}$$

- Average dynamic pressure

$$p_{dynamic_{avg}} = \left(\frac{\Sigma \sqrt{p_{dynamic}}}{n} \right)^2 = 485.4 \ Pa \tag{5.10}$$

where n is the number of Pitot tubes

- Average velocity

$$V_{avg} = \sqrt{\frac{2 \times p_{dynamic_{avg}}}{\rho_{air}}} = 30.28 \ m^3/s \tag{5.11}$$

- Volumetric flow rate

$$Q = V_{avg} \times A_{tube} = 53.5 \ m^3/s \tag{5.12}$$

- Frictional losses between the fan inlet and Pitot tube section

$$Re = \frac{V_{avg} \times D}{\nu_{air}} \rightarrow Re = 3.1 \times 10^6 \tag{5.13}$$

where ν_{air} is the kinematic viscosity of air at 16℃ and 1 atm. Flow is found as turbulent because its value is higher than critical Reynolds number of 2300 [31]

- Pipe friction coefficient from Moody chart [46]

$$f_{pipe} = 0.08 \tag{5.14}$$

- Pressure loss due to viscous shear for circular pipes [46]

$$p_{loss} = f_{pipe} \frac{l_{tube}}{D} \frac{\rho_{air}}{2} V_{avg}{}^2 = 390.78 \, Pa \qquad (5.15)$$

- Total pressure produced by the fan

$$p_{total} = p_{static} + p_{dynamic_{avg}} + p_{loss} = 966.2 \, Pa \qquad (5.16)$$

- Power input to working fluid

$$P_{fluid} = p_{total} \times Q = 51702.6 \, Watt \qquad (5.17)$$

- Power consumption of AC motor

$$P_{motor} = 70 \, kW \qquad (5.18)$$

- The system efficiency

$$\eta_{system} = \frac{P_{fluid}}{P_{motor}} = 0.73 \qquad (5.19)$$

System efficiency consists of the product of five different efficiencies. These efficiencies are hydraulic efficiency, volumetric efficiency, mechanical efficiency, motor efficiency and control panel & power cables efficiency. It is known from the motor and control panel catalogue that motor efficiency is 98% and panel & power cables efficiency is 92%. Mechanical efficiency and volumetric efficiency are assumed as 97%. Therefore, hydraulic efficiency can be calculated as

$$\eta_{hydraulic} = \frac{\eta_{system}}{\eta_{mech} \times \eta_{vol} \times \eta_{motor} \times \eta_{panel}} = 0.86 \qquad (5.20)$$

By following the same procedure, the efficiencies, total pressure differences, and the volumetric flow rates are calculated for the all position of the throttling device. The results are given in Table *5.2*.

Table 5.2. *Experimental Test Results at 1500 rpm*

	Throttling Device Position	Total Pressure Difference (Pa)	Volumetric Flow Rate (m3/s)	Efficiency (%)
1500 rpm	1200 mm	966.18	53.5	73
	900 mm	1056.78	51.6	75
	600 mm	1171.97	45.8	72
	300 mm	1168.91	29.1	60

The performance curve of the current fan can be plotted by using the data in Table *5.2*. It can be seen in Figure 5.13.
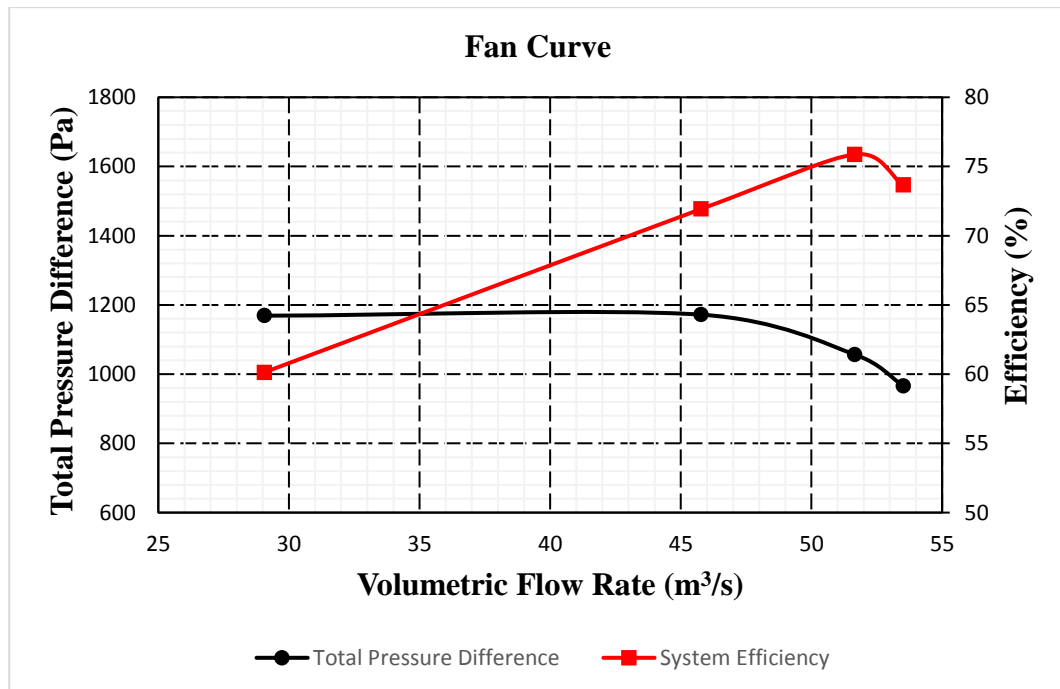

Figure 5.13. Experimental Performance Curves of the Axial Fan

In Figure 5.13, it can be seen that the maximum efficiency point is achieved around a volumetric flow rate of 52 m^3/s. In contrary, the expected volumetric flow rate of the current fan is 50 m^3/s. The difference between them can be acceptable, but one of the possible reasons for this small difference is that the stagger angle of the blades may not be the same with its designed value. In the hub construction part, it is explained that the stagger angle of the blades is adjusted by using handwork, therefore, the small differences can be showed up at the end of the assembly.

In addition, the expected total pressure rise of the fan is 1250 Pa at a volumetric flow rate of 50 m^3/s. It is obtained differently in the real fan curve. The corresponding total pressure rise of the current fan is about 1150 Pa. This difference may be occurred due to the losses not taken into account. The accumulated dust on the inner walls of the test tube can increase frictional pressure loss and small leakages in the test tube can decrease the total pressure.

The velocity profile of the working fluid at a rotational speed of 1500 rpm and a fully opened state of the throttle device is given in Figure 5.14.
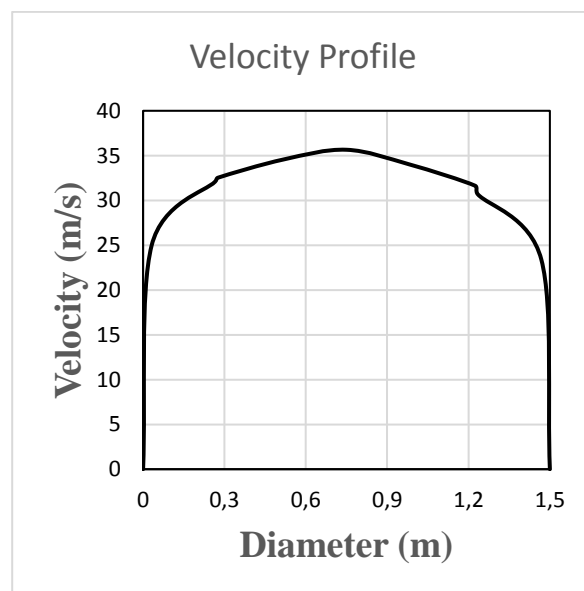
Figure 5.14. Velocity Profile in the Test Tube

110

The test procedure is repeated for the rotational speed of the AC motor, 1000 rpm, and 800 rpm. The obtained data is given in Table *5.3.* and the comparative performance graphs of them can be seen in Figure 5.15.

Table 5.3. *Experimental Test Results at 1000 rpm and 800 rpm*

	Throttling Device Position	Total Pressure Difference (Pa)	Volumetric Flow Rate (m^3/s)	Efficiency (%)
1000 rpm	1200 mm	428.4	34.9	73.5
	900 mm	463.7	34.2	76.2
	600 mm	522.1	30.9	76.4
	300 mm	552.5	23.2	70

	Throttling Device Position	Total Pressure Difference (Pa)	Volumetric Flow Rate (m3/s)	Efficiency (%)
800 rpm	1200 mm	284.9	28.8	75.2
	900 mm	312.5	28.2	78
	600 mm	342.7	24.9	75.4
	300 mm	352.4	17.9	65
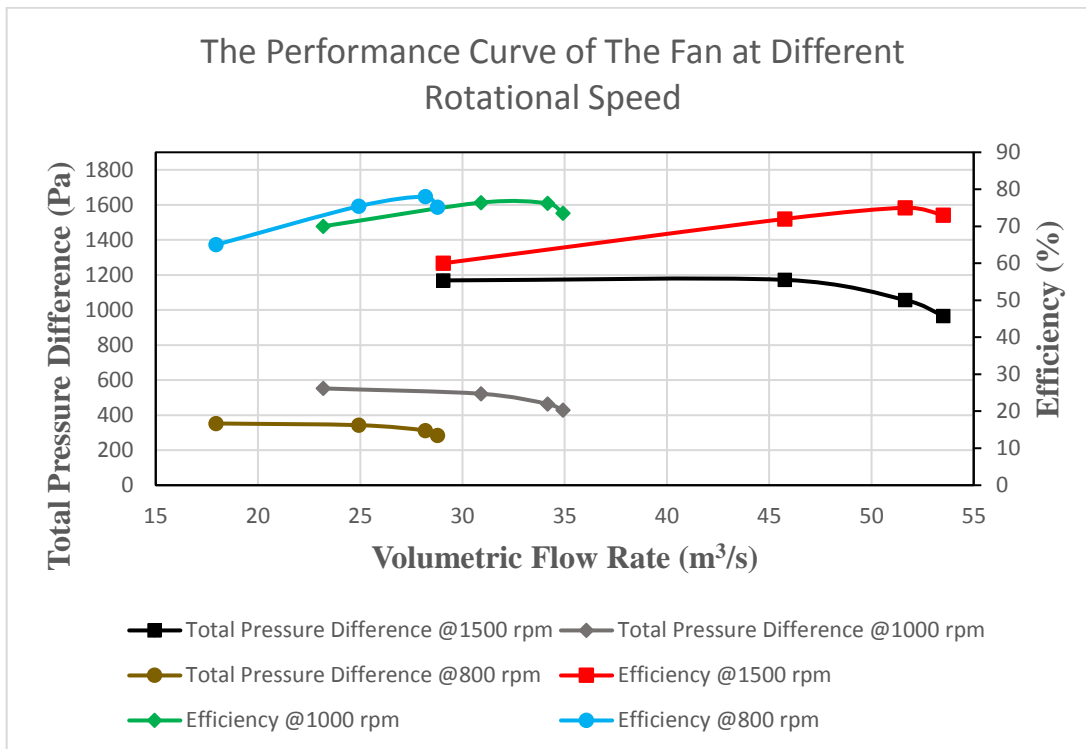
Figure 5.15. Performance Curves of the Fan for Different Rotational Speeds

In Figure 5.15, the performance curves of the same fan operated at different rotational speeds are given. It shows the effect of the rotational speed on the performance of the fan. It is an expected graph since the behavior of the axial fans operated at different rotational speed is a well-known case. These curves can also be obtained by using similarity laws. The calculated parameters are given in Appendix B.

If the density of the working fluid is constant, Equation 2.38, Equation 2.39 and Equation 2.40 are used.

The comparison of the performance curves obtained by using experimental methods and similarity laws are given in Figure 5.16. It can be said that the analytical results are very close to the experimental results. It can also show the consistency of the experimental tests.
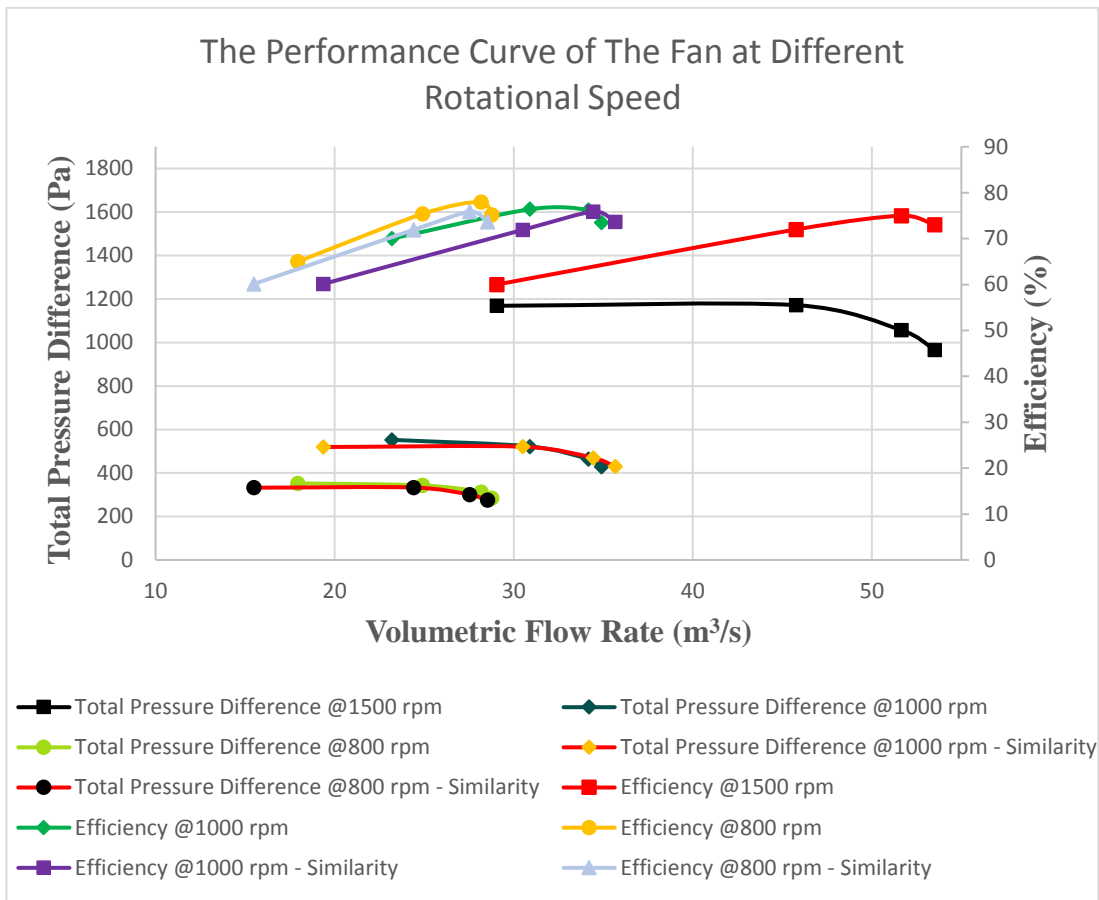
Figure 5.16. Comparison of Experimental and Similarity Performance Curves

The comparison of the performance curves obtained by using experimental methods and numerical methods are given in Figure 5.17.
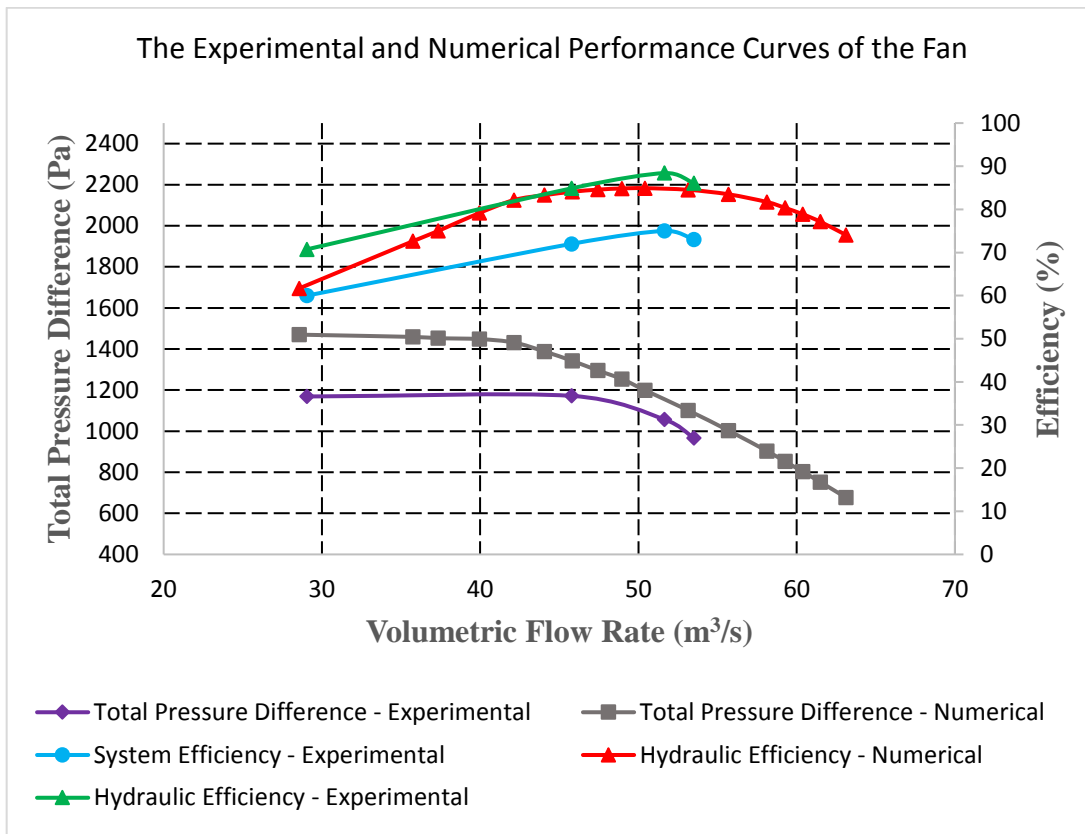
*Figure 5.17.* Comparison of Experimental and Numerical Performance Curves

At the end of all studies, the performance curves obtained from the numerical and the experimental methods are plotted and compared. In Figure 5.17, the comparison of the performance curves is given. The efficiency of the numerical method is hydraulic efficiency, and the efficiency obtained by the experimental method is the system efficiency. In addition, hydraulic efficiency curve of the experimental method is calculated and plotted. It can be said that hydraulic efficiencies of both methods are close to each other. Moreover, the total pressure curves of both methods are also close to each other at the suggested operating range, but there is a difference at the stalling range. The relative error between the numerical and experimental methods is calculated as 19%. There are some reasons of it. First one is that accuracies of both methods are different at the stalling range. When the stall starts in the experiment, the

114

total pressure values read from the pitot tubes fluctuate, and therefore, the recording process of the total pressures get difficult. Moreover, in the analyses, achieving the convergence criteria at the stalling range is also too difficult. Secondly, the movement of the throttling device is imitated by increasing the static pressure at the fan outlet in the numerical analyses. But the effect of the decreasing flow area of the fan outlet is not taken into consideration. Lastly, the inside walls of the test tube are considered as a smooth wall in the analyses, but they are not smooth in real. Therefore, the frictional pressure losses are different. All of these problems of the both methods cause to obtain different total pressure curves at the stalling range. However, these differences end up with different aerodynamic behaviors at the unstable range, the results in the operating range are close to each other.

CHAPTER 6

DISCUSSION AND CONCLUSION

6.1. Discussion

In this study, the design, construction and performance evaluation of axial flow fans are performed. The design process of an axial flow fan is examined in detail, and the experiences gained in the design are presented. It is observed that designing of an axial flow fan is a complicated process. The detailed design takes a long time, and it is possible to make a calculation error during the design process. In addition, there are a lot of empirical graphs used in the design process. Reading of the design parameters from the empirical graphs can also trigger to make mistakes in the design. In order to get rid of design mistakes, to reduce the allocated time to the design and to obtain an accurate axial flow fan, an axial flow fan design software is developed. In the code of the software, the suggestions, the design rules and the empirical graphs regarding the axial flow fans are embedded. In the airfoil selection of the implemented software, the experiences gained in the industry are used. An airfoil database is created to increase the diversity of the airfoil profiles used in the axial flow fan design.

Moreover, an axial flow fan is designed by using design software, and it is manufactured. In order to observe the aerodynamic characteristics of the fluid flow inside the fan and to prevent re-work processes in the manufacturing process, CFD analyses of the designed fan are performed before the manufacturing process. According to the results of the CFD analyses, the accuracy of the implemented software is found enough to start the manufacturing process. In order to obtain the performance curves of the manufactured axial flow fan, a test setup is prepared by obeying the rules in the testing standards. The tests are performed for three different rotational velocities of the AC motor, 800 rpm, 1000 rpm and 1500 rpm. The total and

117

static pressures are recorded by the help of located Pitot tubes in the test tube. The performance curves of the fan are plotted, and a sample calculation is presented.

Implementing a design software takes the most of the labor force, which is spent on this thesis. All the design rules and experiences learned from the literature and the industry are combined to generate a design code. All the empirical data in the design procedure is digitized to use in the code.

Designing of an axial flow fan is an iterative process. The initial and the final values of the lift coefficient and the hydraulic efficiency are compared, and a proper airfoil is selected in each iteration. These iterations are repeated with respect to the number of selected diametral slice points to obtain an airfoil data along the span length of the blade. Therefore, it turns to a complicated process. As a result, in order to supply ease of use, a user interface is developed. App Designer tool of the MATLAB is used for this process. The user-interface is prepared and connected to the design code with App Designer. Then, in order to increase the accuracy of the designs, the number of airfoils used in the database is increased. The data produced by XFOIL is used in this process. There are suggestions regarding the type of airfoil at the result screen of the interface. These airfoils are selected in the generated database.

In the CFD analyses part, the simplified geometry of the fan is analyzed. The main objectives of using CFD are to observe the aerodynamic characteristics of the fluid flow and to prevent re-works in the manufacturing process. Because of not being a CFD based study, the allocated time for the analyses is limited, and therefore, the simplifications are made in the analyzed model of the fan. Typically, there is a one-diameter long inlet tube and a ten-diameters long outlet tube at the inlet and the outlet of the fan model, respectively. The diameter of the fan is calculated as 1.5 meters, and therefore, the suggested length of the fan model for the analyses is computed as 15 meters. The CFD analyses of this kind of a big and detailed fan model take a long time. On the contrary, the allocated time for the analyses is limited due to the timely delivery of the produced fan. As a result, the simplified geometry of the fan model is

drawn. The small ineffective details such as nuts and screws are deleted in the model. Moreover, the size of the mesh file is adjusted with the help of the mesh independency study.

The constructions and experimental tests are performed by using the facilities of TEKNIMA CleanAir Technology. All parts used in the fan assembly except AC motor are constructed in the workplace of the company. The blades are produced by using an aluminum casting process. It is a critical process since the air bubbles in the blades lead to crack. In order to observe the quality of the molded blades, a non-destructive testing method is used. After the production process is completed, the test setup is prepared. There are some testing methods for fans to find their performance ratings. The setup is arranged according to Outlet Duct Setup-Pitot Traverse in Outlet Duct model of AMCA 210.

6.2. Conclusion

It is observed and experienced that there are painful processes in the design of an axial flow fan. In order to get support at the design process, a design code is generated and improved. The number of blades using in the database is increased and a user-interface is added. After the optimization in the design code, an axial flow fan is designed by the suggested output parameters of the software. The 3D model of the fan is constituted and then is analyzed by using numerical methods. According to the results of the analyses, the design is found logical, and the real model of it is constructed and tested experimentally.

According to the results of both experimental and numerical methods, the accuracy of the implemented software is found enough. The desired input parameters used in the implemented software are $50 \ m^3/s$ for the volumetric flow rate and $1250 \ Pa$ for the total pressure difference. The performance curves give around $1150 - 1200 \ Pa$ total pressure difference for the volumetric flow rate of $50 \ m^3/s$. It can be said that the outputs of the implemented software meet the design requirements.

REFERENCES

[1] S. K. Som and G. Biswas, *Introduction to Fluid Mechanics Fluid Machines*, 2nd ed. New Delhi: Tata McGraw-Hill Publishing Company Limited, 2008.

[2] F. P. Bleier, *Fan Handbook*. New York: McGraw-Hill, 1997.

[3] "12AWD Wall Fan Cast Aluminum Propeller Direct Drive," 2019. [Online]. Available: https://allaroundindustrysupply.com/product/12awd-wall-fan-cast-aluminum-propeller-direct-drive/.

[4] "Propeller Exhaust Fan," 2019. [Online]. Available: https://www.indiamart.com/proddetail/propeller-exhaust-fan-11629131062.html.

[5] "Tube Axial Fan," 2019. [Online]. Available: https://www.indiamart.com/proddetail/tube-axial-fan-17918196288.html.

[6] "ABC Ventilation Systems," 2019. [Online]. Available: https://abcventilation.com/ventilation-fans/.

[7] C. A. Nixon and D. J. Brake, "Design and Operational Aspects in the Use of Booster, Circuit and Auxiliary Fan Systems," *Mine Vent. Aust.*, 2006.

[8] I. Air Movement and Control Association International and I. American Society of Heating, Refrigerating and Air Conditioning Engineers, "AMCA 210: Laboratory Methods of Testing Fans for Ratings," 2000.

[9] S. Castegnaro, "A Critical Analysis of the Differences Among Design Methods for Low-Speed Axial Fans," *Proc. ASMA Turbo Expo 2017*, 2017.

[10] S. Castegnaro, "Fan Blade Design Methods: Cascade Versus Isolated Approach - Experimental and Numerical Comparison," *Proc. ASMA Turbo Expo 2016*, 2016.

[11] N. Ahmed, B. S. Yilbas, and M. O. Budair, "Computational Study into the Flow Field Developed Around a Cascade of NACA 0012 Airfoils," *Comput. Methods Appl. Mech. Eng.*, 1998.

[12] M. Masi, S. Castegnaro, and A. Lazzaretto, "A Criterion for the Preliminary Design of High-Efficiency Tube-Axial Fans," *Proc. ASMA Turbo Expo 2016*, 2016.

[13] S. J. Venter and D. G. Kröger, "The Effect of Tip Clearance on the Performance of an Axial Flow Fan," *Energy Convers. Manag.*, 1992.

[14] A. Pogorelov, M. Meinke, and W. Schröder, "Effects of Tip-Gap Width on the Flow Field in an Axial Fan," *Int. J. Heat Fluid Flow*, 2016.

[15] B. S. Yilbas, M. O. Budair, and M. N. Ahmed, "Numerical Simulation of the Flow Field Around a Cascade of NACA 0012 Airfoils-Effects of Solidity and Stagger," *Comput. Methods Appl. Mech. Eng.*, 1998.

[16] W. W. Peng, *Fundamentals of Turbomachinery*. Hoboken: JOHN WILEY & SONS, Inc., 2008.

[17] E. Andreadis, "Design of a Low Speed Vane-Axial Fan," Cranfield University, 2011.

[18] N. Scholz, *Aerodynamics of Cascades*. Neuilly sur Seine: North Atlantic Treaty Organization, 1965.

[19] O. Cordier, "Ähnlichkeitsbedingungen für Strömungsmaschinen," 1953.

[20] P. Epple, F. Durst, and A. Delgado, "A Theoretical Derivation of the Cordier Diagram for Turbomachines," *J. Mech. Eng. Sci.*, 2011.

[21] "SystemAir AXCPV 315 VANE." [Online]. Available: https://catalogue2.systemair.com/index.aspx?doc=%2Fitem%2Fitem.aspx%3 FfamilyId%3D12363%26__frame%3D.

[22] T. Neff and A. Lahm, "Structural Statics and Dynamics on Axial Fan Blades," *10th Int. Mine Vent. Congr.*, 2014.

[23] F. Piolenc and G. E. Wright, *Ducted Fan Design*. Marc de Piolenc, 2001.

[24] R. C. Turner, *Notes on Ducted Fan Design*. London, 1966.

[25] R. J. Downie, M. C. Thompson, and R. A. Wallis, "An Engineering Approach to Blade Designs for Low to Medium Pressure Rise Rotor-Only Axial Fans," *Exp. Therm. Fluid Sci.*, 1993.

[26] S. L. Dixon, *Fluid Mechanics, Thermodynamics of Turbomachinery*, 4th ed. Madras: Pergamon Press Ltd, 1998.

[27] P. R. P. Bruneau, "The Design of an Axial Flow Fan for a Cooling Tower Application," University of Stellenbosch, 1994.

[28] R. A. Wallis, *Axial Flow Fans and Ducts*. JOHN WILEY & SONS, Inc., 1983.

[29] "Ventilation Axial Flow Fan," 2019. [Online]. Available: https://www.indiamart.com/proddetail/ventilation-axial-flow-fan-5363191648.html.

[30] B. Eck, *Design and Operation of Centrifugal, Axial-Flow and Cross-Flow Fans*, 5th ed. Guildford: Pergamon Press, 1973.

[31] M. H. Aksel, *Fluid Mechanics*, 3rd ed. Ankara: METU, 2011.

[32] "NACA6904 Airfoil Details," 2019. [Online]. Available: http://airfoiltools.com/airfoil/details?airfoil=n6409-il.

[33] J. H. Ferziger and M. Peric, *Computational Methods for Fluid Dynamics*, 3rd ed. Berlin: Springer-Verlag, 2002.

[34] D. C. Wilcox, *Turbulence Modelling for CFD*, 1st ed. Glendale: DVW Industries, 1993.

[35] L. Prandtl, "Über ein neues Formelsystem für die ausgebildere turbulenz," 1945.

[36] P. R. Spalart and S. R. Allmaras, "A One-Equatlon Turbulence Model for Aerodynamic Flows," *AIAA J.*, 1992.

[37] B. S. Baldwin and T. J. Barth, "A One-Equation Turbulence Transport Model for High Reynolds Number Wall-Bounded Flows," *NASA Tech. Memo.*, 1990.

[38] V. A. Sai and F. M. Lutfy, "Analysis of the Baldwin-Barth and Spalart-Allmaras One-Equation Turbulence Models," *AIAA J.*, 1995.

[39] "Ansys Fluent Theory Guide." ANSYS, Inc., Canonsburg, 2013.

[40] F. R. Menter, "Two-Equation Eddy-Viscosity Turbulence Models for Engineering Applications," *AIAA J.*, 1994.

[41] W. P. Jones and B. E. Launder, "The Prediction of Laminarization with a Two-Equation Model of Turbulence," *Int. J. Heat Mass Transf.*, 1972.

[42] T.-H. Shih, W. W. Liou, A. Shabbir, Z. Yang, and J. Zhu, "A New k-ε Eddy Viscosity Model for High Reynolds Number Turbulent Flows," *Comput. Fluids*, 1995.

[43] J. E. Bardina, P. G. Huang, and T. J. Coakley, "Turbulence Modeling Validation, Testing, and Development," 1997.

[44] "ANSYS CFX-Solver Theory Guide." ANSYS, Inc., Canonsburg, 2009.

[45] "WhetherOnline Turkey," 2019. [Online]. Available: https://www.havaturkiye.com/weather/maps/city.

[46] R. J. Houghtalen, A. O. Akan, and N. H. C. Hwang, *Fundamentals of hydraulic engineering systems*, 4th ed. Upper Saddle River: Pearson Higher Education, 2010.

APPENDICES

A. Airfoil List

Table 0.1. *Used Airfoil List in Implemented Software*

1	NACA0006
2	NACA0008
3	NACA0009
4	NACA0010
5	NACA0012
6	NACA0015
7	NACA0018
8	NACA0021
9	NACA0024
10	NACA1408
11	NACA1410
12	NACA1412
13	NACA2408
14	NACA2410
15	NACA2411
16	NACA2412
17	NACA2415
18	NACA2418
19	NACA2421
20	NACA2424
21	NACA4412
22	NACA4415
23	NACA4418
24	NACA4421
25	NACA4424
26	NACA6409

27	NACA6412
28	S1223
29	S1210
30	S1223 RTL
31	E423
32	E591
33	EPPLER 1211
34	MH 112
35	CYR 24

B. Calculated Parameters by Using Similarity Laws

Table 0.2. *Similarity for 1000 rpm*

	Throttling Device Position	Total Pressure Difference (Pa)	Volumetric Flow Rate (m3/s)	Power Consumption (W)	Efficiency (%)
1000 rpm - Similarity	1200 mm	429.41	35.67	18903.70	81.04
	900 mm	469.68	34.43	19377.78	83.46
	600 mm	520.88	30.51	20088.89	79.12
	300 mm	519.51	19.37	15496.30	64.94

Table 0.3. *Similarity for 800 rpm*

	Throttling Device Position	Total Pressure Difference (Pa)	Volumetric Flow Rate (m3/s)	Power Consumption (W)	Efficiency (%)
800 rpm - Similarity	1200 mm	274.82	28.54	9678.70	81.04
	900 mm	300.59	27.55	9921.42	83.46
	600 mm	333.36	24.41	10285.51	79.12
	300 mm	332.49	15.50	7934.10	64.94